

*Study of Marine Processes in the
Northern Indian Ocean
using Radiocarbon*

Thesis submitted to

*The Maharaja Sayajirao University of Baroda,
Vadodara, India*

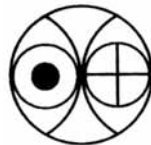
For the degree of

Doctor of Philosophy in Geology

By

Koushik Dutta

October, 2001



Oceanography & Climate Studies Area
Physical Research Laboratory,
Navrangpura, Ahmedabad – 380 009, India

Dedicated to my parents

Acknowledgements

“I hereby take the pleasure of expressing my heartfelt gratitude to Prof. B.L.K. Somayajulu, who introduced me to the wonderful fields of oceanography and carbon cycle. His great enthusiasm and constant encouragement helped a lot in shaping up of this work. I like to express my deep sense of gratitude to Prof. S. Krishnaswami, from whom I learnt how to look into finer details and intricacies in a data, and how to put them in a presentable form. I am also thankful to him for his critical comments and many helpful discussions. I sincerely thank Prof. Nikhil Desai and Prof. P.P. Patel (Dept. of Geology, M.S. University of Baroda), for encouragement and inspiration during the course of this work.

I am very much indebted to Dr. M.M. Sarin, who helped in developing within me the skills necessary to be a good experimental scientist. I learnt from him the techniques of analysis of inorganic carbon in seawater and sediment samples using a CO₂ coulometer, and also of total carbon and nitrogen analysis in sediments using a CN analyzer. I thank Prof. S.K. Bhattacharya for help with stable isotope analysis, and helpful discussions. I also thank Dr. R. Ramesh, for discussions and comments.

I am thankful to Drs. M. Dileep Kumar, (NIO, Goa), John Southon and Tom Guilderson (LLNL, Livermore), Minze Stuiver (Univ. of Washington, Seattle), and Ralph Keeling (Univ. of California, San Diego) for their valuable comments and inputs during various stages of this work. I like to thank Prof. Israel Carmi (Weizmann Institute of Science, Rehovot), who gave me an opportunity to attend the “17th International Radiocarbon Conference”, at Judean Hills, Israel (June, 2000). I also thank Prof. T. Nakazawa (FORGC, Yokohama), for providing me opportunity to attend the “6th International Carbon Dioxide Conference”, at Sendai, Japan (October, 2001).

I am grateful to R. Bhushan, who taught me with great patience the techniques of benzene synthesis and liquid scintillation counting. I will always remember the help provided by him during very tedious onboard oceanographic sampling operations, and also in the lab at other times. I also thank M.G. Yadava, who helped me to use the Quantulus LSC of the PRL radiocarbon laboratory, and R.A. Jani for his help during stable isotope analyses. I am indebted to J.P. Bhavsar, for his experienced technical help in the lab as well as onboard. I also like to thank R. Rengarajan, Soumen Mandal and Tarak Nath Dey, for helping me with computational works.

My sincere thanks to Dr. P.V. Narvekar (NIO, Goa) for his help in onboard CTD measurements, and to Dr. S.W.A. Naqvi (NIO, Goa), for his help and suggestions for various onboard chemical measurements. I gratefully acknowledge the help provided by Rajesh, Amit and Sudheer (PRL), and also by Joythi and Madhu (NIO, Cochin) for various chemical analyses done onboard FORV Sagar Sampada. I also like to thank Leopold (CMFRI, Cochin), Tapan (CMLRE, Cochin), and the staffs of Norinco for their technical help in various oceanographic operations. Help and encouragement provided by V. Ravindranathan (Director, CMLRE, Cochin) is thankfully acknowledged.

I am indebted to Dr. J.R.B. Alfred, (Zoological Survey of India, Calcutta), who provided the archived marine shell samples from the northern Indian Ocean, that are used in this work. Thanks go to Dr. R. Sridharan, who provided the shells of Mandapam and Rameswaram, and also to J.C. Drona, G. Rajagopal and V. Ganesh, who provided known age marine shells from their collections. I also thank Dr. Devesh Kr. Sinha (BHU, Varanasi), who helped in identifying some of the shell samples. I thank Dr. Michael Schulz, (Inst. for Geosciences, Univ. of Kiel), for providing the spectral analysis software, "SPECTRUM" and "REDFIT".

I thank A.R.S. Pandian, G.D. Panchal, and V.G. Shah for help in maintaining the LSC lab. I also thank Pranav and Rahul, who helped in smooth running of various electronic instruments. Excellent glass blowing skills of M.P. Kurup and K.K. Sivasankaran helped in maintaining the complex and delicate glassware of the benzene line, and also in making of various glass parts of instruments as per design. I gratefully acknowledge the help extended by the staffs of the computer center, the library, the workshop and the liquid nitrogen plant.

I will always remember my association with the chemistry lab colleagues, Sunil, Rajesh, Dixit, Tarun, Amit, Anirban, Neeraj, Sudheer and Manish. I thank them all for their help and support in different times. Educative discussions with Rajesh were always stimulating, from which both of us have been benefited. My sincere thank to Pauline for her moral support. I will also cherish the happy moments with the wonderful bunch of friends at the PRL residences (the list is rather too long to include them here!).

I am very much thankful to my parents, whose encouragement and moral support and always kept my ambitions high. My heartfelt thanks goes to my dearest friend, who provided constant mental support during the difficult days of writing this thesis.

Partial financial supports for this work were obtained from DOD-JGOFS, ISRO-GBP, ISRO-PC and PRL."

ABSTRACT

This work focuses on the northern Indian Ocean, to study oceanic carbon cycle and ocean circulation, using natural and nuclear-bomb produced radiocarbon (^{14}C) as tracer. The study involves ^{14}C measurements in the seawater column and in the air overlying the northern Indian Ocean, mainly aiming to determine:

- (1) Temporal and spatial variations of ^{14}C in the atmosphere;
- (2) Present distribution of ^{14}C in the water column, to assess temporal changes in the invasion of bomb- ^{14}C and the air-sea CO_2 exchange rate.

Achievement of some of the goals mentioned above also needs the determination of the pre-nuclear levels of ^{14}C in the surface waters of the northern Indian Ocean. This has been accomplished by ^{14}C measurements in archived marine shells of known age collected from the Arabian Sea and the Bay of Bengal coasts during the pre-nuclear era. The pre-nuclear $\Delta^{14}\text{C}$ values range from -50‰ to -62‰ in the Bay of Bengal, and -78‰ in the northern Arabian Sea. The ^{14}C reservoir ages in the Bay of Bengal are $229\pm 56\text{yr}$, $306\pm 35\text{yr}$ and $350\pm 21\text{yr}$ for the northern Bay of Bengal, the Andaman Sea and the southern Bay of Bengal respectively, corresponding to ΔR correction values of $-65\pm 53\text{yr}$, $11\pm 35\text{yr}$ and $32\pm 20\text{yr}$. In this study the highest ^{14}C reservoir age of $435\pm 29\text{yr}$ has been obtained for the upwelling dominated northern Arabian Sea, corresponding to ΔR value of $163\pm 30\text{yr}$. These ΔR correction values will be useful for calibrating ^{14}C ages of northern Indian Ocean marine sediments, and of calcareous archeological samples from the coastal region.

The mean $\Delta^{14}\text{C}$ values of the atmospheric CO_2 over the northern Indian Ocean were 121‰ (Bay of Bengal), 98‰ (Arabian Sea) and 88‰ (Bay of Bengal) during the springs of 1997, 1998 and 1999 respectively. The inter-annual variations observed beyond the expected exponential decay trend can be due to regional variations of $\Delta^{14}\text{C}$ and/or anomalous CO_2 emissions of biospheric origin during certain years.

The first water column measurements of ^{14}C in the Arabian Sea and the Bay of Bengal were made during 1978, as part of the international GEOSECS Indian Ocean expedition. To study the temporal changes of the distribution of ^{14}C in the northern Indian Ocean, cruises were conducted between 1993 and 1999, onboard FORV *Sagar Sampada*. During 1997, three GEOSECS stations were reoccupied; one of them is in the equatorial Indian Ocean and the other two in the central Bay of Bengal. During 1998, five GEOSECS stations in the Arabian Sea were reoccupied. During 1999, the

regions in the northern and the southern Bay of Bengal and the Andaman Sea were sampled. Samples of seawater were collected in vertical profiles from these stations for ^{14}C and various nutrient measurements. ^{14}C was measured by conventional liquid scintillation counting method, using 100litres of seawater per sample. In this study, ^{14}C results of seven vertical profiles from the northern Indian Ocean stations are reported. These stations are in the Gulf of Aden (reoccupation of GEOSECS 413), equatorial Indian Ocean (reoccupation of GEOSECS 448), southeastern Bay of Bengal (reoccupation of GEOSECS 445), two stations in the Andaman Sea and one station each in the northern and southern Bay of Bengal. During these cruises, $\Delta^{14}\text{C}$ in the air overlying the northern Indian Ocean was also measured by trapping atmospheric CO_2 in NaOH , and subsequently analyzing ^{14}C in the resulting bicarbonate solution.

The water column ^{14}C measurements show only marginal changes in the inventories of nuclear-bomb produced ^{14}C in the Bay of Bengal in two decades, since 1978. The mean penetration depth has increased on an average by ~40% in these two decades. At one station in the equatorial Indian Ocean, both large inventory and mean penetration depth of bomb ^{14}C indicates the importance of the lateral advection of ^{14}C enriched Pacific waters into this region. The air-sea CO_2 exchange rates over the Bay of Bengal, determined from the water column bomb ^{14}C inventories and atmospheric $\Delta^{14}\text{C}$ range from 7 to 17 $\text{mol.m}^{-2}.\text{yr}^{-1}$. These exchange rates are mainly a function of regional long-term wind speeds. From the reported mean seawater pCO_2 measurements, the corresponding atmospheric CO_2 uptake rate by the Bay of Bengal has been estimated to be ~9TgC.yr $^{-1}$.

No changes in the deep-water $\Delta^{14}\text{C}$ values are observed in the northern Indian Ocean as compared to the GEOSECS results, except in the Gulf of Aden, where increase up to 40‰ has been observed at 1500~2500m depths, possibly due to mixing with sinking Red Sea water having higher $\Delta^{14}\text{C}$. The $\Delta^{14}\text{C}$ values of the waters below ~1400m in the enclosed Andaman Basin are depth invariant at -170‰, significantly higher than that in the open Bay of Bengal (-190 to -195‰). This difference is due to rapid mixing of the deeper waters with the intermediate water masses due to convection as a result of high heat flow, and absence of deep-water ventilation. From the distribution of ^{14}C below 700m in the northern Indian Ocean, vertical advection rate of 5 to 14 m.yr^{-1} and vertical eddy diffusivity of 2 to 4 $\text{cm}^2.\text{sec}^{-1}$ was obtained.

Contents

List of tables...	(iv)
List of figures ...	(v)
Chapter 1 Introduction	1–9
1.1 Radiocarbon in the environment and its applications...	2
1.1.1 Application of ^{14}C as a chronometer...	4
1.1.2 Application of ^{14}C as a radiotracer ...	5
1.2 Studies of marine processes in the northern Indian Ocean ...	7
1.3 Scope of the present work ...	8
1.4 Outline of the thesis ...	9
Chapter 2 Materials and methods	10–27
Materials	
2.1 Collection and pretreatment of archived marine shells and corals...	12
2.2 Oceanographic cruises to the northern Indian Ocean...	14
2.2.1 Sampling of atmospheric CO_2...	15
2.2.2 Sampling of seawater ...	16
Methods	
2.3 Shipboard processing and measurements ...	17
2.3.1 Measurement of dissolved oxygen ...	18
2.3.2 Measurement of dissolved inorganic carbon ...	18
2.3.3 Measurement of nutrients ...	19
2.3.4 Measurement of salinity ...	19
2.3.5 On-board extraction of DIC from seawater for ^{14}C analysis ...	20
2.4 Radiocarbon measurements ...	21
2.4.1 Conversion of samples to benzene ...	21
2.4.2 ^{14}C counting of benzene samples...	24
2.4.3 ^{14}C counting of marble and NBS Oxalic Acid-II ...	25
2.4.4 Stable isotope ($\delta^{13}\text{C}$) measurement of CO_2 samples ...	26
2.4.5 Reporting of ^{14}C activities ...	26
2.4.6 Precision of ^{14}C measurements and results of Fourth International Radiocarbon Inter-comparison (FIRI) Exercise ...	26

Chapter 3 Pre-nuclear radiocarbon in the Northern Indian Ocean 28–45

3.1	Introduction: Natural radiocarbon in surface oceans	29
3.1.1	Marine ^{14}C reservoir ages and ΔR correction values	31
3.1.2	Pre-nuclear $\Delta^{14}\text{C}$ in surface oceans	31
3.2	Pre-nuclear surface ocean ^{14}C from marine samples	33
3.3	Pre-nuclear surface water ^{14}C in the northern Indian Ocean	35
3.4	Results of ^{14}C measurements in shells and corals... ..	36
3.5	Discussion on pre-nuclear $\Delta^{14}\text{C}$, $\text{R}(\text{t})$ and ΔR correction values for the northern Indian Ocean	38
3.5.1	Arabian Sea	38
3.5.2	Bay of Bengal... ..	40
3.5.3	Spatial variation of $\Delta^{14}\text{C}$, $\text{R}(\text{t})$ and ΔR correction values of the northern Indian Ocean and comparison with the global pattern	42
3.6	Conclusions	45

Chapter 4 Radiocarbon in atmospheric CO_2 over the Northern Indian Ocean 46–69

4.1	Variations of bomb ^{14}C in the atmospheric CO_2 over the northern Indian Ocean	47
4.2	$\Delta^{14}\text{C}$ in maritime air over the northern Indian Ocean... ..	50
4.3	Trends of $\Delta^{14}\text{C}$ in atmosphere over the northern Indian Ocean	52
4.3.1	Regional variations of $\Delta^{14}\text{C}$ over the northern Indian Ocean	54
4.3.2	Inter-annual variations of $\Delta^{14}\text{C}$ over the northern Indian Ocean	56
4.4	Influence of El Niño/Southern Oscillation on atmospheric CO_2 and its isotopes... ..	56
4.5	Statistical coherence between ENSO and tropospheric $\Delta^{14}\text{C}$	60
4.5.1	Pre-bomb tropospheric $\Delta^{14}\text{C}$ data from Washington, U.S.A.	60
4.5.2	Post-bomb tropospheric $\Delta^{14}\text{C}$ data from Wellington, New Zealand	60
4.5.3	El Niño/Southern Oscillation indices (Niño-3 SST and MEI)	61
4.5.4	Spectral and cross-spectral analyses of detrended ^{14}C and ENSO Indices	64
4.5.5	Discussion on coherence between tropospheric $\Delta^{14}\text{C}$ and ENSO	67
4.6	Conclusions	69

Chapter 5 Radiocarbon in the Bay of Bengal: Two decades after the GEOSECS **70–99**

5.1	Oceanographic features of the northern Indian Ocean	71
5.2	Distribution of ^{14}C in the northern Indian ocean two decades after the GEOSECS... ..	72
5.3	Bomb ^{14}C in the northern Indian Ocean... ..	84
5.3.1	Changes in the inventories and penetration depths of bomb- ^{14}C in the northern Indian Ocean	84
5.3.2	Comparison of the observed changes of bomb- ^{14}C inventories with model simulated bomb- ^{14}C distribution... ..	87
5.4	Air-sea exchange rate of CO_2 based on bomb- ^{14}C inventories... ..	88
5.4.1	Distribution of air-sea CO_2 exchange rate over the northern Indian Ocean	88
5.4.2	Comparison of the bomb- ^{14}C derived air-sea CO_2 exchange rates with climatological wind-speed data	90
5.4.3	Estimate of net air-sea flux of CO_2 over the northern Indian Ocean ...	92
5.5	^{14}C in deep waters of the northern Indian Ocean	96
5.5.1	Estimation of vertical advection and diffusion rates from natural ^{14}C distributions	97
5.6	Conclusions	99

Chapter 6 Synthesis and scope of future research **100–106**

6.1	Important results of this study... ..	101
6.2	Scope of future research	104

<i>Appendix–A</i>	Method of reporting ^{14}C data	107
-------------------	-------------------------------------------------	-----

<i>Appendix–B</i>	Determination of marine ^{14}C reservoir ages & ΔR correction values... ..	109
-------------------	---------------------------------------------------------------------------------------------	-----

<i>Appendix–C</i>	Determination of bomb- ^{14}C inventories & air-sea CO_2 exchange rates	111
-------------------	--------------------------------------------------------------------------------------------------	-----

<i>Appendix–D</i>	Radiocarbon & hydrographic data	114
-------------------	----------------------------------------	-----

<i>References</i>	122–140
-------------------	-------	----------------

<i>List of publications</i>	141–142
-----------------------------	-------	----------------

List of Tables

Table	Page
2–1 Onboard processing and measurements of seawater samples	17
2–2 Comparison of ^{14}C measurements by PRLCH and FIRI consensus values	27
3–1 Results of ^{14}C analyses in archived marine shells and corals of pre-nuclear era from the northern Indian Ocean... ..	37
3–2 Comparison of reservoir ages calculated in this study and in Global Marine Reservoir Correction Database... ..	44
3–3 Summary of pre-nuclear $\Delta^{14}\text{C}$, $R(t)$ and ΔR values for the northern Indian Ocean	45
4–1 ^{14}C measurements in atmospheric CO_2 over the northern Indian Ocean	51
4–2 Spring-time $\Delta^{14}\text{C}$, e-folding time (τ) and residual $\Delta^{14}\text{C}$	54
4–3 Fraction of oceanic CO_2 in the atmospheric CO_2 over the Arabian Sea	56
5–1 Pre-nuclear surface $\Delta^{14}\text{C}$ values adopted for the northern Indian Ocean	73
5–2 Inventory and mean penetration depths of bomb- ^{14}C in the northern Indian Ocean	83
5–3 Bomb- ^{14}C -based air-sea CO_2 exchange rates over the northern Indian Ocean	89
5–4 Compilation of surface water pCO_2 in the northern Indian Ocean (1991–1995)	94
5–5 Estimates of sea to air flux of CO_2 from the northern Indian Ocean ...	95
5–6 1D-model results for advection velocity and vertical eddy diffusivity	98

List of Figures

Fig.		Page
1-1	Rise of ^{14}C in the atmosphere and ocean in response to atmospheric thermonuclear tests	3
2-1	Locations of shell and coral samples from the northern Indian Ocean	12
2-2	Bivalve shell pair <i>Asaphis deflavata</i> , from Stewart Sound, North Andaman Islands	13
2-3	Cruise tracks of FORV <i>Sagar Sampada</i> to the northern Indian Ocean between 1997 and 1999	14
2-4	Apparatus used for onboard sampling of CO_2 from the atmosphere for ^{14}C analysis... ..	15
2-5	Sampling of seawater onboard FORV <i>Sagar Sampada</i>	16
2-6	Closed system circulation for on-board extraction of DIC from seawater samples	20
2-7	Flow diagram for measurement of ^{14}C by liquid scintillation counting of benzene samples	21
2-8	Count-rates of marble (background) and NBS Oxalic Acid-II (standard) with Packard 2250CA LSC	25
3-1	Calibration of radiocarbon ages for marine samples and the concept of ΔR	30
3-2	Spatial gradient of $\Delta^{14}\text{C}$ in surface oceans during 1950 by the LLNL model simulation compared with data from biological archives	32
3-3	Results of ^{14}C measurements in shells and corals from the northern Indian Ocean	36
3-4	Pre-nuclear $\Delta^{14}\text{C}$ in the Bay of Bengal shells, compared with coral measurements in the eastern Pacific	41
3-5	Isopycnal contours for the WOCE section I08, along 8.5°N in the Arabian Sea and along 9.97°N in the Bay of Bengal	42
3-6	Compilation of coastal region ΔR correction values	43
4-1	$\Delta^{14}\text{C}$ versus time for three latitude zones	47
4-2	^{14}C in atmospheric CO_2 from sites near the northern Indian Ocean ...	48

Fig.		Page
4-3	Cruise tracks for maritime CO ₂ sampling over the Arabian Sea and the Bay of Bengal, between 1997 and 1999	50
4-4	Tropospheric $\Delta^{14}\text{C}$ measured from the northern and the southern hemisphere sites with inset plot of average $\Delta^{14}\text{C}$ measured in air overlying the northern Indian Ocean	52
4-5	Long-term observations of ¹⁴ CO ₂ at Izaña, Canary Is. and at Neumayer, Antarctica, from 1983 to 1999	53
4-6	Global atmospheric carbon dioxide growth rate from NOAA–CMDL cooperative air sampling network... ..	57
4-7	Anomalies of ¹⁴ C over the Arabian Sea and the Bay of Bengal	58
4-8	The Niño regions of the equatorial Pacific	61
4-9	Tree-ring ¹⁴ C and El Niño strength during the pre-nuclear era	62
4-10	Southern hemisphere tropospheric $\Delta^{14}\text{C}$ and El Niño strength in the post-nuclear era	63
4-11	Spectral and cross-spectral analysis of the detrended Washington tree-ring $\Delta^{14}\text{C}$ and the Niño-3 SST index (1650–1950 AD)	65
4-12	Spectral and cross-spectral analysis of the detrended Wellington $\Delta^{14}\text{C}$ and the MEI (1970–1993 AD)... ..	66
5-1	θ -S profiles of seawater sampling stations in the northern Indian Ocean	71
5-2	θ -S and radiocarbon profile for the northern Bay of Bengal station SS#172/4030	74
5-3	θ -S and radiocarbon profile for the Andaman Basin station (north) SS#172/4036	75
5-4	θ -S and radiocarbon profile for the Andaman Basin station (south) SS#172/4037	76
5-5	θ -S and radiocarbon profiles for the southern Bay of Bengal stations, GEOSECS 445 and SS#152/3829... ..	77
5-6	θ -S and radiocarbon profile for the southern Bay of Bengal station SS#172/4041	78
5-7	θ -S and radiocarbon profiles for the equatorial Indian Ocean stations (south of Sri Lanka), GEOSECS 448 and SS#152/3846... ..	79

Fig.		Page
5–8	θ -S and radiocarbon profiles in the western Arabian Sea near the Red Sea mouth, GEOSECS 413 and SS#164/4018	80
5–9	Bomb- ¹⁴ C inventories in the northern Indian Ocean during the GEOSECS expedition of 1977–1978... ..	81
5–10	Bomb- ¹⁴ C inventories in the Arabian Sea during 1994–1995	84
5–11	Bomb- ¹⁴ C inventories in the Bay of Bengal during 1997 and 1999, and in the Red Sea mouth during 1998, determined from the ¹⁴ C results obtained from this study... ..	84
5–12	Changes in bomb- ¹⁴ C inventories in the northern Indian Ocean between 1978 and late 1990s, at the GEOSECS reoccupation stations	85
5–13	Predicted changes in bomb- ¹⁴ C inventories for the world ocean between 1981 and 1990 using GFDL world ocean model	87
5–14	Contours of long-term mean scalar wind speed at the surface over northern Indian Ocean region and bomb- ¹⁴ C based air-sea CO ₂ exchange rates... ..	90
5–15	Dependence of ¹⁴ C derived CO ₂ exchange rates with long-term mean scalar wind speed... ..	91
5–16	Underway pCO ₂ in surface seawater and in the atmosphere measured along WOCE sections I01 and I09N in the northern Indian Ocean ...	93
C–1	Demonstration of integrating ¹⁴ C profile to determine bomb- ¹⁴ C inventory in seawater column	112

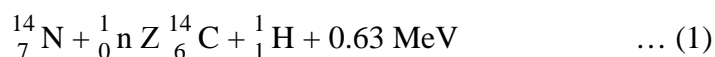
Chapter 1

Introduction

The pathways as well as time scales of the movement of carbon across various reservoirs (atmosphere, ocean and biosphere) can be studied, from the relative variations of the abundances of carbon isotopes in the respective reservoirs. There are three naturally occurring isotopes of carbon — ^{12}C (98.9%), ^{13}C (1.1%) and ^{14}C (10^{-10} %). Comprehensive account on the applications of ^{14}C isotopes in global carbon cycle studies can be found in Stuiver, *et al.*, (2000); Lal and Krishnaswami (1999). The following sections will provide introduction to ^{14}C , with a discussion on its applications in geochronology, global carbon cycle and ocean circulation.

1.1 Radiocarbon in the environment and its applications

The only naturally occurring radioactive isotope of carbon is ^{14}C , commonly known as radiocarbon. Under natural conditions, ^{14}C is produced in the environment by the nuclear interactions of galactic and solar cosmic rays with the atmospheric constituents. ^{14}C is produced mainly in the stratosphere by the $^{14}\text{N}(\text{n,p})^{14}\text{C}$ reaction, by exothermic thermal neutron capture by atmospheric ^{14}N ,



The ‘hot’ and energetic ^{14}C atoms thus formed get quickly oxidized into $^{14}\text{CO}_2$ (through the formation of ^{14}CO). Being chemically indistinguishable from ordinary $^{12}\text{CO}_2$, ^{14}C in the form of $^{14}\text{CO}_2$ gets subsequently transferred to the exchangeable terrestrial reservoirs of carbon, *e.g.*, the biosphere and the oceans, through photosynthesis and air-sea exchange of CO_2 , and takes part in the global carbon cycle. ^{14}C decays to ^{14}N through electron (β^-) emission ($E_{\text{max}}=156\text{keV}$), with a half-life of $5730\pm 40\text{yr}$ (Godwin, 1962),



Prior to 1950, the natural level of ^{14}C in the environment was in equilibrium with its nearly constant cosmogenic production rate in the atmosphere at the rate of $\sim 2.4 \text{ atoms.cm}^{-2}.\text{sec}^{-1}$ at sea level, and its decay in different reservoirs (Lingenfelter and Ramaty, 1970; Damon and Sternberg, 1989). Natural variations of ^{14}C in the atmosphere take place in a wide range of time scales, from less than a decade to about a few millennia (Stuiver, *et al.*, 1991). These are caused mainly through changes in the ^{14}C production rate (due to changes in geomagnetic field variations and solar modulation of galactic cosmic rays) and also through ocean circulation variations, which influence the exchange rates of CO_2 between ocean and atmosphere.

1.1.1 Applications of ^{14}C as a chronometer

The half-life of ^{14}C ($5730\pm 40\text{yr}$) make this isotope most suitable for dating wide range of organic archeological samples, which are either remains of plants (woods, seeds, etc.) or animals (bones, shells, etc.), and are dated between a few hundred years to few tens of kilo-years (Libby, *et al.*, 1949; Libby, 1955). The ^{14}C is used as a chronometer with the assumption that, during their lifetimes these organic materials have exchanged carbon with the ambient ‘reservoir’ or carbon pool—which are atmospheric carbon dioxide in case of terrestrial samples and dissolved inorganic carbon of seawater in case of marine samples. This exchange continued until their death, after which ^{14}C starts decaying. However, the initial $^{14}\text{C}/^{12}\text{C}$ isotopic ratios in various reservoirs are not uniform, either due to production rate changes in the atmosphere or circulation changes in the ocean, or both, which complicates the ^{14}C dating method. It is essential to have precise knowledge about both the spatial and temporal variability of the initial $^{14}\text{C}/^{12}\text{C}$ isotopic ratios in the respective reservoirs.

Variations of ^{14}C in the atmosphere until $\sim 11,900\text{yr}$ back is fairly well known, from large number of high-precision ^{14}C measurements in tree-rings of known calendar age (Stuiver, *et al.*, 1998a). Due to rapid mixing time scale of the tropospheric air, little spatial variation of ^{14}C is seen in global terrestrial ^{14}C ages. Since the zonal mixing rate of the atmosphere is far more rapid (few weeks) than the meridional mixing (months to about a year), zonal variations of tropospheric ^{14}C concentration are negligible as compared to the meridional variations (Braziunas, *et al.*, 1995). However, oceanic mixing time scales are much slower than that of the troposphere, which ranges from few decades in the upper ocean to about a millennium for the global deep-water (Stuiver and Quay, 1983). Upwelling processes, which brings ^{14}C -depleted waters from the deep to the surface, varies considerably for different oceanic regions. These processes, along with slower mixing time scales contribute to the significant spatial variability of natural ^{14}C concentrations in the surface oceans. Thus, unlike terrestrial samples, for ^{14}C dating of marine samples it is not possible to assume geographically uniform values of initial ^{14}C activities of the reservoir (*i.e.*, surface seawater). A region specific correction is required, to account for these regional variations of initial ^{14}C ages. Thus, it is essential to have knowledge of the pre-nuclear surface ^{14}C concentration of different regions of the global ocean. Knowledge on the distribution of pre-nuclear ^{14}C is also essential to quantify the input of bomb- ^{14}C to oceans (Broecker, *et al.*, 1995).

1.1.2 Applications of ^{14}C as a radiotracer

Apart from its most well known application as a dating tool for archeological samples, the ^{14}C isotope can also be used as a tracer to study the pathways of carbon across various reservoirs. Both natural and bomb produced ^{14}C are suitable for the studies of exchangeable carbon reservoirs (oceans, biosphere, soil organic matter), which interact with atmospheric CO_2 reservoir on time scale of decades to centuries (Stuiver, *et al.*, 2000). The inadvertent addition of bomb- ^{14}C in the environment can be used to address a host of problems, pertaining to the global carbon cycling and ocean circulation. The important applications of ^{14}C as a tracer are described here.

(a) ^{14}C as tracer in atmospheric studies:

The natural variations of ^{14}C in the atmosphere depend on the variations of solar magnetic activity and also on the coupled ocean-atmosphere processes (Damon, *et al.*, 1978, 1989, 1999; Stuiver and Quay, 1981; Stuiver and Braziunas, 1993b). Anthropogenic variations of this isotope in the environment take place either through dilution from ^{14}C -free fossil fuel emissions, or increase in ^{14}C due to thermonuclear explosions or other nuclear emissions (Levin, *et al.*, 1980). After the post-bomb excursion of ^{14}C in the atmosphere during mid 1960s (Fig. 1–1), the bomb- ^{14}C pulse in the environment has been fruitfully used as a transient tracer to study atmospheric circulation and monitoring fossil fuel emissions (Levin, *et al.*, 1980, 1985; Manning, *et al.*, 1994). The ^{14}C observation in the atmosphere has played a crucial role to understand the global sources and sinks of carbon.

During 1990s, the interannual variations of $\Delta^{14}\text{C}$ became much smaller than during late 1960s, due to the quasi-exponential decreasing trend of atmospheric $\Delta^{14}\text{C}$. Therefore, the long-term atmospheric $\Delta^{14}\text{C}$ monitoring programs were discontinued at several locations of the world during 1990s, when the interannual $\Delta^{14}\text{C}$ variations became appreciably small and atmospheric $\Delta^{14}\text{C}$ attained a quasi-natural equilibrium state. However, subtle natural variations of atmospheric $\Delta^{14}\text{C}$ both in the pre-bomb and post-bomb era can be induced by anomalous changes in the CO_2 sources and sinks from the oceans and biosphere, which are triggered by complex coupled ocean-atmosphere processes (Stuiver and Braziunas, 1993b; Rozanski, *et al.*, 1995). It is important to understand these processes, which influence the natural variation of ^{14}C in the atmosphere on short time scales (<10yr), to disentangle the anthropogenic variations from the natural ones (Stuiver and Braziunas, 1998).

Observations of $\Delta^{14}\text{C}$ in the maritime atmosphere far from influences of continental fossil fuel sources, offer a means to study such processes. Study of ^{14}C variations in the atmosphere, undisturbed from human influences for the past several centuries, can also provide clues to these processes. Such data can be retrieved from high-precision ^{14}C measurements in long tree-ring records (Stuiver, *et al.*, 1998b).

(b) ^{14}C in oceanographic studies:

^{14}C in oceans has long been employed as a useful tracer to study the processes of air-sea CO_2 exchange and circulation at different time scales. Oceans, which cover about 72% of the earth's surface, are a huge reservoir of heat energy and play a very important role in regulating the climate of the Earth. Global oceans absorb about 55% of the CO_2 emitted by fossil fuel burning anthropogenic activities, thus acting as an enormous buffer against the atmospheric rise of this greenhouse gas. Concentration of atmospheric CO_2 was $\sim 370\text{ppm}$ at the end of 20th century (Keeling and Whorf, 2001), and is increasing at an alarming rate of $\sim 2\text{ppm.yr}^{-1}$ due to fossil fuel burning and land use changes. To meet the energy demands of the ever-increasing population and industry, global consumption of fossil fuel and land use changes are expected to rise, making the upward trend of atmospheric CO_2 inevitable. Oceans being one of the major sinks of CO_2 , detailed knowledge about the uptake rate of for different oceanic basins of the world is essential to model the future rise of CO_2 in the atmosphere.

Oceanic distribution of ^{14}C can be used to trace circulation processes on a wide range of time scales. Distribution of natural (cosmogenic) ^{14}C in oceans, provide time constants for large-scale circulation of the oceans (Bien, *et al.*, 1965; Stuiver and Quay, 1983). Since 1955, global surface oceans showed a measurable increase in ^{14}C concentration, due to transfer of bomb- ^{14}C from the atmosphere to the oceans (Rafter and Ferguson, 1957). The increase in oceanic inventory of bomb- ^{14}C depends on the local air-sea CO_2 exchange rate, diffusivity, vertical and lateral movement of seawaters. Since the bomb- ^{14}C concentration in the upper layers of the ocean changes on time scale of decades, it is an ideal tracer to study air-sea CO_2 exchange processes and to trace decadal mixing processes in the thermocline (Quay and Stuiver, 1980; Broecker, *et al.*, 1985, 1995; Druffel, 1989). Measurement of ^{14}C in oceans is also important for validating the ocean general circulation models, primarily used for predicting the CO_2 uptake rates and used to simulate the oceanic ^{14}C distribution (Toggweiler, *et al.*, 1989b; Jain, *et al.*, 1995; Guilderson, *et al.*, 2000a).

1.2 Studies of marine processes in the northern Indian Ocean

The two northern Indian Ocean basins surrounding India are the Arabian Sea and the Bay of Bengal. They are characterized by contrasting oceanographic features, which result in distinct differences in their circulation pattern in the thermocline region, and also in the magnitude and direction of sea-air CO₂ fluxes. The Bay of Bengal receives large amount of fresh water throughout the year from seven major rivers, with peak input during the southwest monsoon season (June to September). Therefore the surface waters of the Bay of Bengal are much less saline than those of the Arabian Sea. This low salinity water creates a low-density layer at the surface, thereby creating a steep gradient of the isopycnal surfaces and reducing the vertical mixing. This, coupled with high biological productivity keeps the surface seawater pCO₂ in this oceanic region lower than that in the atmosphere, making it a sink of atmospheric CO₂ (Kumar, *et al.*, 1996). Whereas in the Arabian Sea, the pCO₂ of surface waters is greater than that in the atmosphere mainly due to strong wind induced upwelling of CO₂ rich deep waters, making it a net source of CO₂ to the atmosphere (Kumar, *et al.*, 1992; Sarma, *et al.*, 1998). These contrasting physical oceanographic settings and the wind speed regimes of the two basins influence the regional ocean-atmosphere fluxes of CO₂. In addition, these will also influence the isotopic composition of carbon in the concerned reservoirs, *i.e.*, both in the oceanic DIC as well as in the atmospheric CO₂ overlying this ocean.

The northern Indian Ocean is a region of considerable interest, to study past climate changes, from the geochemical records of marine sediments. The paleoclimate studies done in this region mainly focus on past monsoon variations in the southern Asia during the Quaternary, deciphered from analyses of geochemical proxies in marine sediments (Duplessy, 1982; Sarkar, *et al.*, 1990; von Rad, *et al.*, 1999; Sarkar, *et al.*, 2000). For the studies of temporal climate variations, these analyses must be supported with a reliable chronology. The ¹⁴C method of dating is most suited for the chronology of marine sediments, deposited within few tens of kilo years. ¹⁴C ages of shells of marine calcareous microfossils are generally used for this purpose. Due to complex circulation pattern in the surface northern Indian Ocean, large regional variations of ¹⁴C reservoir ages are expected in this region. However, so far there were very few pre-nuclear ¹⁴C measurements from this region, which can be used to determine ¹⁴C reservoir ages, for dating these marine sediments by the ¹⁴C method.

Complex and contrasting ocean circulation patterns in the Arabian Sea and the Bay of Bengal complicate the modeling of the distribution of tracers in this region. The first measurements of radiocarbon in the water column of the Arabian Sea and the Bay of Bengal were done during 1977 and 1978, as a part of the international GEOSECS program (Stuiver and Östlund, 1983). Based on reoccupation of three Arabian Sea GEOSECS stations, Bhushan, *et al.* (2000) described temporal changes in radiocarbon distribution about two decades after GEOSECS.

To study the temporal changes in the distribution of radiocarbon in the Bay of Bengal, cruises were led during 1997 and 1999, onboard FORV *Sagar Sampada*. During the 1997 cruise, three GEOSECS stations were reoccupied, one of them is in the equatorial Indian Ocean and the other two in the central Bay of Bengal. During 1999, stations in the northern and the southern Bay of Bengal and in the Andaman Sea were occupied. The results obtained from the Bay of Bengal in this study have been compared with those of the Arabian Sea. In another cruise to the Arabian Sea during 1998, five GEOSECS stations in the Arabian Sea were reoccupied, which included one station in the Gulf of Aden near the Red Sea mouth.

During these cruises, samples of seawater were collected in vertical profiles for measurements of ^{14}C . Atmospheric CO_2 was also collected during these cruises for ^{14}C measurements. Pre-nuclear marine shells of known age, collected from northern Indian coasts were procured from different sources, to determine pre-nuclear ^{14}C and ^{14}C reservoir ages for this oceanic region.

1.3 Scope of the present work

The present investigation deals with studies of the oceanographic processes in the northern Indian Ocean using ^{14}C as a tracer. The main aims of this study are:

- (i) To determine the spatial variability of pre-nuclear ^{14}C in the oceanic mixed layer from ^{14}C measurements in archived marine shells from pre-nuclear era. This will help to calculate ^{14}C reservoir ages in selected northern Indian Ocean regions for marine ^{14}C age calibration.
- (ii) To measure the present level of ^{14}C in atmospheric CO_2 and its spatial and temporal variations over the northern Indian Ocean; examine the coupled ocean-atmosphere phenomena, which influence the natural variations of ^{14}C in the atmosphere on sub-decadal time scales.

- (iii) Evaluating the temporal variations in the distribution and inventory of nuclear bomb produced radiocarbon in the northern Indian Ocean water column, with focus on the Bay of Bengal region, two decades after the GEOSECS expedition; To assess the spatial variability in the air-sea exchange rate of CO₂ over the northern Indian Ocean from the bomb ¹⁴C inventories and atmospheric ¹⁴C variations, and estimation of the average uptake rate of CO₂ by the region; To determine the vertical advection and diffusion rates based on the distribution of natural ¹⁴C in deep water.

1.4 Outline of the thesis

This thesis has been divided into six chapters. The contents of the other five chapters are outlined below:

Chapter 2 describes the experimental procedures of ¹⁴C analysis of various samples, such as seawater, atmospheric air and shells. Onboard measurement procedures of various chemical and hydrographic parameters are also described.

Chapter 3 gives the pre-nuclear distribution of ¹⁴C in the northern Indian Ocean from ¹⁴C measurements in archived marine shells. The patterns of the ¹⁴C reservoir ages and the ΔR correction factors in this region have been discussed.

Chapter 4 discusses the results of atmospheric Δ¹⁴C measurements over the northern Indian Ocean between 1993 and 1999. Variation of atmospheric Δ¹⁴C on sub-decadal time scales from different parts of the world — both for the pre-nuclear and the post-nuclear periods have been discussed, with the underlying causes.

Chapter 5 presents the results of radiocarbon measurements from different stations of the Arabian Sea, the equatorial Indian Ocean and the Bay of Bengal. Changes in the inventory and penetration of bomb-¹⁴C two decades after the GEOSECS expedition, bomb-¹⁴C based air-sea CO₂ exchange rates are discussed in this section. The net uptake rate of CO₂ by the northern Indian Ocean has been estimated from the bomb-¹⁴C based air-sea CO₂ exchange rates and reported surface seawater pCO₂ measurements. Vertical advection and diffusion rates are estimated based on the natural ¹⁴C in the intermediate and deep waters.

Chapter 6 synthesizes the results obtained in this study, highlighting the important findings. Scope for further research to improve the understanding of carbon cycling and the circulation processes of the northern Indian Ocean is included.

Chapter 2

Materials and Methods

The main aim of this thesis, as described in the earlier chapter is to determine air-sea exchange of CO₂ and circulation in the northern Indian Ocean region — from ¹⁴C measurements in archived pre-nuclear marine shells, contemporary atmospheric carbon dioxide and seawater samples. Sampling of these materials involved:

1. Procuring archived marine shells of pre-nuclear era for the measurement of ¹⁴C;
2. Collection of maritime atmospheric carbon dioxide over the ocean surface for the measurement of ¹⁴C; and
3. Collection of seawater samples in vertical profiles, for the measurement of ¹⁴C and other physical and chemical properties

Measurement of various physical properties and chemical constituents of seawater samples were carried out onboard. The primary physical properties measured were pressure, temperature and salinity, using a conductivity-temperature-depth (CTD) profiler. From these, other parameters such as depth, potential temperature (θ) and potential density (σ_θ) were derived. The chemical components measured in the seawater samples were dissolved oxygen, dissolved inorganic carbon (DIC or ΣCO_2), and nutrients — which included silicate (SiO₂), phosphate (PO₄) and nitrate (NO₃).

The radiocarbon measurements were done, using conventional liquid scintillation counting (β -assaying) of the benzene samples, prepared from CO₂ extracted from shells, atmospheric air and seawater samples.

Quality of all measurements was monitored, by analyzing suitable standard reference materials and repeat analyses. The quality of radiocarbon measurements was checked by analysis of a set of samples distributed for an international laboratory inter-comparison exercise during this study.

In the following the sampling locations, methods of sample collection and the procedures of various analytical techniques employed are described.

2.1 Collection and pretreatment of marine shells and corals

(a) Collection of shell and coral samples:

The sampling locations of the shell and coral samples used in this study are shown in Fig. 2–1. The bivalve shells from Stewart Sound and Chilika Lake were collected in 1935 and 1954 respectively by the Zoological Survey of India (ZSI). Specimens of these samples were procured from the archives of ZSI at Calcutta for ^{14}C measurements.

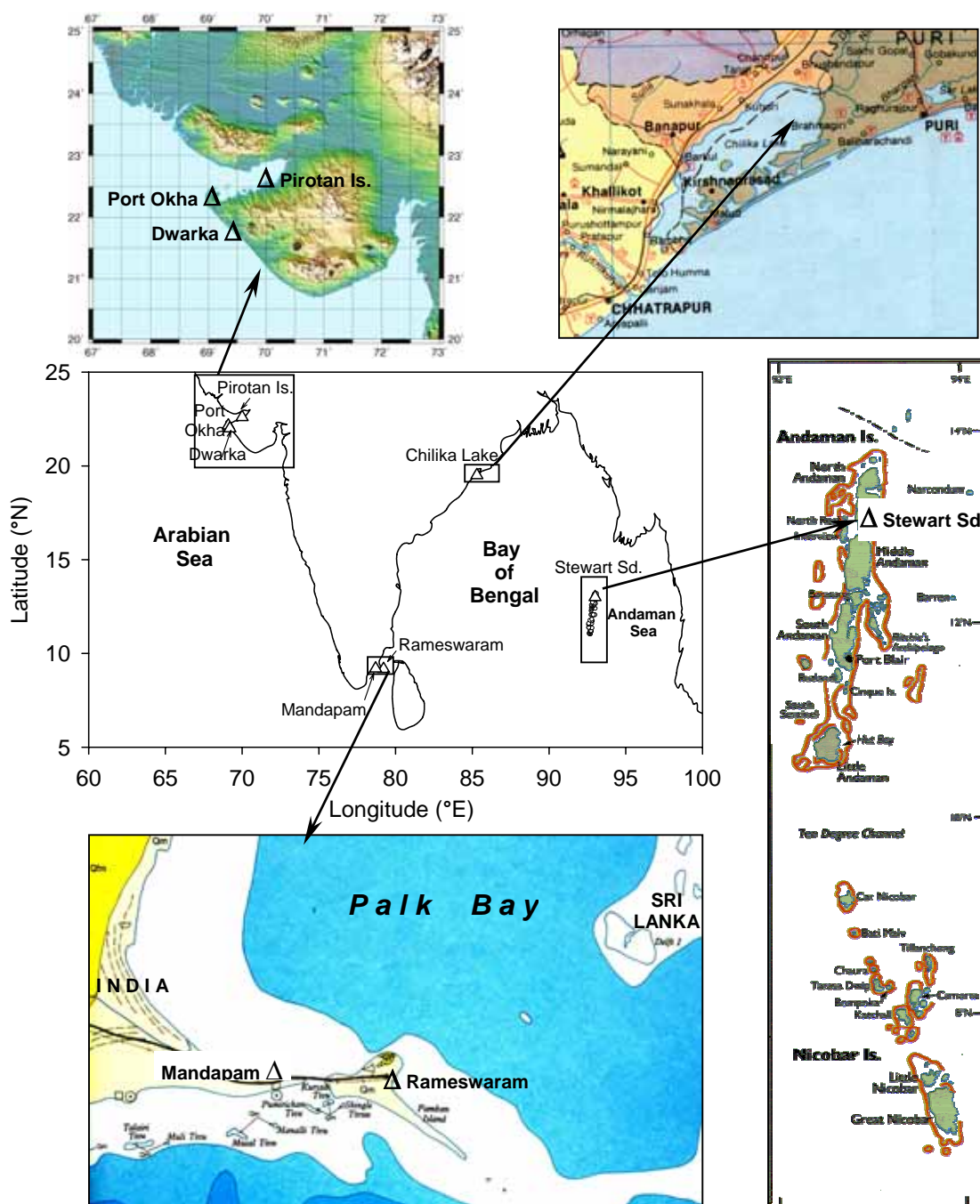


Figure 2–1 Locations of shell and coral samples from the northern Indian Ocean. Figure in the center shows locations of all samples with respect to India. Enlarged views of each location are also shown.

The bivalve collected from Stewart Sound is shown in Fig. 2–2. Bivalve and gastropod samples from Port Okha, Dwarka, Mandapam and Rameswaram were obtained from different shell collectors. The detailed locations of all pre-nuclear shells analyzed in this study are given in Table 3–1.

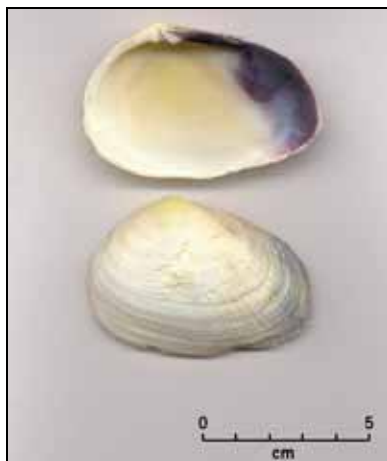


Figure 2–2 Bivalve shell pair Asaphis deflavata, collected from Stewart Sound, North Andaman Islands.

The coral *Favia speciosa* was collected alive from the Gulf of Kutch in 1990 (Chakraborty, 1993). The ^{14}C results of the combined growth bands of this coral formed during 1949–1951 and 1952–1954, as reported by Bhushan, *et al.* (1994) are used as additional supporting data in this work.

(b) Pretreatment of shells and corals prior to ^{14}C analysis:

The bivalve and gastropod samples were initially washed free of surface contamination with distilled water. They were then rinsed in 0.1N HNO_3 and sonified with distilled water in an ultrasonic bath to dislodge surface organic coatings. The outer layers of the shells were etched off by dipping them in 2N HCl for about 2 minutes, to remove surface calcareous contaminants. They were then washed thoroughly with de-ionized water and oven dried at 90°C . Before analysis, the shells were finely powdered in an agate mortar and homogenized. About 20g of powdered shells were used for each analysis (*sec.* 2.4). Procedures of pre-treatment and ^{14}C analysis of the coral samples have been described in Chakraborty, (1993). In that study, the annual coral growth bands were identified by X-radiography and cut using a diamond wheel. The cut bands were dried by heating overnight at $\sim 90^\circ\text{C}$ and powdered using a *Tema* mill. About 15g of powdered coral were used for ^{14}C analysis. For bands with smaller growth rates, 2 to 3 bands were combined to get sufficient material for ^{14}C analysis.

2.2 Oceanographic cruises to the northern Indian Ocean

During this study three cruises were undertaken to the Arabian Sea and the Bay of Bengal onboard FORV *Sagar Sampada* (Dept. of Ocean Development, Govt. of India), for seawater sampling in the northern Indian Ocean. Cruise SS#152 was during February 1997 to the Bay of Bengal, SS#164 during March–April 1998 to the Arabian Sea and SS#172 during February 1999 to the Bay of Bengal. The cruise tracks of these expeditions are shown in Fig. 2–3.

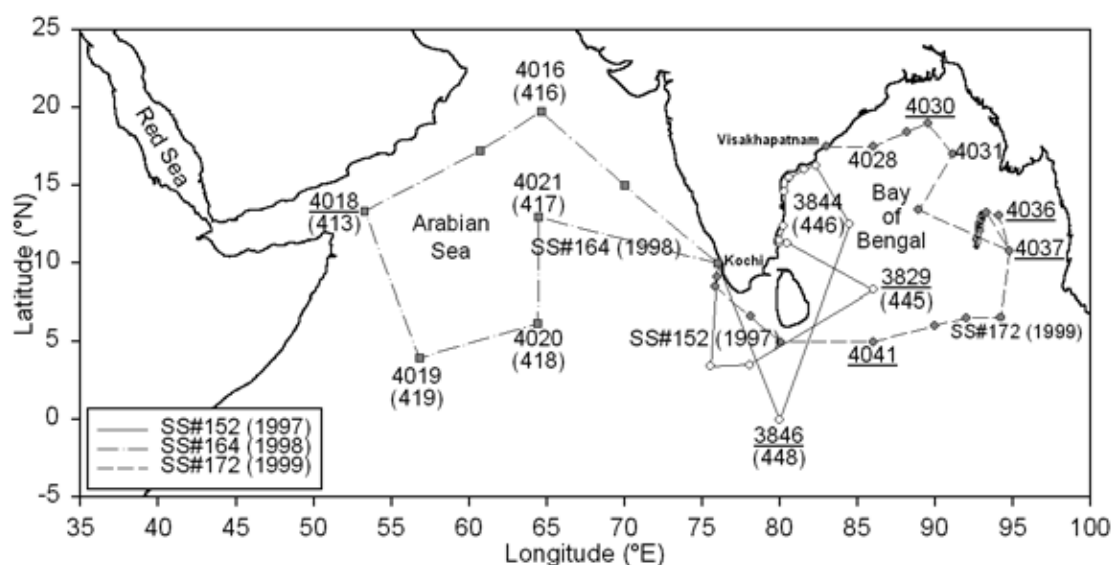


Figure 2–3 Cruise tracks of FORV *Sagar Sampada* to the northern Indian Ocean during 1997, 1998 and 1999.

During the 1997 cruise, three stations occupied during the GEOSECS expedition (1977–1978) were revisited. While during the 1998 cruise, five GEOSECS stations were reoccupied. The reoccupied GEOSECS stations are marked in parentheses in Fig. 2–3.

Depth profiles of seawater were collected in these stations for the measurements of ^{14}C , dissolved inorganic carbon (ΣCO_2), dissolved oxygen and nutrients. About 20 samples were collected for each profile — sampled approximately every 100m in the top 500m and every 200m for the rest of the profile. CO_2 in the atmospheric air was collected along the cruise tracks, for the measurement of $\Delta^{14}\text{C}$ in the air over the northern Indian Ocean. In this work, ^{14}C results of seawater samples are reported for the stations, which are underlined in Fig. 2–3.

2.2.1 Sampling of atmospheric CO₂:

The apparatus used for collection of atmospheric CO₂ is shown in Fig. 2–4. The sampling unit consists of a greaseless air compressor, which takes in atmospheric air. The air is allowed to pass through three plastic bottles kept in series fitted with glass dispersion tubes. The first of the two bottles were filled with 2N NaOH solution (freed from inorganic carbon, prepared by dissolving 20g of pure NaOH pellets in pre-boiled and cooled distilled water). The last bottle was filled with distilled water to

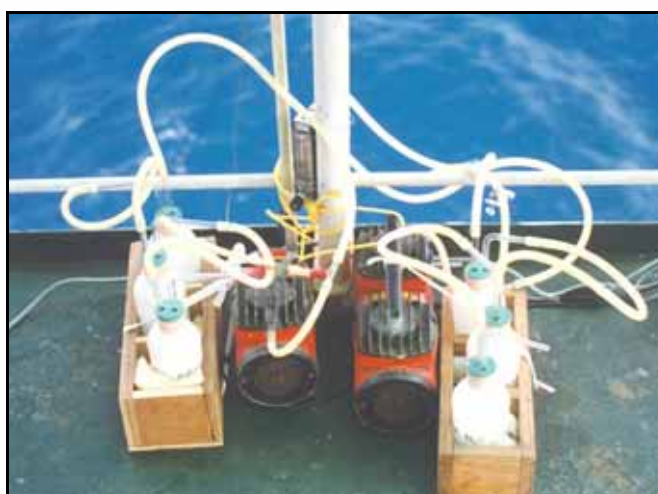
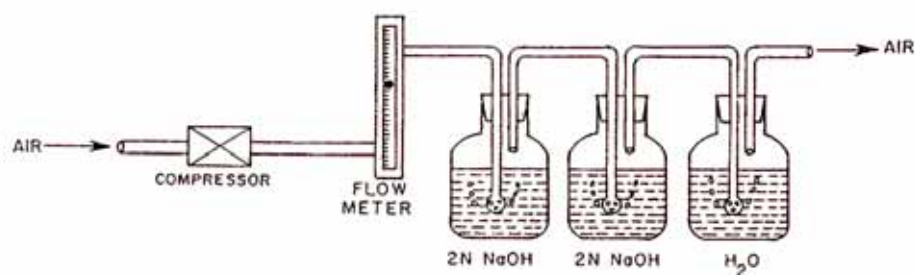


Figure 2–4 Apparatus used for onboard sampling of CO₂ from maritime atmosphere for ¹⁴C analysis. Top: schematic of the apparatus; Bottom: the actual assembly onboard.

trap any escaping alkali aerosols. Atmospheric air was allowed to bubble through the NaOH solution to trap the CO₂ present in it. The air intake rate was maintained at about 5lit.min⁻¹ by a flow meter. Samplings were done for about 2 to 3 days to collect enough CO₂ for ¹⁴C analysis. Two of these samplers were run in parallel, for collecting samples in duplicate along a cruise track (Fig. 2–3).

Precautions were taken to avoid any contamination from fossil fuel CO₂, both from ships emission and continental air. The sampling assemblies were installed in the front deck of the ship to collect air, which were uncontaminated with ship's emission. The samplers were allowed to run only while the ship was sailing, and when it was at least 200km away from the shore.

2.2.2 Sampling of seawater:

Seawater samples were collected using 30lit PVC *Go-Flo* bottles (General Oceanics, Miami, Florida, USA) attached with a 12-position rosette. The rosette was fitted with eight bottles as shown in Fig. 2–5. Continuous profiles of temperature, salinity, dissolved oxygen and beam attenuation (particles) were obtained using a *SeaBird* CTD instrument package. The system consists of a *SBE 9* underwater unit mounted with the sampling rosette and a *SBE 11* deck unit for receiving the digital data (Fig. 2–5).



Figure 2-5 Sampling of seawater onboard FORV Sagar Sampada. Left: Rosette attached with eight 30lit Go-Flo bottles and SBE 9 underwater CTD unit being lowered for temperature - salinity profiling and seawater sampling. Right: The SBE 11 deck unit onboard, for data acquisition and monitoring the sampling operation. Real time profiles of temperature (red), salinity (blue), oxygen (green) and beam attenuation (brown) can be seen on the monitor.

The temperature sensor of the CTD was calibrated before the cruises. The software package SEASOFT (version 4.232) was used for processing the raw CTD data and deriving potential temperature (θ) and potential density (σ_θ). The CTD temperature and salinity values are expressed following the conventions of ITS-90 (degree Celsius) and PSS-78 (PSU) respectively. The dissolved oxygen and salinity values from CTD were calibrated by comparing the onboard measurements of O_2 by Winkler's titration and salinity by Autosol salinometer in collected seawater samples (*sec. 2.3*). Water samples were collected from selected depths, from the surface to a few hundred meters above the sea floor, on the basis of the CTD profiles. Usually two samples were collected from each cast, by tripping four bottles at the desired depth. Therefore about 120lit of seawater was collected for each depth, aliquots of this was used for measurements of all parameters.

2.3 Shipboard processing and measurements

Immediately after the collection, seawater was sampled from the *Go-Flo* bottles for various shipboard measurements. The sequence of sampling followed, with the approximate sample volume for each are:

- (1) Dissolved oxygen ~125ml;
- (2) Dissolved inorganic carbon ~125ml;
- (3) Nutrients (silicate, nitrate and phosphate) ~500ml; and
- (4) Salinity ~200ml.

The rest of the seawater (~100lit) was utilized for the extraction of DIC for ^{14}C measurements (*sec. 2.3.5*). The analytical protocols of these shipboard measurements are described in JGOFS report no. 19 (1996), and mentioned here in brief. The results of dissolved oxygen, dissolved inorganic carbon and nutrients are expressed in micromoles per kg ($\mu\text{mol.kg}^{-1}$).

Various onboard processing and measurements and the methods employed to analyze the collected seawater samples are summarized in Table 2–1.

Table 2–1:
Onboard processing and measurements of seawater samples

Measurement	Method
Dissolved oxygen	Winkler's titration
Dissolved inorganic carbon (DIC or ΣCO_2)	Coulometry
Nutrients (silicate, nitrate & phosphate)	Autoanalyzer & Spectrophotometry
Salinity	Autosal
Extraction of DIC for ^{14}C analysis	Acidification and trapping CO_2 in a closed system circulation

2.3.1 Measurement of dissolved oxygen

Dissolved oxygen was measured by a modified Winkler titration method (Carpenter, 1965). A *Metrohm 655 Dosimat* auto-titrator was used for the titration. The end point of titration was detected using starch solution as visual indicator. Based on repeat analyses, the average precision (1σ) of dissolved oxygen measurements by Winkler titration was $\pm 2\mu\text{mol.kg}^{-1}$.

2.3.2 Measurement of total dissolved inorganic carbon (ΣCO_2)

The total dissolved inorganic carbon (ΣCO_2) of seawater is defined as the total molar concentrations of all species of inorganic carbon present in dissolved phase, given by,

$$\Sigma\text{CO}_2 = [\text{CO}_2^*] + [\text{HCO}_3^-] + [\text{CO}_3^{2-}]$$

where the brackets represent total concentrations of these constituents in solution (in mol.kg^{-1}) and $[\text{CO}_2^*]$ represents the total concentration of all un-ionized dissolved carbon dioxide (as H_2CO_3 or CO_2). The measurements of ΣCO_2 in the seawater samples were carried out by coulometric method, following the procedures outlined by Johnson, *et al.* (1985) and in D.O.E. handbook (1994).

An aliquot of seawater sampled from each depth in the PVC *Go-Flo* bottles is collected in 125ml *Borosilicate* glass bottles. Immediately after collection the samples were poisoned with 25 μl of saturated mercuric chloride solution (5% HgCl_2), to stop biological production. The bottles were sealed with greased ground glass stoppers (with *Apeizon-N* grease), and kept refrigerated at $\sim 2^\circ\text{C}$ until their analysis.

ΣCO_2 was measured in the samples using a *UIC model 5012* CO_2 coulometer (UIC Inc., Joliet, Illinois, USA). A fixed volume of ($\sim 25\text{ml}$) of seawater sample was drawn in the reaction chamber of an extraction system and CO_2 was extracted from it by adding 3ml of 40% (v/v) H_3PO_4 . CO_2 free air was used as carrier gas to purge CO_2 from the acidified sample to the titration cell of the coulometer. The cell contains a DMSO based titration solution (mono ethanol amine), sensitive for pH changes to change its transmittance at 610nm. The coulometer was calibrated by measuring Na_2CO_3 solutions of known concentrations (prepared by dissolving anhydrous Na_2CO_3 in de-ionized water). Based on repeat analyses of seawater samples, typical precision of ΣCO_2 measurements was $\pm 3\mu\text{mol.kg}^{-1}$ (1σ). The accuracy of ΣCO_2

measurements was checked from analyses of certified reference seawater (Batch#42, December, 1997), supplied by Prof. Andrew G. Dickson of Scripps Institute of Oceanography, USA. The mean ΣCO_2 measured during this study for this standard seawater is $1983.2 \pm 2.3 \mu\text{mol.kg}^{-1}$ (1σ , $n=20$), in good agreement with its certified value of $1985.1 \pm 0.8 \mu\text{mol.kg}^{-1}$.

2.3.3 Measurement of nutrients

About 500ml of seawater was used for the analysis of nutrients — silicate, total nitrate (nitrate + nitrite) and phosphate. The samples were kept refrigerated until analysis. Silicate and nitrate were measured onboard using a *Technicon* auto-analyzer. Phosphate was measured by spectrophotometry using a *Beckman model 26* spectrophotometer, using the procedure of Strickland and Parsons (1972).

Based on repeat measurements of seawater samples, the precisions ($\pm 1\sigma$) of silicate, total nitrate and phosphate measurements were 1.34%, 1.36% and 1.63% respectively of the measured values. Accuracies of silicate and nitrate measurements were about $\pm 5\%$, as checked by analyzing *CSK* standard solutions (Wako Chemical Industries Ltd., Japan).

2.3.4 Measurement of salinity

Salinity of the seawater samples was determined using a *Guildline AutoSal model 8400A* salinometer. The instrument determines the conductivity ratio (K_{15}) of a sample — defined by the ratio of conductivity of a sample at 15°C and 1 standard atmosphere pressure, to that of a potassium chloride (KCl) solution containing 32.4356g of KCl in 1kg of solution. R_t is the conductivity ratio at $t^\circ\text{C}$. The instrument displays twice the R_t values, from which salinity was determined using an empirical relationship (UNESCO, 1978). The software SEACALC (included in the SEASOFT package) was used to calculate salinity from R_t values. The salinometer was calibrated using IAPSO standard seawater. The precision of salinity measurements by *Autosal* was typically $\pm 0.0005\text{PSU}$, based on repeat measurements of seawater samples. The CTD salinity values were calibrated using the values measured by *Autosal*.

2.3.5 On-board extraction of DIC from seawater for ^{14}C analysis

For ^{14}C analysis, about 100lit of seawater was collected. This amount of seawater has sufficient amount of DIC (~2.5g), for ^{14}C measurement by LSC. To minimize exchange of CO_2 with the atmosphere, extraction of DIC from seawater was done soon after sample collection, and carried out using a closed circulation system as shown in Fig. 2-6. About 50kg of seawater was directly transferred from the PVC *Go-Flo* bottles into each of the two 60lit plastic (LLDPE) carboys. The carboys were sealed airtight using rubber stoppers fitted with glass dispersion tube and separatory

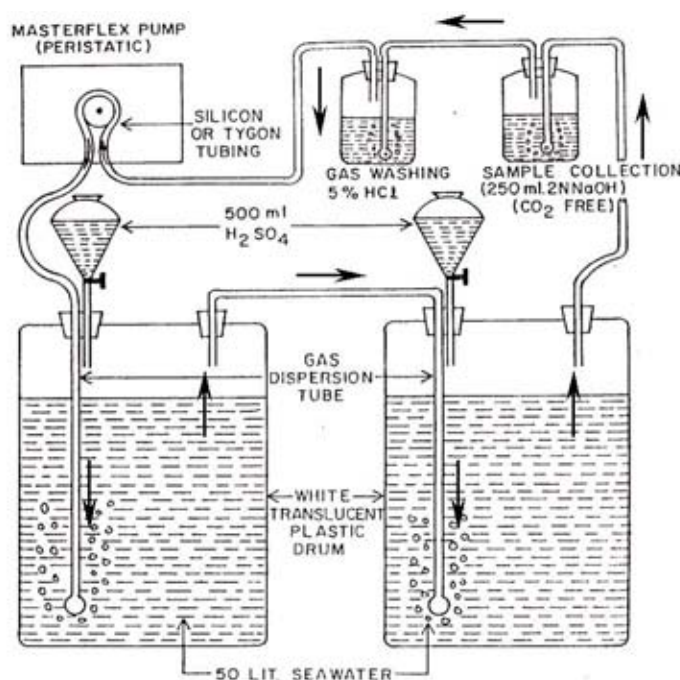


Figure 2-6 Closed system circulation for on-board extraction of DIC from seawater samples.

funnel containing 500ml of conc. H_2SO_4 . The outlets were connected with *Tygon* tubes to a sample collection bottle containing 250ml of 2N NaOH solution (free from CO_2), with another bottle kept in series containing 5% HCl (gas scrubber). A continuous closed system circulation is maintained within the system using a peristaltic pump. After ensuring absence of leaks in the system, the pump was turned on and the acid was slowly added to the seawater. The small volume of air within the system was used as the carrier gas. The quantity of CO_2 in the enclosed air is too small (10^{-5} mole) to cause any serious contamination of the liberated CO_2 . The circulation was allowed to continue for ~8 hours at the rate of $1.5\text{lit}\cdot\text{min}^{-1}$ to ensure complete extraction of the DIC. After the extraction, the NaOH bottle was stoppered and sealed airtight with Teflon tape until further shore based analysis of ^{14}C (*sec. 2.4*).

2.4 Radiocarbon measurements

The radiocarbon assay of all samples was done by conventional technique of β -activity measurement from the ^{14}C atoms — by liquid scintillation counting (LSC) of benzene prepared from the carbon of the samples (Bhushan, *et al.*, 1994). The entire procedure of ^{14}C measurement using LSC technique is summarized by the flow diagram in Fig. 2–7.

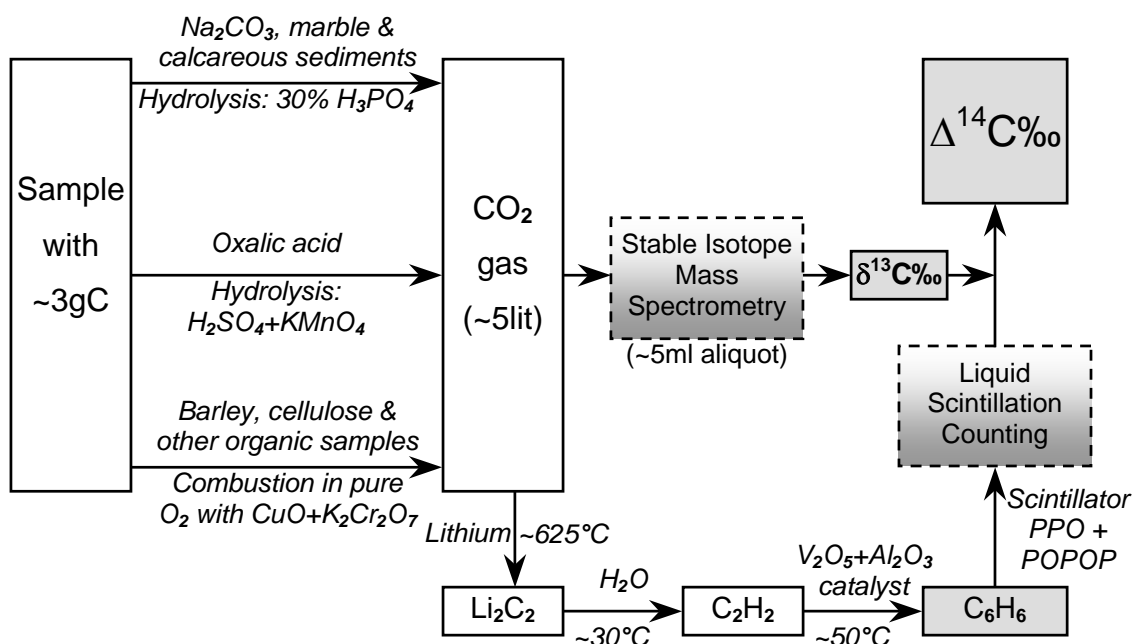


Figure 2–7 Flow diagram for measurement of ^{14}C by liquid scintillation counting of benzene samples.

2.4.1 Conversion of samples to benzene

Benzene was prepared from the samples, following the procedures outlined by Noakes, *et al.*, (1965) and Gupta and Polach (1985), which involves following steps:

- Liberation of CO_2 from samples (by acid hydrolysis or dry combustion)
- Reduction of CO_2 to lithium carbide (Li_2C_2)
- Hydrolysis of Li_2C_2 to acetylene (C_2H_2)
- Trimerization of C_2H_2 to benzene (C_6H_6)

For all samples reported in this work, benzene was prepared following the above steps, using a commercially available benzene synthesizer supplied by Technical & Applied Knowledge Inc. (TASK), Athens, Georgia, U.S.A.

(a) ***Liberation of CO₂ from different sample types:***

Depending on the sample, various methods were employed to convert its carbon into CO₂ prior to benzene synthesis, as outlined below.

Carbonate samples: From carbonate samples, CO₂ was liberated by acid hydrolysis. Solid carbonate samples, *e.g.*, shells, marine sediments, and marble were finely powdered (after necessary pretreatment). The sample amounts were chosen so that they contained at least 20g of carbonate as CaCO₃. The liquid samples include the alkaline solutions obtained after trapping CO₂ from air or seawater samples. The samples were taken in glass reaction vessel connected to the TASK benzene synthesizer. The lines were evacuated and 30% (v/v) H₃PO₄ was added with stirring, after attaining sufficient vacuum (~1torr).

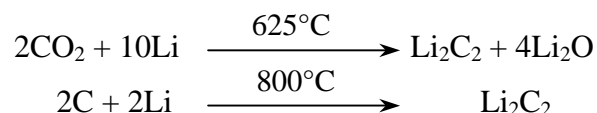
Oxalic acid: CO₂ from the NBS Oxalic Acid-II standard (NIST SRM 4990C, *sec. 2.4.3*) was obtained by oxidizing it with acidified KMnO₄. In the reaction vessel, 22.5g of oxalic acid were dissolved in 225ml of distilled water. The solution was acidified, by adding 15ml of conc. H₂SO₄. An oxidizing solution was prepared by dissolving 18g of KMnO₄ in 300ml of distilled water and acidified with 7.5ml of conc. H₂SO₄. CO₂ was liberated by slowly adding the acidified KMnO₄ solution to the oxalic acid solution under vacuum.

Organic samples: Organic samples, *e.g.*, samples of tree-rings, barley, cellulose and humic acid (*sec. 2.4.5*) were oxidized directly by combusting them in a stream of medical grade oxygen. The tree-ring samples were processed to extract the α -cellulose to completely get rid of resins and volatile matters, following the procedure of Hua, *et al.*, (2000), modified from Head (1979). To complete the combustion, the gases were passed through heated cupric oxide (CuO) wires and potassium dichromate (K₂Cr₂O₇) kept at 600°C.

Purification of CO₂: The CO₂ obtained from the samples was purified in the vacuum line of the TASK system, to remove moisture and traces of air. Moisture was removed from the liberated CO₂ by passing it through three water traps kept in series (cooled at -80°C by LN₂+acetone slush), and finally through a silica gel trap. An additional trap, containing glass beads coated with chromic acid was introduced after the combustion chamber while combusting organic samples, to remove volatile organic matter. The purification of CO₂ is essential for smooth reduction of CO₂ and avoiding formation of impurities like ammonia, etc. during the hydrolysis of Li₂C₂.

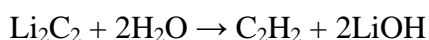
(b) Reduction of CO₂ to Li₂C₂:

About 15g of Li metal (supplied by Lithco Corp., USA) was used for each 5lit of CO₂. The purified CO₂ was slowly allowed to react with molten lithium (135°C), which leads to an exothermic reaction with the formation of lithium carbide (Li₂C₂):



(c) Hydrolysis of Li₂C₂ to C₂H₂:

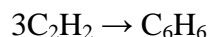
The Li₂C₂ was hydrolyzed at room temperature to form acetylene gas (C₂H₂),



Double distilled old ground water from PRL (pumped from a well ~300m deep) was used for this hydrolysis, to avoid contamination with tritium. The liberated acetylene was dried and purified, by passing it through a series of traps containing LN₂+acetone, P₂O₅ and *Ascarite* (vermiculite coated with NaOH, supplied by Thomas Scientific Inc., USA).

(d) Trimerization of C₂H₂ to C₆H₆:

The trimerization of acetylene to benzene was done using Al₂O₃/V₂O₅ catalyst (alumina granules coated with vanadium pentoxide, supplied by Commercia Chemie, Hannover, Germany). Prior to acetylene formation, the catalyst was activated by heating overnight at ~300°C under vacuum. About 35g of catalyst were used for 5lit of CO₂. After cooling the catalyst to ~50°C, the frozen acetylene was allowed to slowly sublime over it, when the following trimerization reaction took place,



The pressure was maintained at about 250 torr during this reaction. The catalyst trap was kept immersed in water to maintain it at room temperature (~25°C), during exothermic polymerization reaction. After complete absorption of acetylene by the catalyst, the reaction was allowed to complete by leaving it for 3 hours. Benzene was then distilled off from the catalyst by heating it at 120°C.

The average efficiency of conversion of CO₂ to benzene was within 80~90%. Thus from 5lit of CO₂, typically ~2g of benzene samples were obtained. The yield was found to be sensitively dependent upon the purity of CO₂ and the temperature of formation of Li₂C₂.

2.4.2 ^{14}C counting of benzene samples:

For counting the benzene samples by LSC they were transferred to a 7ml glass scintillation vial and weighed. Scintillator grade non-radioactive benzene was added if necessary to the sample benzene, to make the volume to 3ml (2.637g) — the standard volume used for counting. A scintillator cocktail was prepared by dissolving 0.42g of PPO (diphenyl oxazole) and 0.007g of POPOP (2, 2'-p-phenylene-bis-5 phenyl oxazole) in 10ml (8.87g) of scintillator grade benzene. Before counting, 0.5ml of this scintillator cocktail was added to the sample benzene and mixed well.

Most of the benzene samples in this study (coded PRLCH-) were counted in a low background *Packard Tri-Carb 2250CA* Liquid Scintillation Analyzer (Packard Instruments Co., Meriden, Connecticut, USA), following the procedures outlined by Bhushan, *et al.* (1994). This spectrometer operates in two modes, normal mode and low level count mode (LLCM). In LLCM, an electronic background discriminator reduces the background internally using Three-dimensional Spectral Analysis (Kessler, 1989). Addition of a *PICO-XL*TM plastic vial holder, supplied by the manufacturer, further reduced the background to ~40% with a marginal reduction in ^{14}C counting efficiency by ~5% (Noakes and Valenta, 1989). The counter was operated in LLCM mode along with the vial holder. The Packard LSC has a 3-channel provision to measure count rates. The optimum intervals chosen for 3 channels were,

Channel A	0.0–18.6 keV
Channel B	11.0–98.0 keV
Channel C	0.0–156.0 keV

Channel A is the energy window, which predominantly records tritium counts if any, from the sample. The β -particles emitted from tritium have lower energy (11–18.6 keV) and interfere at the low-energy side of the ^{14}C window (Channel B). Count-rates in channel A for scintillator-grade benzene and benzene prepared from marble was similar — which confirmed that there was no measurable tritium contamination during benzene synthesis.

Some of the samples (coded Q) were counted using a *Quantulus 1220* Liquid Scintillation Counter (LKB Wallac, Turku, Finland). Background counts are minimized in this counter by the use of active and passive shielding. A 7ml *Teflon* counting vial provided with gilded copper cap was used. This instrument incorporates 2 dual programmable MCAs, which enables simultaneous measurement of 4 spectra, each with 1024-channel resolution. Channels 39 to 467 were used for ^{14}C counting.

2.4.3 ^{14}C counting of marble (background) and NBS Oxalic Acid-II (standard)

To ascertain the background count-rates for ^{14}C , several blanks were run using benzene prepared from fresh marble, mined from Precambrian Raialo Formation, of Rajasthan, India. NBS Oxalic Acid-II (SRM 4990C) was used as the modern ^{14}C standard, which was run 2 to 3 times per year. The long-term variation of count-rates of marble background and the net count-rates of the NBS Oxalic acid standard, as obtained for the Packard counter for the period 1991 to 2000 are shown in Fig. 2–8.

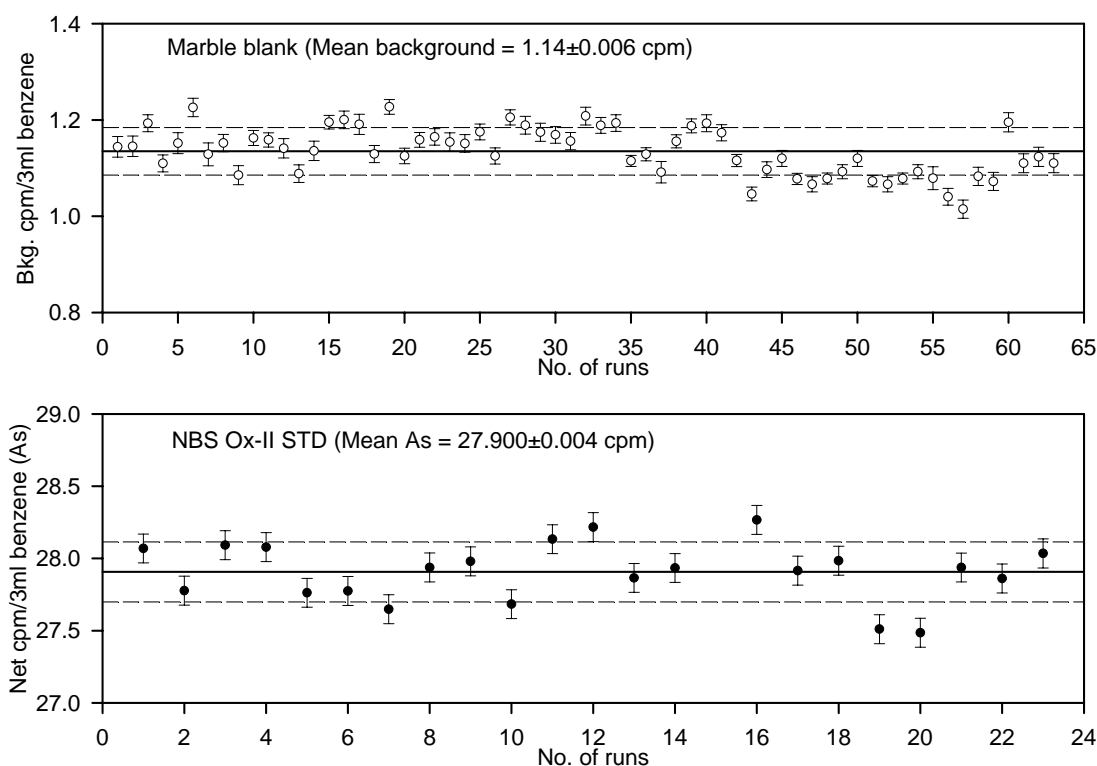


Figure 2-8 Count-rates of marble (background) and NBS Oxalic Acid-II (standard) with the Packard 2250CA LSC. The measurements were done from 1991 through 2000. Individual error bars are $\pm 1\sigma$. The horizontal solid and dashed lines are the long-term mean and $\pm 1\sigma$ limits respectively.

The mean background and net standard count-rates for 3ml (2.637g) benzene with the Packard counter are 1.14 ± 0.006 and 27.900 ± 0.004 cpm respectively (1σ standard error). With the Quantulus counter, the count-rates for the same volume of background and the standard benzenes are 0.605 ± 0.005 and 39.90 ± 0.06 cpm respectively. The typical count rates for the seawater, atmospheric and shell samples range from 5~20cpm with the Packard counter and 10~30cpm with the Quantulus counter — depending on their age and the amount of benzene sample counted.

2.4.4 Stable isotope ($\delta^{13}\text{C}$) measurement of CO_2 samples:

To correct the ^{14}C activities for isotopic fractionation, an aliquot of CO_2 was collected prior to benzene synthesis for measurement of stable isotopic ratio ($\delta^{13}\text{C}$). The $\delta^{13}\text{C}$ measurements were done using an upgraded *VG Micromass 902D* or a *PDZ Europa Geo 20–20* stable isotope mass-spectrometer. The results are expressed relative to V-PDB standard (Gonfiantini, 1984). Typical precisions of $\delta^{13}\text{C}$ measurements were $\pm 0.05\%$.

The $\delta^{13}\text{C}$ values of CO_2 from the seawater samples ranged from -1 to 5% , bulk of them centered within $2\pm 1\%$. A value of 0% are assumed for the seawater samples, in which $\delta^{13}\text{C}$ is not measured (shown in parentheses in Appendix–D). Considerable fractionation was observed in case of $\delta^{13}\text{C}$ values of CO_2 extracted from the air samples, which range from -7 to -15% . Most of these are significantly depleted than the normal atmospheric values of about -8% (Massarie, *et al.*, 2000). Such depletions in $\delta^{13}\text{C}$ values of CO_2 during absorption in alkaline solutions are also reported earlier (Nydal, 1966). However, for a given cruise the values were more or less constant (Table 4–1).

2.4.5 Reporting of ^{14}C activities

The ^{14}C activities are reported here for all samples after correcting for isotopic fractionation to $\delta^{13}\text{C}$ of -25% , following the procedures of Stuiver and Polach (1977). The detailed procedure is outlined in Appendix–A. For the seawater and atmospheric CO_2 samples, the ^{14}C activities are reported as $\Delta^{14}\text{C} \%$ (permil). For other samples (shells and FIRI samples), they have also been reported as BP (year Before Present) or PMC (Percent Modern Carbon), wherever they are appropriate.

2.4.6 Precision of ^{14}C measurements and results of Fourth International Laboratory Inter-comparison (FIRI) exercise:

The internal precision (1σ) of $\Delta^{14}\text{C}$ measurements based on modern samples (using 3ml benzene) is $\pm 5\%$ for the Packard counter and $\pm 3\%$ for the Quantulus counter. The average reproducibility of the $\Delta^{14}\text{C}$ measurements, based on duplicate measurements done in atmospheric samples (Table 4–1) is better than $\pm 8\%$.

To check the consistency of the ^{14}C measurements with other labs, the radiocarbon lab of PRL Chemistry Laboratory (PRLCH) participated in the recent Fourth International Radiocarbon Inter-comparison (FIRI) exercise of 2000. In this exercise radiocarbon labs of 37 different countries participated and reported 92 data sets (25 AMS, 18 gas proportional counting and 49 LSC). A total of 10 samples were distributed, of varied sample types and wide range of radiocarbon ages. These include marine turbidite (calcareous sediment), humic acid (extracted from soil), cellulose (extracted from wood), modern barley mash, wood, etc. From PRL Chemistry lab, ^{14}C measurements in 5 FIRI samples were done using the Packard counter. The results are tabulated in Table 2–1. The FIRI results shown are the preliminary consensus values (with $\pm 1\sigma$ standard errors) as agreed upon at the FIRI workshop, held in Edinburgh during 2001. The samples G and J are duplicates. The sample J was measured twice.

Table 2–2:
Comparison of ^{14}C measurements by PRLCH and the FIRI consensus values

FIRI Sample	PRLCH results	FIRI results (Preliminary consensus values*)	
		Mean of all labs (AMS, GPC, LSC)	Mean of LSC labs only
C (Turbidite)	17,730 \pm 130 BP	18,173 \pm 11 BP	18,140 \pm 25 BP
E (Humic acid)	11,720 \pm 100 BP	11,778 \pm 7 BP	11,707 \pm 17 BP
G (Barley)	110.497 \pm 0.528 PMC	110.69 \pm 0.09 PMC	110.82 \pm 0.08 PMC
J (Barley)	111.672 \pm 0.466 PMC [†]		
G & J (mean)	110.873 \pm 0.469 PMC		
I (Cellulose)	110.707 \pm 0.248 PMC	4,485 \pm 5 BP	4,499 \pm 11 BP

* As reported in the FIRI workshop. Subject to change after further analysis.

[†] Rejected for calculating mean. Combustion was incomplete for this sample.

PRLCH measurements of all five FIRI samples are in excellent agreement with their consensus values, except sample C, which yielded slightly younger age.

Chapter 3

Pre-nuclear Radiocarbon in the Northern Indian Ocean

3.1 Introduction: Natural radiocarbon in surface oceans

The concentration of ^{14}C in the dissolved inorganic carbon (DIC) of surface ocean waters is in quasi-equilibrium with air-sea exchange of atmospheric CO_2 , and diffusive and advective mixing with ^{14}C -depleted waters of the deep ocean. This causes the ^{14}C concentration for the surface oceans to be 5% lower on the average than that in the atmosphere, hence the ^{14}C -ages of surface ocean waters are older than contemporary terrestrial plants by about 400yr (Taylor and Berger, 1967). While the long-term temporal variations of surface ocean ^{14}C -ages are a function of the contemporary atmospheric ^{14}C levels and vertical mixing rates of the global ocean, their spatial variations also depend on the regional circulation patterns within the thermocline and regional air-sea CO_2 exchange rates. This causes considerable spatial variations of the steady-state (or natural) distribution of $\Delta^{14}\text{C}$ in the surface oceans and regional offsets of marine ^{14}C -reservoir ages from the global mean value, making it difficult to use a common calibration curve to determine ^{14}C -ages of marine samples.

The introduction of ^{14}C produced from atmospheric nuclear tests during the late 1950's and early 1960's had considerably enhanced the ^{14}C levels of the atmosphere. Mixing of bomb- ^{14}C contaminated atmospheric CO_2 resulted in steady increase of the level of ^{14}C in the surface oceans. This injection of bomb ^{14}C in surface waters though obliterated the natural (pre-nuclear) ^{14}C signatures; its inventory in the water column provided a means of determining the air-sea exchange of CO_2 . However, a knowledge of the pre-nuclear level of ^{14}C in the surface ocean waters is necessary, to determine:

- (i) Offsets of regional reservoir ages from the modeled global mean — to calibrate the ^{14}C -ages of marine calcareous fossils, which grew during the pre-nuclear period and used for dating of marine sediments.
- (ii) Temporal variations of bomb- ^{14}C in water column and to use its inventory to assess the air-sea CO_2 exchange rates and decadal circulation in the thermocline;

The above applications are explained in the following sub-sections in further detail.

3.1.1 Marine ^{14}C reservoir ages and ΔR correction values

For a given region (s) at any given time (t), the reservoir age $R(s, t)$ is defined as the difference between the measured conventional ^{14}C -age of the reservoir and that of the contemporary atmosphere as derived from tree rings. ^{14}C reservoir ages can be determined from ^{14}C analysis of pre-nuclear marine calcareous samples of known calendar age (Appendix–B). Considerable spatial variability is seen in the regional marine reservoir ^{14}C -ages from the global mean value, mainly due to variations in local ocean circulation patterns and regional exchange rates of CO_2 with the atmosphere. For a given region (s) at any given time, the difference between the regional marine ^{14}C -age and that of the modeled global surface ocean is expressed by the term $\Delta R(s)$, which account for regional deviations of reservoir ages from the global mean value (Stuiver and Braziunas, 1993a). The regional ΔR correction values can be determined from the difference of regional ^{14}C reservoir age and that of the modeled global ocean (Appendix–B). It is implicit in this definition that temporal variations of regional reservoir ages will parallel those of the global ocean, thus $\Delta R(s)$ is assumed to be time independent for a given region (Stuiver *et al.*, 1986, 1998b). Due to considerable variations in regional ^{14}C reservoir ages, knowledge of regional ΔR values is necessary for accurate calibration of ^{14}C -ages of marine samples.

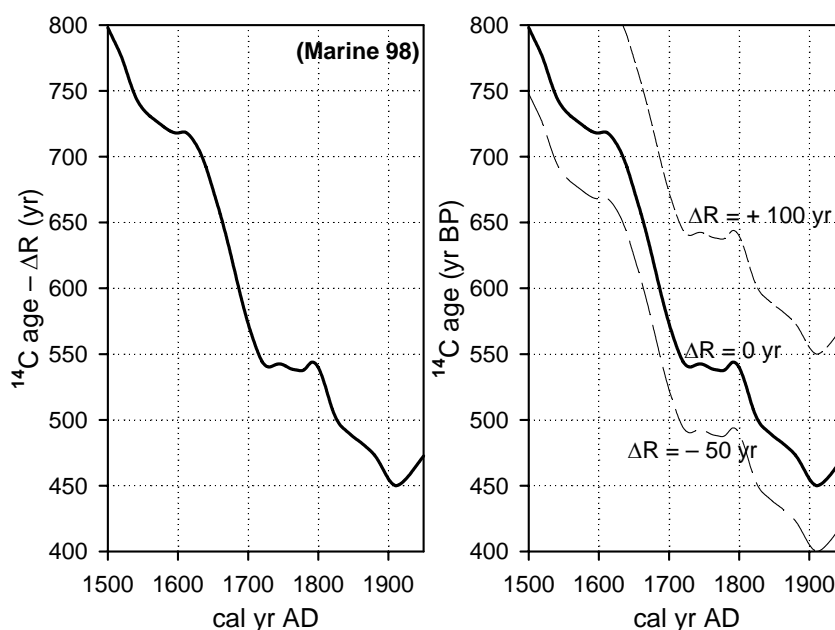


Figure 3–1 Calibration of radiocarbon ages for marine samples and the concept of ΔR . Left: The MARINE 98 calibration curve (Stuiver, *et al.*, 1998b). Right: Reconstructed marine ^{14}C ages at three hypothetical locations. Top curve: in an upwelling region for which reservoir ^{14}C -age is higher than global mean ($\Delta R = +100\text{yr}$). Middle curve: in an oceanic area that resembles the average world ocean ($\Delta R = 0\text{yr}$). Bottom curve: an oceanic area with lower vertical mixing with deeper waters where reservoir ^{14}C -age is younger than global mean ($\Delta R = -50\text{yr}$).

The reconstruction of regional marine ^{14}C -age calibration curve for three hypothetical oceanic regions is demonstrated in Fig. 3–1. The MARINE 98 calibration curve (Stuiver, *et al.*, 1998b) is shown in the left graph, calculated from the decadal tree-ring ^{14}C data, using the carbon cycle model after Oescheger, *et al.*, (1975). Regional ΔR correction values must be added to this curve to obtain the regional marine calibration curves, which are shown in the right graph.

3.1.2 Pre-nuclear $\Delta^{14}\text{C}$ in surface oceans

Oceanic measurements of ^{14}C started during the mid 1950's — about the same time when bomb- ^{14}C started penetrating the world oceans. Soon, it was realized that bomb- ^{14}C can be used as a powerful tracer to study air-sea exchange rates of CO_2 and mixing in the thermocline region on decadal time scales, from the temporal variations of ^{14}C concentrations (Rafter and O'Brien, 1973; Broecker, *et al.*, 1978; Broecker and Peng, 1982). The need for information about the pre-nuclear surface ocean ^{14}C levels was felt, while attempting to determine the increase of the surface ^{14}C levels from the pre-nuclear values. To determine the penetration depth and inventory of bomb- ^{14}C in oceans, it is essential to have knowledge about the surface pre-nuclear $\Delta^{14}\text{C}$ (Broecker, *et al.*, 1985). Several approaches have been made to determine these pre-nuclear surface ocean ^{14}C values from the analyses of suitable marine samples from the pre-nuclear era. Broecker, *et al.*, (1985) estimated the pre-nuclear $\Delta^{14}\text{C}$ values for different oceanic regions of the world within $\pm 10\text{‰}$. These values range from a minimum of -140‰ in polar oceans to -50‰ in mid latitudes. However, the surface circulation patterns of the global oceans are far from simple, to adopt a uniform scheme for meridional pre-nuclear $\Delta^{14}\text{C}$ variations for different oceans.

The results of state-of-the-art ocean general circulation models (GCMs), which predict the future rise of greenhouse gases in the atmosphere, must be verified through observations before they can be used for planning of policies to control anthropogenic CO_2 emissions. Such models can be used for simulating the steady state distributions of pre-nuclear $\Delta^{14}\text{C}$ in the world oceans (Maier-Reimer, 1993; Toggweiler, *et al.*, 1989a). Comparison of these model results with direct measurements of ^{14}C in surface dwelling marine calcareous organisms from the pre-nuclear era offer a way to check the validity of these models and also test their predictive capabilities. Guilderson, *et al.*, (2000a) compared modeled pre-nuclear

$\Delta^{14}\text{C}$ for the world ocean surface with a large compilation of pre-nuclear $\Delta^{14}\text{C}$ values obtained from biological archives and direct seawater ^{14}C measurements done in early 1950's. The model results are from the Lawrence Livermore National Laboratory's (LLNL) enhanced variant of the Geophysical Fluid Dynamics Laboratory's Modular Ocean Model (GFDL-MOM) after Pacanowski, *et al.*, (1991). The result of model simulated pre-nuclear $\Delta^{14}\text{C}$ distribution and its comparison with actual measurements of $\Delta^{14}\text{C}$ in pre-nuclear shells and seawater (unpublished) are shown in Fig. 3–2.

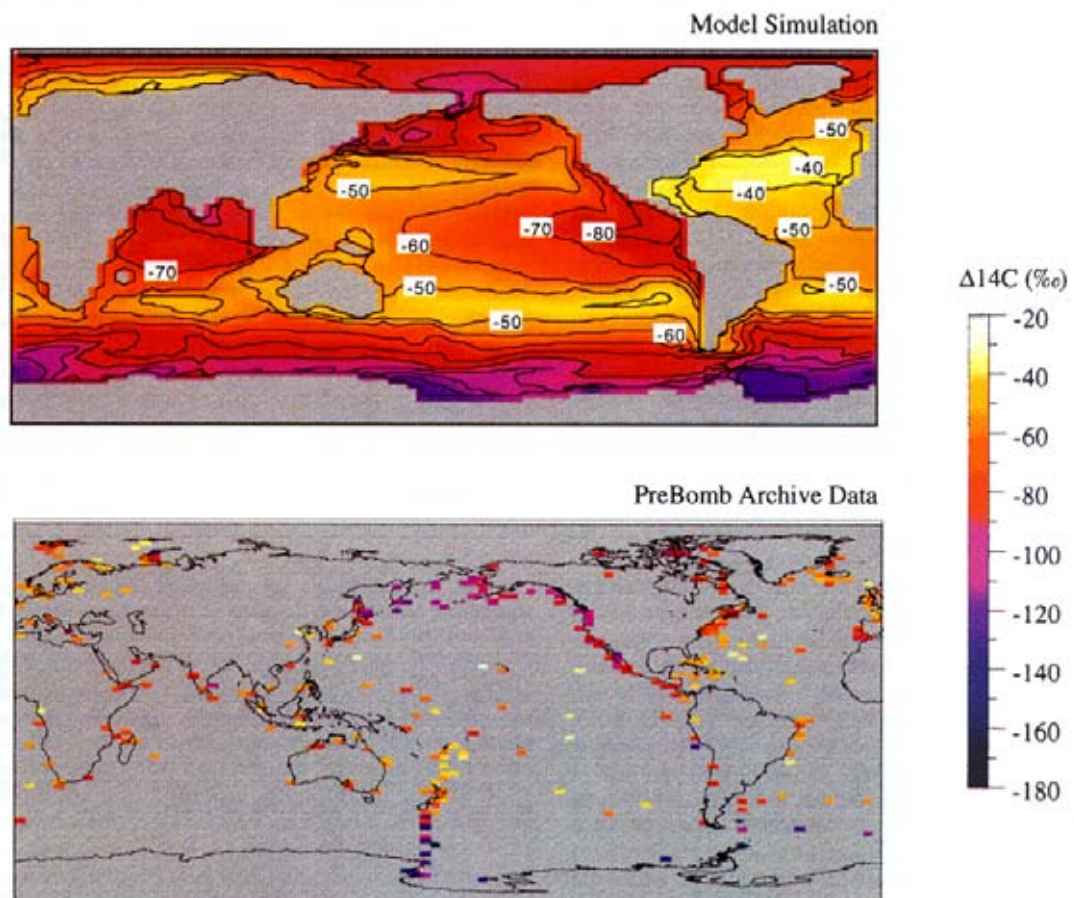


Figure 3–2 Spatial gradient of $\Delta^{14}\text{C}$ in surface oceans during 1950 simulated by the LLNL model (top) compared with unpublished pre-bomb data from biological archives (bottom) (Guilderson, *et al.*, 2000a).

The modeled pre-nuclear $\Delta^{14}\text{C}$ in the Bay of Bengal is -80 to -90‰ , while in the Arabian Sea this is around -70‰ . The lower $\Delta^{14}\text{C}$ in the Bay of Bengal requires more intense upwelling to occur in this oceanic region, compared to that in the Arabian Sea. As will be seen later from the measurements done in this work (as discussed in *sec.* 3.5.3), this requirement is not met, in reality the reverse occurs, *i.e.*, more upwelling takes place in the Arabian Sea. Guilderson, *et al.*, (2000a) attributed these low $\Delta^{14}\text{C}$ values in the Bay of Bengal, to an artifact of advective processes in the model.

3.2 Pre-nuclear surface seawater $\Delta^{14}\text{C}$ from marine samples

An ideal approach to determine the ^{14}C -age of seawater is to measure directly ^{14}C in its DIC (Fonselius and Östlund, 1959). Since direct measurements of ^{14}C in oceans began too late — only after the onset of nuclear weapons testing in the early 1950's (Rubin and Suess, 1955), nearly all seawater samples collected for ^{14}C determinations were contaminated with bomb ^{14}C . To determine pre-nuclear surface ocean $\Delta^{14}\text{C}$, ^{14}C reservoir ages [R(t)] and ΔR correction values, one must rely on the analysis ^{14}C in marine samples of known age, which were grown or collected before 1950. Some of the methods commonly used for this purpose are described below.

(i) *Marine shells:*

Measurement of ^{14}C in archived marine calcareous shells (*e.g.*, bivalves or gastropods), collected prior to the nuclear-testing era is the most common approach to determine pre-nuclear levels of surface water $\Delta^{14}\text{C}$ (Stuiver, *et al.*, 1986; Siani, *et al.*, 2000). Short-lived and epifaunal (non burrowing) mollusk species are preferred, with well-documented collection dates. One can also measure ^{14}C in long-lived giant calms (*e.g.*, *Tridacna* or *Arctica islandica*), which forms well-developed annual growth bands (Weidman and Jones, 1993).

(ii) *Corals:*

Hermatypic or reef building corals form annual growth bands of aragonite (CaCO_3), with $^{14}\text{C}/^{12}\text{C}$ composition identical to that of the ambient seawater DIC. Once deposited, these aragonite bands do not exchange their carbonate with any other source. In a coral collected alive these bands can be precisely dated back in time by counting, as in tree-rings. Past changes of $^{14}\text{C}/^{12}\text{C}$ ratio in the DIC of surface-oceans can be determined from ^{14}C measurements in coral growth bands. Some of the earliest ^{14}C measurements in coral skeletons were reported by Moore, *et al.*, (1973), Buddemeier, *et al.* (1974) and, Moore and Krishnaswami (1974). Continuous records of ^{14}C variations in surface oceans can be deciphered from long corals, extending back to several hundred years in the pre-nuclear era (Nozaki, *et al.*, 1978; Druffel and Linick, 1978; Druffel, 1981; Druffel and Suess, 1983; Druffel and Griffin, 1993). The major disadvantage of using corals is their restricted geographical distribution. They generally grow only in the tropical or limited sub-tropical regions.

(iii) Charcoal & marine shell pairs:

Direct determination of the atmosphere-ocean ^{14}C -age difference can be obtained from ^{14}C measurements in co-existing terrestrial charcoal and marine shell pairs collected from same stratigraphic horizon — capturing the oceanic and terrestrial events simultaneously (Southon, *et al.*, 1990, 1992; Talma, 1990; Ingram, 1998). As in corals, this method can determine past variations of regional reservoir ages in response to the ocean circulation changes for a much longer timescale. To measure fossil reservoir ages, Bard (1988) had suggested comparing the ^{14}C -age of a short and well-defined event both on land and in deep-sea sediments (*e.g.*, deposition of a volcanic ash layer).

(iv) Otoliths:

Otoliths are calcareous deposits that grow in the inner ears of teleost or bony fish, primarily used by them as gravity and auditory receptors. Otoliths, like corals, are also made of aragonite and form annual growth bands. AMS ^{14}C measurements in otoliths of known age marine fishes can be used for reconstructing the ^{14}C evolution in surface water (Higham and Hogg, 1995; Kalish, 1993; Kalish, *et al.*, 2000). Advantage of using fish otoliths over other methods is their large geographical range. Fish being nektonic (*i.e.*, free swimming), their otoliths can integrate the past ^{14}C signals over much wider oceanic region — unlike other archives (*e.g.*, shells or corals) which records oceanic ^{14}C variations only at their growth location.

Most of the methods described above have their own merits and demerits, and are often fraught with problems too. In spite of the availability of several established methods, pre-nuclear surface water ^{14}C data for many key oceanic regions are sparse, mainly owing to non-availability of suitable known-age marine samples. The northern Indian Ocean is a region, for which knowledge of pre-nuclear surface water ^{14}C is too meager. This oceanic region is an area of considerable interest from the perspective of paleoclimate studies, *e.g.*, South Asian monsoon variations in during the Late Quaternary (Duplessey, 1982; Sarkar, *et al.*, 1990; Sarkar, *et al.*, 2000). Spatial data of ^{14}C -reservoir ages for the northern Indian Ocean region are too meager to report reliable ^{14}C chronologies essential for paleoceanographic studies.

3.3 Pre-nuclear surface water $\Delta^{14}\text{C}$ in the northern Indian Ocean

The earliest seawater ^{14}C measurements in the tropical Indian Ocean region were done during the expeditions *Monsoon* (10°S, 99°E; November, 1960), *Lusiad* (8°N, 71°E; October, 1962) and *Dodo* (6°S, 55°E; September, 1964) of the Scripps Institute of Oceanography (Linick, 1975). The surface $\Delta^{14}\text{C}$ values measured during these periods ranged from -38 to -24‰ , for the latitude band of 24°S to 11°S during the *Monsoon* expedition. These results, however, could not provide pre-nuclear $\Delta^{14}\text{C}$ values for the region. These values are significantly higher than those obtained from pre-nuclear $\Delta^{14}\text{C}$ in biological archives — indicating the penetration of bomb ^{14}C even during early 1960s. More extensive studies of surface water $\Delta^{14}\text{C}$ measurements were made during 1977–1978 as a part of the international GEOSECS Indian Ocean expedition (Stuiver and Östlund, 1983). To calculate the bomb ^{14}C inventories from the GEOSECS ^{14}C measurements, Broecker, *et al.*, (1985) assumed pre-nuclear surface $\Delta^{14}\text{C}$ values of -60 to -65‰ for the northern Indian Ocean. In a later report, Broecker, *et al.*, (1995) assumed surface natural $\Delta^{14}\text{C}$ -59‰ in the equatorial Indian Ocean (GEOSECS 448), and a steadily decreasing $\Delta^{14}\text{C}$ trend was followed towards the north, assuming minimum $\Delta^{14}\text{C}$ value of -68‰ for the northern Arabian Sea (GEOSECS 416).

Moore and Krishnaswami (1974) first reported measurement of ^{14}C in the growth bands of corals from the Gulf of Kutch. $\Delta^{14}\text{C}$ of coral growth bands grown during 1950s have been reported for corals from the Red Sea and Gulf of Aden (Cember, 1989) and also from the Gulf of Kutch (Chakraborty, *et al.*, 1994).

The work done as part of this thesis provides the first detailed measurements of ^{14}C in archived marine shells, aiming to determine pre-nuclear $\Delta^{14}\text{C}$, ^{14}C -reservoir ages and ΔR correction values for the northern Indian Ocean (Dutta, *et al.*, 2000b, 2001a). These values are determined for the northern Arabian Sea, the northern and the southern Bay of Bengal, from ^{14}C analysis of seven marine mollusk samples collected between 1930 and 1954. The ^{14}C reservoir ages and ΔR correction values have also been calculated from the reported $\Delta^{14}\text{C}$ values of the annual bands of corals from the Gulf of Kutch in the northern Arabian Sea (Chakraborty, 1993; Bhushan, *et al.*, 1994).

3.4 Results of ^{14}C measurements in shells and corals

The results of ^{14}C measurements in shells made in this study are given in Table 3–1. The ^{14}C -ages are reported following the convention of Stuiver and Polach (1977). The modeled global marine ^{14}C -ages are from the MARINE 98 data (Stuiver, *et al.*, 1998b), reported for decadal samples. The tree-ring ^{14}C -ages are from the INTCAL 98 data for the northern hemisphere (Stuiver, *et al.*, 1998a). The details of calculation of ^{14}C -reservoir ages and ΔR values are given in Appendix–B. Errors quoted on $\Delta^{14}\text{C}$, ^{14}C -ages, $R(t)$ and ΔR are 1σ .

Stuiver, *et al.* (1986), recommended the use of pooled mean for reporting regional mean reservoir ages. Where a number of measurements are available, the error weighted pooled mean of $\Delta^{14}\text{C}$, $R(t)$ and ΔR values have been calculated using the method explained in Appendix–B. The results of ^{14}C measurements are summarized in Fig. 3–3, where the pooled mean $\Delta^{14}\text{C}$, $R(t)$ and ΔR values are given for each region. Table 3–1 and Fig. 3–4 also shows $\Delta^{14}\text{C}$ measured in corals from the Gulf of Kutch (Chakraborty, 1993; Bhushan, *et al.*, 1994).

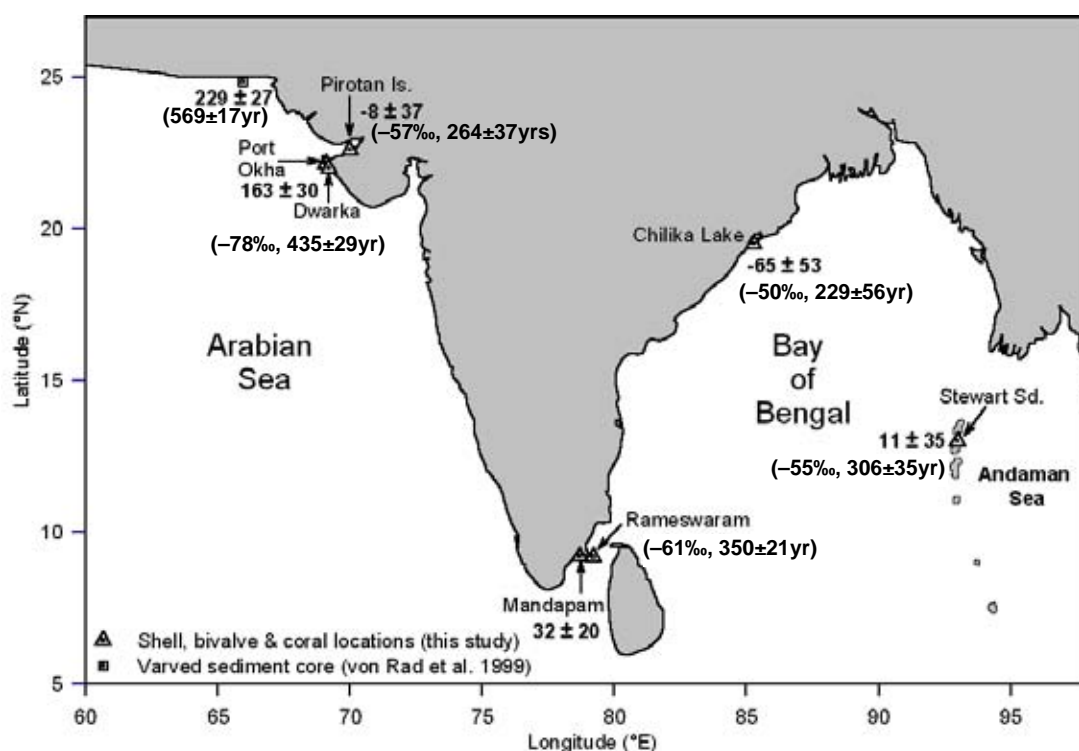


Figure 3–3 Results of ^{14}C measurements in shells and corals from the northern Indian Ocean. Pooled mean ΔR values (in years) are given for each region. Pooled mean $\Delta^{14}\text{C}$ (‰) and $R(t)$ (in years) are given in parentheses. Except for the Stewart Sound sample, the regional $\Delta^{14}\text{C}$ values are calculated only considering the samples that were collected in late 1940s or early 1950s (i.e., pre-nuclear).

Table 3–1:
Results of ^{14}C analyses in archived pre-nuclear marine shells and corals from the northern Indian Ocean

Sample Code (PRLCH)	Species [b- bivalve, g- gastropod and c- coral]	Sample location		Year of collection or growth (t)	$\delta^{13}\text{C}$ (‰)	$\Delta^{14}\text{C}$ (‰)	Sample ^{14}C -age (yr)	Model age (yr)	Tree-ring ^{14}C -age (yr)	Reservoir age R(t) (yr)	ΔR correction (yr)
		Place	Lat., Long.								
<i>Arabian Sea coasts</i>											
319	<i>Turbobrunneus</i> sp.(g)	Port Okha, Gujarat	22°28'N,69°05'E	1953	2.18	-83±5	693±44	473±13	193±15	500±46	220±46
543	<i>Turbobrunneus</i> sp.(g)	Dwarka, Gujarat	22°16'N,68°57'E	1952	2.36	-72±4	598±35	473±13	208±14	390±38	125±37
542	<i>Conus monule</i> (g)	Dwarka, Gujarat	-do-	1952	2.08	-173±3	1524±30	473±13	208±14	1316±33	1051±33 [†]
541	<i>Nerita oryzorcem</i> (g)	Dwarka, Gujarat	-do-	1952	3.39	-116±4	988±37	473±13	208±14	780±40	515±39 [†]
339	<i>Architectonica</i> sp. (g)	Dwarka, Gujarat	-do-	1952	1.66	-141±4	1219±38	473±13	208±14	1011±40	746±40 [†]
340	<i>Nassarius</i> sp. (g)	Dwarka, Gujarat	-do-	1952	*	-126±4	1080±37	473±13	208±14	872±39	607±39 [†]
87	<i>Favia speciosa</i> (c)	Pirotan Is., Gulf of Kutch	22°36'N,70°E	1952–1954	-0.65	-53±6 [‡]	434±51	473±13	193±15	241±53	-39±53
88	<i>Favia speciosa</i> (c)	Pirotan Is., Gulf of Kutch	-do-	1949–1951	-0.79	-60±6 [‡]	497±51	473±13	210±14	287±53	24±53
<i>Bay of Bengal coasts</i>											
320	<i>Marcia pinguis</i> (g)	Chilika Lake, Orissa	19°43'N,85°37'E	1954	0.76	-50±6	408±51	473±13	179±23	229±56	-65±53
539	<i>Asaphis deflavata</i> (b)	Stewart Sd., N. Andaman	13°01'N,92°58'E	1935	0.98	-55±4	469±34	458±4	150±15	319±37	11±35
545	<i>Cyprea</i> sp. (g)	Rameswaram, Tamilnadu	9°15'N,79°29'E	1930	2.02	-56±4	483±34	458±4	137±10	346±35	25±35
544	<i>Cyprea</i> sp. (g)	Rameswaram, Tamilnadu	-do-	1949	2.42	-60±4	498±34	465±7	213±14	385±37	33±35
526	<i>Cyprea</i> sp. (g)	Mandapam, Tamilnadu	9°12'N,78°42'E	1953	2.36	-62±4	511±34	473±13	193±15	318±37	38±36

$\Delta^{14}\text{C}$ and conventional ^{14}C ages are as defined by Stuiver and Polach (1977).

Details of R(t) and ΔR calculations are given in Appendix–B.

* $\delta^{13}\text{C}$ not measured, 2‰ assumed (mean value of other similar samples).

[†]Not used for regional R(t) and ΔR calculation. See text for details.

[‡]From Bhushan, et al. (1994).

3.5 Discussion on pre-nuclear $\Delta^{14}\text{C}$, $R(t)$ and ΔR correction values for the northern Indian Ocean

3.5.1 Arabian Sea

(a) Dwarka and Port Okha (Northeastern Arabian Sea coast):

Two samples of *Turbo-brunneus* (PRLCH 319 and 543) collected from Port Okha and Dwarka in the northeastern Arabian Sea coast during 1952 and 1953, yielded average $\Delta^{14}\text{C}$ of $-78\pm 3\text{‰}$ (^{14}C -age $635\pm 27\text{BP}$), which correspond to mean $R(t)$ $435\pm 29\text{yr}$ and ΔR $163\pm 30\text{yr}$.

From ^{14}C measurements in corals from the Red Sea and the Gulf of Aden in the western Arabian Sea, Cember, (1989) reported $\Delta^{14}\text{C}$ values of -76‰ to -73‰ ($\pm 8\text{‰}$), for the bands formed during 1951. These values are comparable to the pre-nuclear $\Delta^{14}\text{C}$ of the northeastern Arabian Sea, as obtained from the pre-nuclear shells of Port Okha and Dwarka. Based on AMS- ^{14}C measurements in planktonic foraminifers from varved sediments in a core off Pakistan ($24^{\circ}50'\text{N}$, $65^{\circ}55'\text{E}$), von Rad, *et al.*, (1999) estimated local marine ^{14}C -age of 640BP. This is based on ^{14}C -ages of $664\pm 25\text{BP}$ and $705\pm 23\text{BP}$ for varves deposited in 1926 and 1898 AD respectively, in a core about 300km northwest of Port Okha (Fig. 3–2). These ages correspond to local mean $R(t)$ $569\pm 17\text{yr}$ and ΔR $229\pm 27\text{yr}$ (Reimer and Reimer, 2001). These $R(t)$ and ΔR values from northern Arabian Sea off Pakistan are higher than that derived from shells of Port Okha and Dwarka. These higher ^{14}C -ages possibly indicate stronger upwelling off Pakistan than in the northeastern Arabian Sea near Port Okha and Dwarka. However, it is possible for foraminifers to record systematically older ^{14}C -ages than coastal shells. The $\Delta^{14}\text{C}$ of foraminifers, which grow within top 100m of the ocean, is expected to be a few tens of permil more than that of contemporary coastal shells or corals, which derives carbon mainly from the DIC of surface ocean. Thus $\sim 130\text{yr}$ difference seen above in the ^{14}C -reservoir ages of shells and foraminifers from nearly same locality could be due to difference in their habitat.

Four samples of gastropods collected from Dwarka yielded much older ^{14}C -ages, between 989 and 1524BP (Table 3–1), and have been excluded for regional $R(t)$ and ΔR calculations. The anomalous ages of the four gastropod samples from Dwarka could be due to incorporation of ^{14}C -free or ‘dead’ carbonates from the surrounding sediments in their shells. The beaches of Port Okha and Dwarka in the western India are composed of calcareous sediments derived from Late Quaternary miliolite

limestone and old coral reefs. The $^{230}\text{Th}/^{234}\text{U}$ ages of these miliolite limestones range from 30 to 235kyr (Somayajulu, 1993). The coral reefs from this region fall in two groups, one around 6kyr and the other between 118 to 176kyr (Somayajulu, *et al.*, 1985). There is a possibility that the shells living in this region are incorporating sediment derived ^{14}C -free carbonates. Effects of Pleistocene limestone substrate on the apparent ages of known age marine shells have been reported by Dye, (1994). The apparent ^{14}C -ages of known age marine shells, collected from limestone beaches were found to be ~620yr older than contemporary samples from a volcanic coast. According to Dye, (1994), incorporation of ^{14}C -free carbon in shells takes place either directly by scraping the limestone as they browse, or indirectly from the algae that they live on.

(b) Pirotan Island (Gulf of Kutch, northeastern Arabian Sea):

The coral *Favia speciosa* was collected from the Pirotan Island within the Gulf of Kutch (Chakraborty, 1993). The $\Delta^{14}\text{C}$ of the band formed in 1949–'51 in this coral is measurably higher (by ~18‰) than the contemporary open Arabian Sea shells. The mean R(t) and ΔR for the two coral bands formed between 1949 and 1954 are $264 \pm 35\text{yr}$ and $-8 \pm 37\text{yr}$ respectively. These ages are significantly younger than that for the Arabian Sea samples from Port Okha and Dwarka.

The average water depth of the Gulf of Kutch is less than 30m (Chakraborty, *et al.*, 1994). The lower ^{14}C -age in the gulf compared to the open Arabian Sea appears to reflect faster equilibration time for the shallow gulf, with respect to atmosphere-ocean CO_2 exchange. Absence of mixing with deeper ^{14}C -depleted waters can also result in younger ^{14}C -ages. Even in the post bomb era during the late 1970s, the Gulf of Kutch recorded higher level of ^{14}C than in the open Arabian Sea. The mixed layer $\Delta^{14}\text{C}$ at the GEOSECS station 416 in the northern Arabian Sea was $59 \pm 4\text{‰}$ during 1977 (Stuiver and Ostlund, 1983), while the Pirotan Island coral recorded mean $\Delta^{14}\text{C}$ $112 \pm 7\text{‰}$ during the year 1975 and 1978 (Chakraborty, 1993).

It can be noted that $\Delta^{14}\text{C}$ of the band formed during 1952–1954 ($-53 \pm 6\text{‰}$) is slightly higher than that formed during 1949–'51 ($-60 \pm 6\text{‰}$), although these values are same within the measurement uncertainty. Since in both cases three bands have been combined for analysis, it is possible that the band of 1954 may have incorporated some amount of bomb- ^{14}C in it.

3.5.2 Bay of Bengal

(a) *Rameswaram and Mandapam (Palk Bay, Southern Bay of Bengal):*

Three samples analyzed were collected from Rameswaram and Mandapam (southern India) in the shallow Palk Bay region. The $\Delta^{14}\text{C}$ of these samples range from $-56\pm 4\text{‰}$ to $-62\pm 4\text{‰}$ (^{14}C -ages 483 ± 34 to $511\pm 34\text{BP}$), corresponding to mean $R(t)$ $350\pm 21\text{yr}$ and ΔR $32\pm 20\text{yr}$.

The Palk Bay is a shallow strait between India and Sri Lanka, where average water depth is less than 100m. During the NE monsoon season (November to January) this region is flushed with waters from the northern Bay of Bengal, while during the SW monsoon (June to September), Arabian Sea waters enter this strait. Thus, the ^{14}C -reservoir ages of the Palk Bay waters are intermediate between the Arabian Sea and the Bay of Bengal values.

(b) *Stewart Sound (Andaman Sea):*

The $\Delta^{14}\text{C}$ of the sample collected in 1935 from Stewart Sound, North Andaman Island is $-55\pm 4\text{‰}$ (^{14}C -age $469\pm 34\text{BP}$), corresponding to $R(t)$ $319\pm 37\text{yr}$ and ΔR $11\pm 35\text{yr}$. The ^{14}C -age of this sample is statistically indistinguishable from that of the Palk Bay sample collected in 1930 (PRLCH-545).

(c) *Chilika Lake (Northern Bay of Bengal):*

The $\Delta^{14}\text{C}$ of the shell sample collected from Chilika Lake is $-50\pm 6\text{‰}$ (^{14}C -age $408\pm 51\text{BP}$), youngest compared to all the northern Indian Ocean samples analyzed in this study. The ^{14}C -reservoir age for the Chilika Lake is $229\pm 56\text{yr}$, slightly younger than that obtained for the southern Bay of Bengal region at Palk Bay.

Chilika Lake is a shallow brackish water lagoonal lake in the northern Bay of Bengal, with maximum depth of only 4m. Younger ^{14}C -reservoir ages in enclosed shallow lagoons are expected due to absence of upwelling of ^{14}C -depleted deeper waters and faster equilibration rate with the atmosphere. This is similar to the case for the Pirotan Island coral in the shallow Gulf of Kutch. Although the Chilika Lake sample was collected in 1954, the effect of contamination with bomb- ^{14}C is expected to be less in this case. Bivalves form annual growth layers, the last one forming the outermost periphery of the shell. Therefore, small contamination of bomb- ^{14}C from the last layer would have been significantly diluted with the 10~15 previously formed layers (assuming they lived for ~15yr).

A closer look at the $\Delta^{14}\text{C}$ values of three samples from the Palk Bay and the sample from the Andaman Sea show a decreasing trend, which, if confirmed with more analysis, possibly points to depletion of surface ocean DIC in ^{14}C due to invasion of ^{14}C -free CO_2 from fossil fuel burning in this region. Invasion of fossil fuel CO_2 to the oceans caused significant depletion of surface ocean $\Delta^{14}\text{C}$ values between 1900 and early 1950s (Druffel, 1981; Druffel and Suess, 1983; Toggweiler, *et al.*, 1989a). As shown in Fig. 3–4, the trend of $\Delta^{14}\text{C}$ recorded in four shell samples from the southern Bay of Bengal, possibly hints to the presence of a marine Suess effect in this region. The $\Delta^{14}\text{C}$ in the surface waters of the southern Bay of Bengal appear to have been reduced by $\sim 6\%$, over a period of two decades between 1930 and 1953. The $\Delta^{14}\text{C}$ for these shells samples show statistically significant decreasing trend of $3 \pm 2\%$ [$r^2 = 0.9$ (Bevington, 1969)]. Further measurements are needed from this region to confirm this trend and reduce the uncertainty. Druffel (1981) reported post-industrial and pre-nuclear $\Delta^{14}\text{C}$ recorded in corals from the Urvina Bay, Galapagos Island, in the eastern equatorial Pacific. The $\Delta^{14}\text{C}$ trend for Urvina Bay is compared with that of the Bay of Bengal shells in Fig. 3–4. Both records show similar magnitude of Suess effect of $\sim 6\%$ between 1930 and 1953. It must be mentioned here that the dates assigned to the shell samples are their collection dates, but not their mean growth periods. The life spans of individual shell samples are also not same. Thus the actual decrease of $\Delta^{14}\text{C}$ in Palk Bay and Andaman Sea shells may differ by a few permil from this value. However, the actual reduction of $\Delta^{14}\text{C}$ in DIC is recorded by the Urvina Bay data, where ^{14}C was measured in the annual coral growth bands.

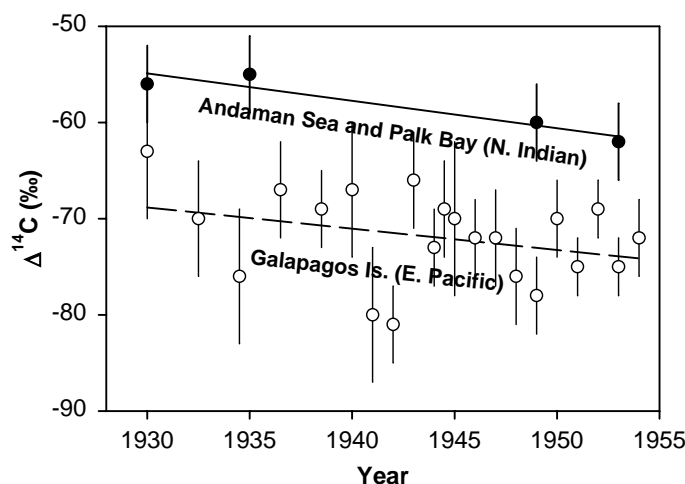


Figure 3–4 Pre-nuclear $\Delta^{14}\text{C}$ in shells from the Bay of Bengal (filled circles), compared with $\Delta^{14}\text{C}$ in annual coral bands from the eastern equatorial Pacific (open circles) (Druffel, 1981). The solid and dashed straight lines are the linear fits to the respective $\Delta^{14}\text{C}$ data.

Since all the samples from the Arabian Sea (which do not have anomalous ^{14}C -ages) were collected during a short span of time between 1949 and 1954, it is not possible to assess the marine ^{14}C Suess effect on them. The presence of this Suess effect in the Indian Ocean can be confirmed from ^{14}C analysis in long coral cores from this region, which dated back to 1900 AD.

3.5.3 Spatial variation of $\Delta^{14}\text{C}$, $R(t)$ and ΔR values in the northern Indian Ocean and comparison with the global pattern

The $R(t)$ values for the open Arabian Sea (ranging from $569\pm 17\text{yr}$ to $435\pm 29\text{yr}$) are distinctly higher than those for the Bay of Bengal (ranging from $229\pm 56\text{yr}$ to $350\pm 21\text{yr}$). Uniform increasing trend in ^{14}C reservoir ages (or lower $\Delta^{14}\text{C}$) is evident, from the northern Bay of Bengal—southern Bay of Bengal—northeastern and northern Arabian Sea (Fig. 3–3), which can be explained in terms of regional variation of circulation patterns within the thermocline.

In the northeastern Arabian Sea, vertical mixing is favored by (i) seasonal upwelling during southwest monsoon and (ii) convective processes associated with winter cooling (Madhupratap, *et al.*, 1996). The apparent ^{14}C -ages in the Arabian Sea are older than that of the modeled world ocean ($\Delta R \approx 0$), due to upwelling induced mixing with deeper ^{14}C -depleted water. The Bay of Bengal, which receives large amount of fresh water from the north by seven major rivers (Milliman and Mead, 1983), has steep gradients of the isopycnal surfaces within the top 200m. This condition is illustrated in Fig. 3–5 from the isopycnal contours obtained for the WOCE transect I08 along $\sim 9^\circ\text{N}$.

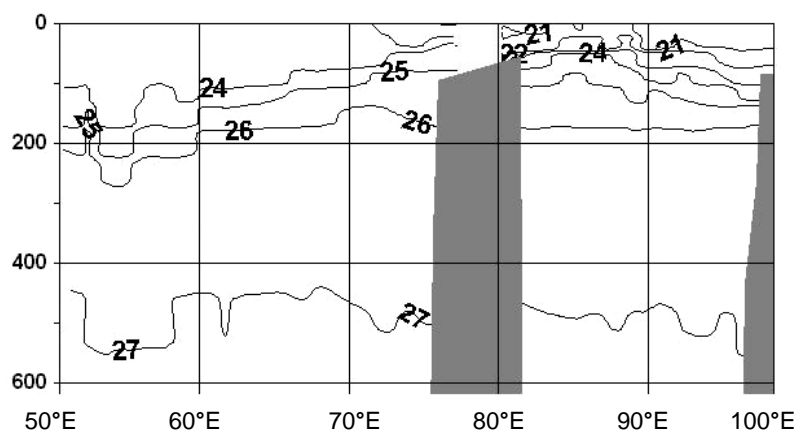


Figure 3–5 Isopycnal contours for the WOCE section I08, along 8.5°N in the Arabian Sea and along 9.97°N in the Bay of Bengal (ODV 5.5, Schlitzer, 2001). Vertical axis is the water depth (in meters) and the contours are of constant potential density (or σ_θ). Steeper gradient of σ_θ is evident in the top 200m of the Bay of Bengal, than in the Arabian Sea.

Steep isopycnal gradient in the Bay of Bengal greatly reduces the vertical mixing rate, retarding vertical advection of deeper ^{14}C depleted water. As a result, relatively younger reservoir ages are likely to be observed in the Bay of Bengal compared to the Arabian Sea. However, input of riverine DIC depleted in ^{14}C will tend to counteract this effect (Little, 1993). Higher reservoir ages in the Arabian Sea compared to the Bay of Bengal shows that greater vertical mixing is the dominant process, which determines the observed pattern of ^{14}C reservoir ages in the northern Indian Ocean.

The modeled pre-nuclear surface ocean $\Delta^{14}\text{C}$ distribution by Toggweiler, *et al.*, (1989a) and Guilderson, *et al.*, (2000a), predicts more positive $\Delta^{14}\text{C}$ values in the Arabian Sea than in the Bay of Bengal. This is in contrary to the present observed values from the ^{14}C analysis of pre-nuclear shells.

In Fig. 3–6, the coastal region ΔR values for the northern Indian Ocean region are compared with a compilation for other oceanic regions (Stuiver and Braziunas, 1993a). In the midst of considerable scatter of the regional ΔR values, it can be observed from Fig. 3–6, that upwelling regions (*e.g.*, the Gulf of California), and the polar-regions are characterized by higher ΔR values. Shallow oceans (*e.g.*, the Mediterranean Sea) have lowest ΔR values. The ΔR for the northern Arabian Sea is typical of an upwelling regime, while the average ΔR for the Bay of Bengal is close to that of mean global modeled ocean.

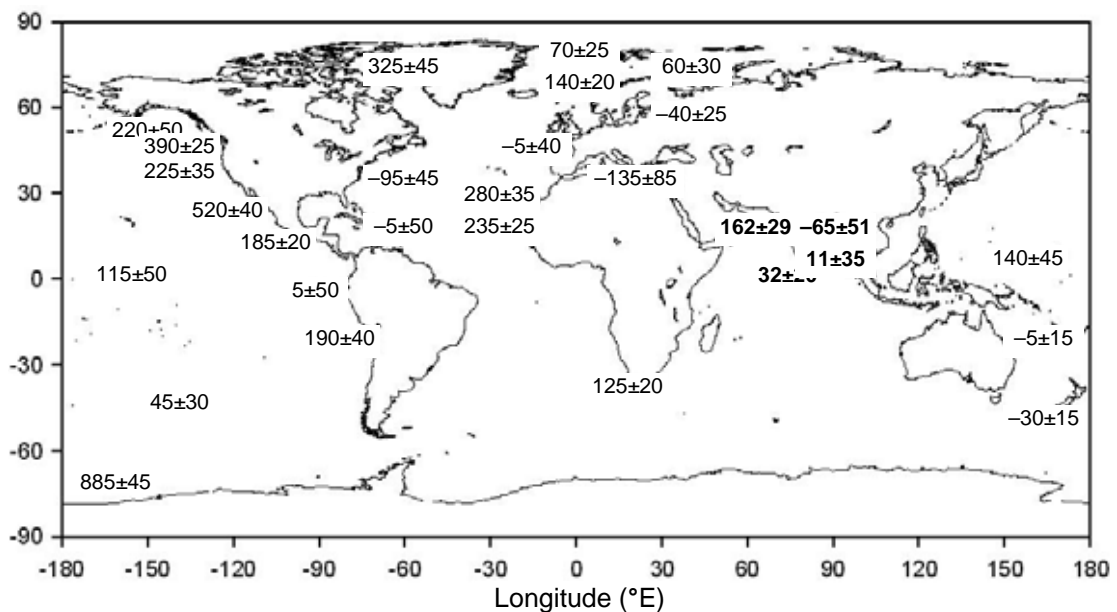


Figure 3–6 Compilation of coastal region ΔR correction values Stuiver and Braziunas (1993a). Results from the northern Indian Ocean obtained from this work are given in bold (Dutta, *et al.*, 2001a).

These new results of pre-nuclear ^{14}C measurements from the northern Indian Ocean obtained from this work have been included in the Global Marine Reservoir Correction Database, maintained jointly by the Queen's University of Belfast and the University of Washington, Seattle (Reimer and Reimer, 2001). The $R(t)$ and ΔR correction values have been calculated in this database by taking the atmospheric ^{14}C -ages from a 5-point moving average of the INTCAL 98 data for the northern hemisphere (Stuiver, *et al.*, 1998a). This is unlike that calculated in this work, which used decadal average of atmospheric ^{14}C -ages (Appendix-B). The comparisons of $R(t)$ and ΔR values calculated using the two methods are shown in Table 3-2. As it is evident, the difference arising for using these two methods is insignificant.

Table 3-2:
Comparison of reservoir ages calculated in this study and in
Global Marine Reservoir Correction Database

Region and Sample code	Dutta, <i>et al.</i> , (2001a)		Global Marine Reservoir Correction Database (Reimer and Reimer, 2001)	
	$R(t) \pm 1\sigma$ (yr)	$\Delta R \pm 1\sigma$ (yr)	$R(t) \pm 1\sigma$ (yr)	$\Delta R \pm 1\sigma$ (yr)
<i>Northern Arabian Sea</i>				
PRLCH-319	500±46	220±46	499±47	221±46
PRLCH-543	390±38	125±37	404±39	126±37
<i>Gulf of Kutch</i>				
PRLCH-87	241±53	-39±53	240±54	-38±53
PRLCH-88	287±53	24±53	303±54	25±53
<i>Chilika Lake</i>				
PRLCH-320	229±56	-65±53	214±54	-64±53
<i>Southern Bay of Bengal</i>				
PRLCH-539	319±37	11±35	306±35	7±34
PRLCH-545	346±35	25±35	334±35	25±34
PRLCH-544	385±37	33±35	305±37	26±36
PRLCH-546	318±37	38±36	317±38	39±36

3.6 Conclusions

The present work provides the first detailed results of pre-nuclear $\Delta^{14}\text{C}$, ^{14}C reservoir ages and ΔR correction values for the two northern Indian Ocean basins — the Arabian Sea and the Bay of Bengal, obtained from apparent ^{14}C -ages of archived marine shells of the pre-nuclear era, and coral bands which formed around 1950.

The pre-nuclear $\Delta^{14}\text{C}$ of the northern Indian Ocean range from -50‰ in the northern bay of Bengal to -78‰ in the northeastern Arabian Sea. Intermediate $\Delta^{14}\text{C}$ values of about -60‰ were obtained for the southern Bay of Bengal. The surface circulation patterns of these basins are reflected on the distribution of regional ^{14}C reservoir ages. The northern Arabian Sea has a mean ΔR of $163 \pm 30 \text{yr}$. For the enclosed Gulf of Kutch the ΔR is $-8 \pm 37 \text{yr}$, as obtained from ^{14}C measurements reported in annual coral bands. The surface seawater of the Bay of Bengal has younger apparent ^{14}C -age than that of the Arabian Sea, with ΔR values of $11 \pm 35 \text{yr}$ for the Andaman Sea and $32 \pm 20 \text{yr}$ for the southern Bay of Bengal. The lowest ΔR of $-65 \pm 53 \text{yr}$ is obtained for the Chilika Lake, a shallow brackish water lagoon in the northern Bay of Bengal. The decreasing trend of $\Delta^{14}\text{C}$ between 1930 and 1953, observed from ^{14}C measurements in four bivalves from the Palk Bay and the Andaman Sea possibly point to marine ^{14}C Suess effect in the Bay of Bengal. The magnitude of this Suess effect is $3 \pm 2\text{‰}$ per decade, between 1930 and 1953.

The pre-nuclear $\Delta^{14}\text{C}$, $R(t)$ and ΔR values from the northern Indian Ocean regions obtained from this study, are summarized in Table 3–3. These new set of ΔR values would be useful in calibrating the ^{14}C ages of marine microfossils for dating marine sediments and also for dating coastal calcareous archeological samples from the northern Indian Ocean region.

Table 3–3:

Summary of pre-nuclear $\Delta^{14}\text{C}$, $R(t)$ and ΔR values for the northern Indian Ocean

Region	Pre-nuclear $\Delta^{14}\text{C} \pm 1\sigma$ (‰)	$R(t) \pm 1\sigma$ (yr)	$\Delta R \pm 1\sigma$ (yr)
Northern Arabian Sea	-78 ± 3	435 ± 29	163 ± 30
Gulf of Kutch	-57 ± 4	264 ± 35	-8 ± 37
Palk Bay	-61 ± 3	350 ± 21	32 ± 20
Andaman Sea	-55 ± 4	306 ± 35	11 ± 35
Chilika Lake Lagoon	-50 ± 6	229 ± 56	-65 ± 53

Chapter 4

Radiocarbon in Atmospheric CO₂ over the Northern Indian Ocean

4.1 Variations of bomb ^{14}C in the atmospheric CO_2 over the northern Indian Ocean

One of the aims of this study is to measure ^{14}C in atmospheric CO_2 over the northern Indian Ocean and to assess its regional and interannual variations.

The knowledge of post bomb atmospheric $\Delta^{14}\text{C}$ history over oceanic regions is necessary, to determine the input of bomb- ^{14}C to the oceans and the air-sea CO_2 exchange rates from the oceanic inventory of bomb- ^{14}C (Broecker, *et al.*, 1985; Stuiver, 1980). The atmospheric $\Delta^{14}\text{C}$ history for a given region can be determined either from direct measurement of ^{14}C in atmospheric CO_2 or indirectly from the $\Delta^{14}\text{C}$ measurements in tree-rings. The post-bomb tropospheric $\Delta^{14}\text{C}$ histories are fairly well known for the three latitudinal bands (northern hemisphere, tropics and the southern hemisphere), based on large number of atmospheric measurements in both hemispheres (Nydal, 1963; Munnich and Roether, 1967; Levin, *et al.*, 1980; Nydal and Lövseth, 1983). The $\Delta^{14}\text{C}$ trends for these latitude bands are synthesized in Fig. 4-1. The meridional differences in $\Delta^{14}\text{C}$ are due to (i) larger number of thermonuclear detonations in the northern hemisphere and (ii) time lag of meridional mixing of air of northern and southern hemisphere. These trends have been adopted for determining the input of bomb- ^{14}C to the world oceans (Broecker, *et al.*, 1985, 1995).

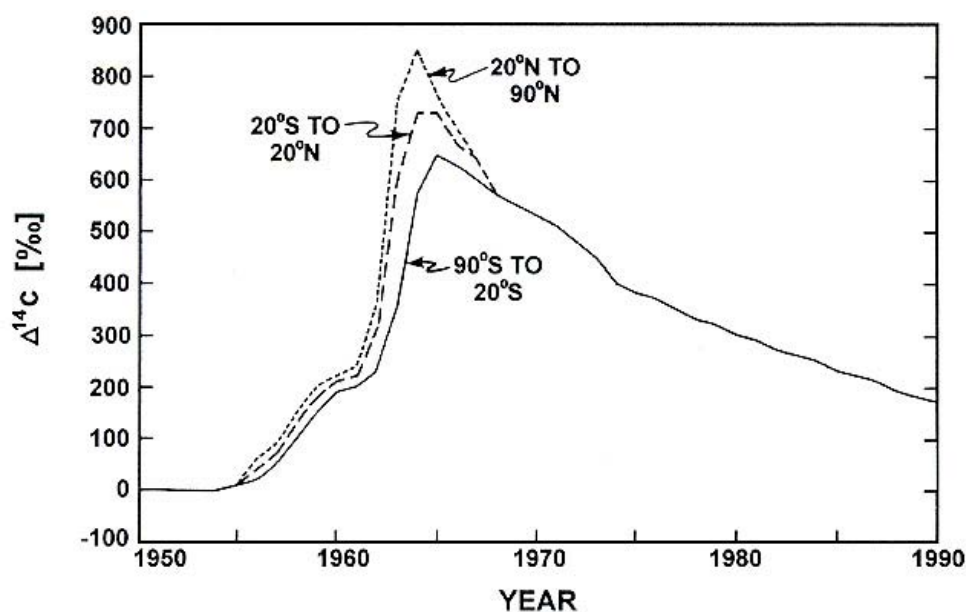


Figure 4-1 Temporal variation of atmospheric $\Delta^{14}\text{C}$ for three latitude zones (Broecker, *et al.*, 1995). The trends are based on large number of $\Delta^{14}\text{C}$ measurements in tropospheric CO_2 , in the northern and southern hemispheres (Nydal, 1963; Munnich and Roether, 1967; Levin, *et al.*, 1980; Nydal and Lövseth, 1983).

For regions adjacent to the northern Indian Ocean, only two sufficiently long tree-ring ^{14}C records exist which can be used to reconstruct the regional atmospheric $\Delta^{14}\text{C}$ history. The first between them is ^{14}C measurements (β -counting) in tree-rings of teak (*Tectona grandis*), from Thane ($19^{\circ}14'\text{N}$, $73^{\circ}24'\text{E}$) near Mumbai (formerly Bombay), India (Chakraborty, 1993). The other record is ^{14}C measurements (by AMS) in tree-rings of three-leaf pine (*Pinus kesiya*), from Doi Inthanon National Park ($18^{\circ}33'\text{N}$, $98^{\circ}34'\text{E}$) in the northwestern Thailand (Hua, *et al.*, 2000). These tree-ring ^{14}C data are shown in Fig. 4–2a.

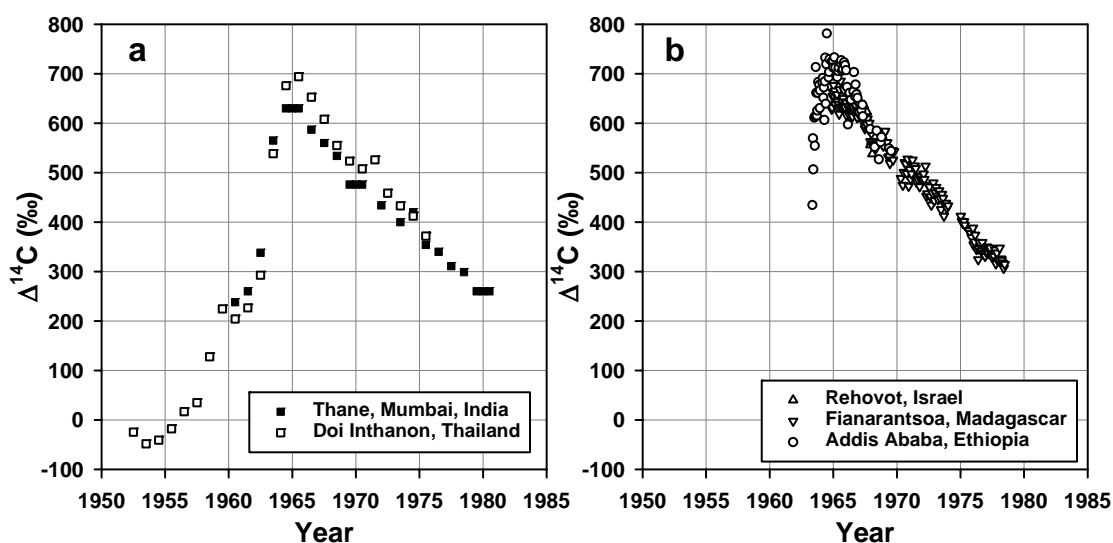


Figure 4–2 ^{14}C in atmospheric CO_2 from sites near the northern Indian Ocean region. (a) $\Delta^{14}\text{C}$ in tree-rings of teak from Thane, India (filled squares, Chakraborty, 1993) and in three-leaf pine from Doi Inthanon National Park, Thailand (open squares, Hua, *et al.*, 2000). For the Thane tree, the rings of 1964–1965, 1969–1970 and 1979–1980 were combined for ^{14}C analysis. (b) $\Delta^{14}\text{C}$ in atmospheric CO_2 from continental air-sampling sites at Israel, Madagascar and Ethiopia (Nydal and Lövseth, 1983, 1996).

Atmospheric $\Delta^{14}\text{C}$ time series from the continental stations near the Indian Ocean region are short, spanning maximum about 15yr, but the main bomb pulse of atmospheric ^{14}C was recorded. Atmospheric $\Delta^{14}\text{C}$ measured from Mumbai (19°N , 73°E , 0m) and Kodaikanal (10°N , 77°E , 2300m) between 1963 and 1965 ranged from 660‰ to 800‰ (Kusumgar, 1965; Lal and Rama, 1966). Nydal and Lövseth, (1983, 1996) reported measurements from Rehovot, Israel ($31^{\circ}50'\text{N}$, $34^{\circ}50'\text{E}$, 1967–1968); Debre Zeit, Ethiopia ($8^{\circ}40'\text{N}$, $38^{\circ}58'\text{E}$, 1900m, 1963–1969); and Fianarantsoa, Madagascar ($21^{\circ}27'\text{S}$, $47^{\circ}05'\text{E}$, 1100m, 1964–1978). The $\Delta^{14}\text{C}$ trends for these stations near the northern Indian Ocean coasts are shown in Fig. 4–2b.

Most of the tree-ring and the atmospheric data from locations near the northern Indian Ocean show that $\Delta^{14}\text{C}$ attained its peak at $700\pm 50\text{‰}$ over this region around 1965. However, the Thane tree-ring shows peak $\Delta^{14}\text{C}$ of $630\pm 8\text{‰}$ in the combined ring-sample grown between 1964 and 1965. This is lower than Thailand tree-ring $\Delta^{14}\text{C}$ values, where it peaks at $694\pm 7\text{‰}$ in the ring of 1965. As can be observed from Fig. 4–2, for most years, the tree-ring $\Delta^{14}\text{C}$ values from Thane are lower than that at Thailand. The peak $\Delta^{14}\text{C}$ value recorded in the Thane tree-rings is also apparently lower than the mean continental $\Delta^{14}\text{C}$ value of 705‰ between 1964 and 1965, measured at Debre Zeit, Ethiopia (Nydal and Lövseth, 1983, 1996). The low $\Delta^{14}\text{C}$ value recorded at Thane could be either due to averaging of two years — with lower $\Delta^{14}\text{C}$ for 1964 and a higher value for 1965, or its proximity with upwelling regions of the Arabian Sea, or a combination of both. Regional depletions of $\Delta^{14}\text{C}$ in the atmosphere are commonly observed near upwelling regions, since CO_2 evading out from upwelled ocean waters is depleted in ^{14}C relative to that in the atmosphere (Jiricovic and Kalin, 1993; Damon, 1995; McCormac, *et al.*, 1995; Damon, *et al.*, 1999).

Direct measurements of $\Delta^{14}\text{C}$ in the atmosphere over the northern Indian Ocean were done between 1993 and 1999, collecting maritime atmospheric CO_2 during scientific cruises in this region (Bhushan, *et al.*, 1997; Dutta, *et al.*, 2000a, 2001b). Spatial variability of $\Delta^{14}\text{C}$ over the contrasting upwelling regimes of the Arabian Sea and the Bay of Bengal has been analyzed in this study, to observe the imprint of oceanic CO_2 in the atmospheric ^{14}C signature.

Both the atmospheric concentration of CO_2 and its isotopic ratio of $^{13}\text{C}/^{12}\text{C}$ show significant interannual variations, in response to changes of fast cycling global sources and sinks of carbon (*e.g.*, biosphere and ocean) during the El Niño/Southern Oscillation events, which also influences the global climate. The interannual variations of $\Delta^{14}\text{C}$ observed over the northern Indian Ocean are compared in this study with the El Niño events. High precision atmospheric $\Delta^{14}\text{C}$ record obtained from sites near the tropical Pacific Ocean are also analyzed to look for statistical coherence with the El Niño events.

4.2 $\Delta^{14}\text{C}$ in maritime air over the Northern Indian Ocean

Tropospheric $^{14}\text{CO}_2$ in the maritime air was measured over the Arabian Sea and the Bay of Bengal during early to late spring months of 1993 to 1999 (except in 1996, when there was no cruise), aiming to determine the contemporary $\Delta^{14}\text{C}$ in the atmosphere overlying these basins. Unlike CO_2 sampling from fixed land-based stations, advantage of sampling CO_2 from a ship is that the $\Delta^{14}\text{C}$ values can be integrated over a much wider area. The sampling areas are shown in Fig. 4–3.

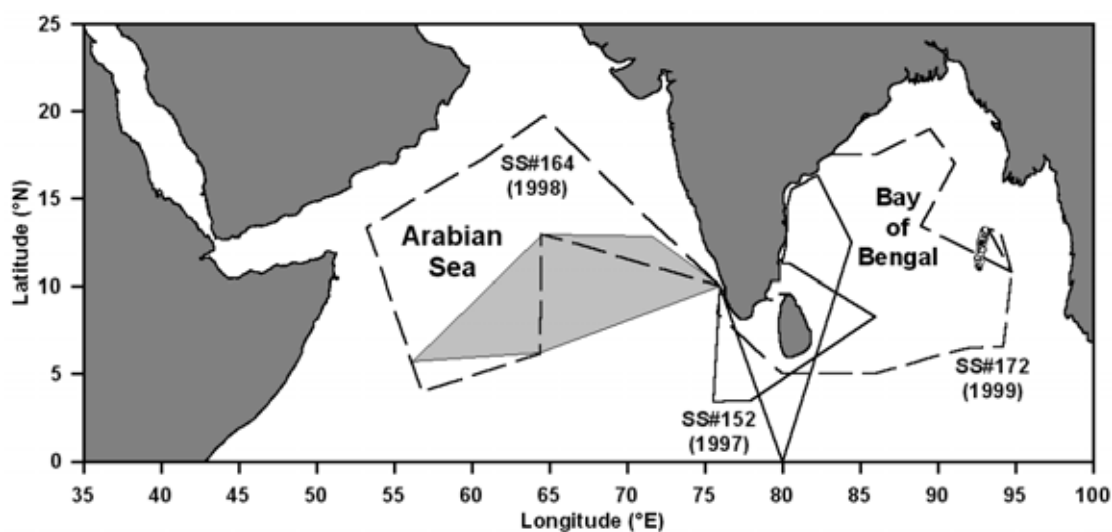


Figure 4–3 Cruise tracks for maritime CO_2 sampling over the Arabian Sea and the Bay of Bengal, between 1997 and 1999. Area sampled during 1993, 1994 and 1995 over the Arabian Sea is shaded.

About 3 to 4 samples were collected during 1993 to 1995 and between 8 to 10 samples (some in duplicate) during 1997 to 1999. The $\Delta^{14}\text{C}$ values in individual samples of each year and their error-weighted means are given in Table 4–1. Data for 1993–1995 are from Bhushan, *et al.*, (1997). A and B are duplicate samples collected along the same cruise track. AB denotes combined duplicate samples — due to insufficient CO_2 in each of the repeats, they were combined to obtain sufficient quantity of CO_2 for $\Delta^{14}\text{C}$ measurement. The codes SK and SS represent the samples collected during ORV *Sagar Kanya* and FORV *Sagar Sampada* cruises respectively.

Absorption of CO_2 from air in aqueous NaOH solution causes significant fractionation, depleting $\delta^{13}\text{C}$ by as much as 20‰ (Nydal, 1966). However, dynamic pumping of air into NaOH solution reduces this fractionation to some extent. The $\delta^{13}\text{C}$ values listed in Table 4–1 are therefore not representative of normal atmospheric values, which range from -7.7 to -8 ‰ (Masarie, *et al.*, 2000). The measured $\delta^{13}\text{C}$ in liberated CO_2 were only used to calculate $\Delta^{14}\text{C}$.

Table 4-1:
 ^{14}C measurements in atmospheric CO_2 over the northern Indian Ocean

Lab code (PRLCH)	Sample code	Sampling track		$\delta^{13}\text{C}_{\text{PDB}}$ (‰)	$\Delta^{14}\text{C} \pm 1\sigma$ (‰)
		Begin (Lat°N, Long°E)	End (Lat°N, Long°E)		
<i>Cruise SK-83 (Apr – May, 1993) Arabian Sea</i>					
194	SK-83-A1	15.0, 73.0	12.5, 67.0	*-15.0	124.0 ± 6.0
196	SK-83-A2	12.5, 67.0	13.0, 68.0	-15.1	119.1 ± 5.2
201	SK-83-A3	13.0, 68.0	12.5, 69.5	-15.3	118.8 ± 4.7
204	SK-83-A4			*-15.0	121.0 ± 8.0
Mean =				-15.2	120 ± 3
<i>Cruise SS-117 (Jan – Feb, 1994) Arabian Sea</i>					
240	SS-117-A1	6.0, 74.0	8.0, 73.0	*-15.0	104.0 ± 5.0
315	SS-117-A2	8.0, 73.0	13.0, 64.8	-16.4	135.2 ± 5.0
316	SS-117-A3	13.0, 64.8	12.8, 71.6	-14.6	109.5 ± 5.5
Mean =				-15.5	117 ± 3
<i>Cruise SS-132 (Apr – May, 1995) Arabian Sea</i>					
326	SS-132-A1	11.0, 75.0	13.0, 64.5	-11.5	101.3 ± 4.7
327	SS-132-A2	13.0, 64.5	5.7, 56.2	-18.0	121.6 ± 5.7
328	SS-132-A3	5.7, 56.2	6.2, 64.4	-8.0	104.2 ± 5.0
329	SS-132-A4	6.2, 64.4	8.0, 75.0	-8.2	91.6 ± 6.7
Mean =				-11.4	105 ± 3
<i>Cruise SS-152 (Feb – Mar, 1997) Bay of Bengal</i>					
351	SS-152-1A	7.2, 76.0	3.9, 78.1	-7.7	†75.7 ± 7.0
398	SS-152-1B			-9.3	105.8 ± 7.7
392	SS-152-2A			-9.0	119.9 ± 8.6
399	SS-152-2B	3.9, 78.1	8.5, 86.0	-8.8	120.1 ± 6.5
393	SS-152-3A			-13.6	111.5 ± 7.4
400	SS-152-3B	8.5, 86.0	16.3, 82.3	-15.0	99.8 ± 7.6
394	SS-152-4AB	16.3, 82.3	7.4, 83.8	-13.6	99.8 ± 6.7
395	SS-152-5AB	7.4, 83.8	0.0, 80.0	-7.1	†82.1 ± 6.4
396	SS-152-6AB	0.0, 80.0	0.0, 80.0	-13.8	112.3 ± 8.5
397	SS-152-7AB	2.2, 79.0	7.2, 76.0	-10.8	106.5 ± 7.7
Mean =				-10.9	109 ± 3
<i>Cruise SS-164 (Mar – Apr, 1998) Arabian Sea</i>					
424	SS-164-1A	12.0, 74.2	16.5, 69.0	-14.1	95.7 ± 7.7
425	SS-164-1B			-17.1	100.3 ± 6.4
426	SS-164-2A			-13.9	83.4 ± 7.5
427	SS-164-2B	16.5, 69.0	19.8, 64.6	-14.9	†56.3 ± 6.7
428	SS-164-3AB1			-17.0	†119.8 ± 6.8
429	SS-164-3AB2	19.8, 64.6	17.2, 60.7	-17.0	106.5 ± 6.7
430	SS-164-4A			-16.1	104.5 ± 6.3
431	SS-164-4B	17.2, 60.7	14.3, 54.9	-19.6	105.1 ± 6.2
432	SS-164-5AB	13.3, 53.2	3.9, 56.8	-10.7	93.0 ± 6.9
433	SS-164-6A			-16.5	99.0 ± 7.1
434	SS-164-6B	3.9, 56.8	6.2, 64.3	-17.3	93.4 ± 6.0
435	SS-164-7A			-10.2	95.7 ± 6.2
437	SS-164-7B	6.2, 64.3	12.9, 64.5	-17.9	89.1 ± 6.6
Mean =				-15.6	97 ± 2
<i>Cruise SS-172 (Feb, 1999) Bay of Bengal</i>					
466	SS-172-1A	17.5, 85.9	17.0, 91.1	-12.6	89.3 ± 7.3
467	SS-172-1B			-10.6	94.5 ± 8.3
468	SS-172-2A			-13.1	84.2 ± 5.4
469	SS-172-2B	16.9, 91.1	13.4, 88.9	-8.2	85.2 ± 5.9
470	SS-172-3AB	13.4, 88.9	13.0, 93.0	-14.0	95.1 ± 5.1
471	SS-172-4AB1			-13.2	91.7 ± 5.0
472	SS-172-4AB2	10.8, 93.2	6.5, 91.7	-13.2	88.7 ± 5.4
473	SS-172-5AB	6.5, 91.7	5.0, 86.0	-15.1	80.5 ± 4.8
474	SS-172-6AB	5.0, 86.0	8.0, 76.0	-9.3	†67.5 ± 4.7
Mean =				-12.1	88 ± 2

Data for 1993, 1994 and 1995 are from Bhushan, et al., (1997).

* $\delta^{13}\text{C}$ not measured, mean value of -15‰ have been used for $\Delta^{14}\text{C}$ calculation.

† Rejected for mean calculation, due to possible fractionation or contamination.

4.3 Trends of $\Delta^{14}\text{C}$ in atmosphere over the Northern Indian Ocean

The $\Delta^{14}\text{C}$ values over the northern Indian Ocean are compared with the global trend of tropospheric $\Delta^{14}\text{C}$ in Fig. 4–4. The $\Delta^{14}\text{C}$ values given in Table 4–1 and Fig. 4–4 (inset) are the mean obtained along the cruise tracks and represents the springtime $\Delta^{14}\text{C}$ averaged over a wide area of ocean basin. The mean seasonal cycle of $\Delta^{14}\text{C}$ in tropical maritime atmosphere, as recorded between 1985 and 1995 at the maritime air sampling station at Izaña, Canary Islands (28°18'N, 16°29'W), has a peak-to-peak amplitude of ~6‰ (Levin, *et al.*, 1999). The turn over of seasonal $\Delta^{14}\text{C}$ cycle occurs during January and June. Thus, springtime $\Delta^{14}\text{C}$ values measured over the northern Indian Ocean are expected to be close to the annual mean, within the limits of experimental uncertainty.

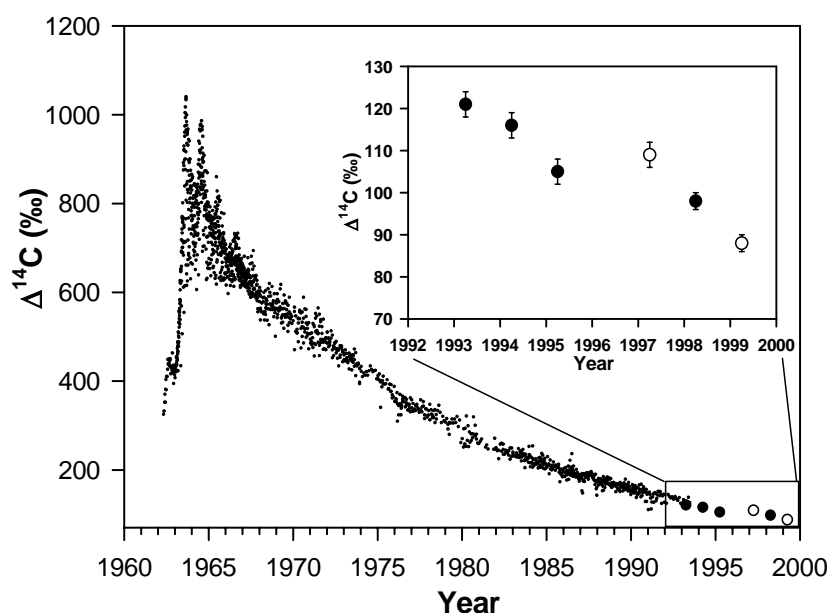


Figure 4–4 Tropospheric $\Delta^{14}\text{C}$ measured from the northern and the southern hemisphere sites (dots) (Nydal and Lövseth, 1983, 1996). Inset, enlarged plot of average $\Delta^{14}\text{C}$ measured in air overlying the Arabian Sea (filled circles) and the Bay of Bengal (open circles) (Dutta, *et al.*, 2001b). Arabian Sea data for 1993, 1994 and 1995 are from Bhushan, *et al.*, (1997).

The $\Delta^{14}\text{C}$ values over the northern Indian Ocean are in good agreement with the global quasi-exponential decaying trend (Fig. 4–4), and with the measurements made at Izaña, as shown in Fig. 4–5 (Levin and Hesshaimer, 2000). A more critical analysis of the data, however, show that the values obtained over the Arabian Sea between 1993 and 1995 are lower by about 10‰, than that at Izaña. Further, contrary to the expected decrease, $\Delta^{14}\text{C}$ measured in 1997 over the Bay of Bengal is equal to or higher than that over the Arabian Sea in 1995. The rate of $\Delta^{14}\text{C}$ decrease over the Arabian Sea was slower between 1995 and 1998, than between 1993 and 1995.

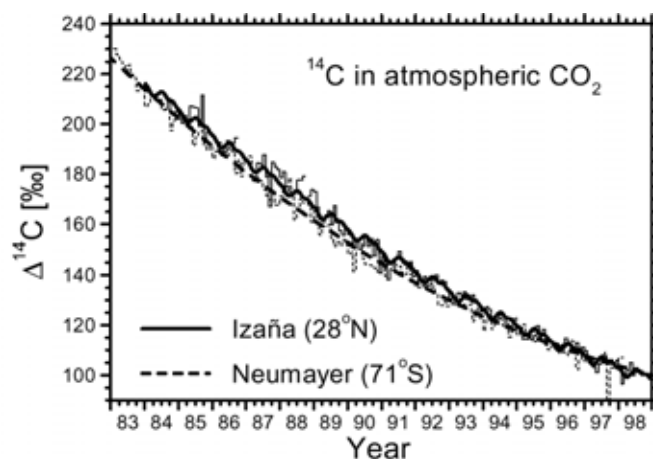


Figure 4-5 Long-term observations of $^{14}\text{CO}_2$ at Izaña, Canary Is. (solid curve and histogram) and at Neumayer, Antarctica (dashed trend curve and histogram) (Levin, *et al.*, 1999).

The exponential decreasing trend of tropospheric $^{14}\text{CO}_2$ at any given location can be characterized by its decay (or e-folding) time constant τ . The average e-folding time is $\sim 16\text{yr}$ in the northern hemisphere (Levin and Kromer, 1997a) and about $\sim 17\text{yr}$ in the southern hemisphere (Manning, *et al.*, 1990). Recent atmospheric measurements from a network of seven background air-sampling stations between 82°N to 71°S , revealed the current trend of tropospheric $\Delta^{14}\text{C}$ (Levin, *et al.*, 1997b; Levin and Hesshaimer, 2000). Their data show, the global decreasing trend closely follows an exponential curve with a time constant of $18.70 \pm 0.15\text{yr}$, thus changing the rate of $\Delta^{14}\text{C}$ decrease from about $-13\text{‰}\cdot\text{yr}^{-1}$ in 1982 to about $-4\text{‰}\cdot\text{yr}^{-1}$ in 1998.

In the present study, the e-folding times (τ) are calculated for different years (by choosing 1980 as the base year) from the relation, $\Delta^{14}\text{C}_t = \Delta^{14}\text{C}_{1980}e^{-\Delta t/\tau}$ where $\Delta^{14}\text{C}_t$ is the measured $\Delta^{14}\text{C}$ value for a given year 't' and Δt is the number of years elapsed since 1980. $\Delta^{14}\text{C}_{1980}$ is taken as 265‰ , from the tropical maritime tropospheric ^{14}C measurements at Izaña, Canary Islands (Nydal and Lövseth, 1996). The calculated e-folding times are summarized in Table 4-2. The uncertainties include only the measurement error of $\Delta^{14}\text{C}$ for a given year. The e-folding times over the northern Indian Ocean range from 16.0 to $18.8(\pm 0.5)\text{yr}$, with error-weighted mean of $17.0 \pm 0.2\text{yr}$. This compares well with the e-folding time of 16.6yr reported earlier for this region (Bhushan, *et al.*, 1997), obtained relative to the base years 1970 with $\Delta^{14}\text{C}_{1970} = 550\text{‰}$ and correcting for Suess effect of $-0.68\text{‰}\cdot\text{yr}^{-1}$. To resolve the interannual variations, the ^{14}C data have been detrended by removing an exponentially decaying trend. The residual of $\Delta^{14}\text{C}$ obtained after detrending is given by, $\Delta^{14}\text{C}_{\text{res}} = \Delta^{14}\text{C}_t - \Delta^{14}\text{C}_{1980}e^{-\Delta t/17.0}$. The residual $\Delta^{14}\text{C}$ values are also tabulated in Table 4-2.

Table 4–2:
Spring-time $\Delta^{14}\text{C}$, e-folding time (τ) and residual $\Delta^{14}\text{C}$

Years (t) / Region	$\Delta^{14}\text{C}_t \pm 1\sigma$ (‰)	$\tau \pm 1\sigma$ (yr)	$\Delta^{14}\text{C}_{\text{res}} \pm 1\sigma$ (‰)
1993 / Arabian Sea	120 ± 3	16.2 ± 0.5	-4.5 ± 3.0
1994 / Arabian Sea	117 ± 3	16.6 ± 0.5	-2.7 ± 3.0
1995 / Arabian Sea	105 ± 3	16.0 ± 0.5	-5.9 ± 3.0
1997 / Bay of Bengal	109 ± 3	18.8 ± 0.5	9.4 ± 3.0
1998 / Arabian Sea	97 ± 2	17.7 ± 0.4	3.7 ± 2.0
1999 / Bay of Bengal	88 ± 2	16.9 ± 0.4	-0.7 ± 2.0

The $\Delta^{14}\text{C}$ values of CO_2 over the northern Indian Ocean show deviations from the normal exponential decreasing trend in certain years. These deviations (anomalies) may not be random, they may reflect either regional variations of $\Delta^{14}\text{C}$ over this region, or interannual $\Delta^{14}\text{C}$ variation in the overlying atmosphere resulting from anomalous ocean-atmosphere CO_2 exchange or biospheric CO_2 flux, or a combination of both.

4.3.1 Regional variations of $\Delta^{14}\text{C}$ over the Northern Indian Ocean

It is apparent from Table 4–2, the $\Delta^{14}\text{C}$ values over the Arabian Sea are less than over the Bay of Bengal, indicated by negative residual $\Delta^{14}\text{C}$ values for all years except 1998. Regional upwelling induced ^{14}C depletion was documented from tree ring $\Delta^{14}\text{C}$ measurements from northwestern Thailand (Hua, *et al.*, 2000) and from coastal South Africa (Damon, *et al.*, 1999). Considering the close proximity of the Arabian Sea and the Bay of Bengal, rapid zonal mixing is expected to smooth out any such variation across these two basins. But this regional difference appears to be consistent, when the tree-ring $\Delta^{14}\text{C}$ values of Thane and Thailand are compared (Fig. 4–2). The Thane $\Delta^{14}\text{C}$ are in general lower by about 20‰ between 1965 and 1975 relative to the Thailand values. This regional variation can be explained by the contrasting upwelling characteristics of the Arabian Sea and the Bay of Bengal. Arabian Sea being a perennial source of CO_2 from upwelling of CO_2 rich deep water (Sarma, *et al.*, 1998), the regional atmospheric $\Delta^{14}\text{C}$ is expected to be lower than contemporary values due to evasion of ^{14}C -depleted CO_2 . The Bay of Bengal being a sink of atmospheric CO_2 (Kumar, *et al.*, 1996), such regional depletion of atmospheric $\Delta^{14}\text{C}$ would be smaller.

Using a simple two-component mixing model, the contribution of oceanic CO₂ necessary for the observed depletions of $\Delta^{14}\text{C}$ over the Arabian Sea have been estimated. In this model, the CO₂ in air overlying the Arabian Sea is assumed to be a mixture of normal tropospheric CO₂ and oceanic CO₂ from the Arabian Sea evaded through upwelling. Measured values from Izaña, Canary Islands (Nydal and Gislefoss, 1996; Levin *et al.*, 1999) are assumed to be representative of tropical tropospheric $\Delta^{14}\text{C}$. The oceanic regions of tropical Atlantic surrounding the Canary Islands are not significant source of oceanic CO₂ (Takahashi, *et al.*, 1997). Thus it is unlikely that $\Delta^{14}\text{C}$ in air over Canary Islands has signatures of oceanic CO₂. The $\Delta^{14}\text{C}$ for the year 1978 at Izaña has been extrapolated from the 1980 mean value (265‰, Nydal and Lövsseth, 1996), assuming that $\Delta^{14}\text{C}$ has been decreasing at 15‰.yr⁻¹ during this time. The $\Delta^{14}\text{C}$ of the evaded oceanic CO₂ from the Arabian Sea is assumed to be same to that of its surface water. The mean $\Delta^{14}\text{C}$ in 1978, of the Arabian Sea surface water is from the GEOSECS ¹⁴C measurements (Stuiver and Ostlund, 1983). The 1994 and 1995 surface water $\Delta^{14}\text{C}$ values are the mean obtained over the Arabian Sea during these two years (Bhushan, *et al.*, 2000). The 1993 and 1998 values are extrapolated.

If f_{CO_2} is the fraction of oceanic CO₂ in the atmosphere over the Arabian Sea, $\Delta^{14}\text{C}_{\text{sea}}$ be the $\Delta^{14}\text{C}$ of Arabian Sea surface water, and $\Delta^{14}\text{C}_{\text{Iz}}$ be the tropospheric $\Delta^{14}\text{C}$ values at Izaña, then from a simple two component mixing process the tropospheric $\Delta^{14}\text{C}$ value over the Arabian Sea ($\Delta^{14}\text{C}_{\text{Ar}}$) is given by,

$$\Delta^{14}\text{C}_{\text{Ar}} = f_{\text{CO}_2}(\Delta^{14}\text{C}_{\text{sea}}) + (1-f_{\text{CO}_2})\Delta^{14}\text{C}_{\text{Iz}}$$

or,

$$f_{\text{CO}_2} = (\Delta^{14}\text{C}_{\text{Iz}} - \Delta^{14}\text{C}_{\text{Ar}}) / (\Delta^{14}\text{C}_{\text{Iz}} - \Delta^{14}\text{C}_{\text{sea}})$$

The f_{CO_2} values calculated from the above relation are given in Table 4–3, shows up to ~17% of the CO₂ in the atmosphere over the Arabian Sea is of oceanic origin.

Table 4–3:
Fraction of oceanic CO₂ in the atmospheric CO₂ over the Arabian Sea

Year	Atmospheric $\Delta^{14}\text{C}$ (‰)		Arabian Sea surface $\Delta^{14}\text{C}$ (‰)	f_{CO_2} (%)
	Above Izaña	Above Arabian Sea		
1978	(295 ± 10)	299 ± 6	75 ± 10	-1.8
1993	130 ± 6	120 ± 3	(49 ± 10)	12.3
1994	123 ± 6	117 ± 3	47 ± 10	7.9
1995	117 ± 6	105 ± 3	47 ± 10	17.1
1998	100 ± 6	97 ± 2	(40 ± 10)	5.0

(extrapolated values are shown in parentheses)

4.3.2 Inter-annual variations of $\Delta^{14}\text{C}$ over the Northern Indian Ocean

It is interesting to note from Table 4–3, that the $\Delta^{14}\text{C}$ over the Arabian Sea are comparable to the Izaña values during certain years (1978, 1994 and 1998). These differences point to interannual $\Delta^{14}\text{C}$ variations in the atmosphere over this region. The $\Delta^{14}\text{C}_{\text{res}}$ for the Arabian Sea for the years 1998 is nearly 10‰ higher than that in 1995, similar to the $\Delta^{14}\text{C}_{\text{res}}$ difference for the Bay of Bengal between 1997 and 1999. The anomalously high values of residual $\Delta^{14}\text{C}$ during 1997 and 1998 coincide with the very strong El Niño event of 1997–1998. The years 1978 and 1994 are also marked by strong El Niño events, when the atmosphere over the Arabian Sea recorded relatively higher $\Delta^{14}\text{C}$. The El Niño/Southern Oscillation (ENSO) events are known to cause significant perturbation of the global carbon cycle, through changes in the growth rates of atmospheric CO_2 and its isotopic composition. The possible relationship between atmospheric $\Delta^{14}\text{C}$ and El Niño are discussed in the next section.

4.4 Influence of El Niño/Southern Oscillation on atmospheric CO_2 and its isotopes

The El Niño/Southern Oscillation events are interannual variability of atmospheric and oceanic circulation that occur every 2 to 10yr (Rasmusson and Wallace, 1983; Enfield, 1988). These events are commonly associated with anomalous high sea surface temperature (SST) in the eastern equatorial Pacific due to reduction in westerly wind stress, which retards the upwelling of deeper colder waters. Anomalous growth rates of atmospheric CO_2 , higher by 1 to 2ppm.yr⁻¹ were observed during the El Niño events (Bacastow, 1976; Bacastow, *et al.*, 1980; Keeling and Revelle, 1985; Keeling, *et al.*, 1989; Elliot, *et al.*, 1991; Keeling, *et al.*, 1995; Keeling and Piper, 2000). The magnitude of these CO_2 anomalies which may correspond to ~6PgC.year⁻¹ during very strong El Niño events cannot be explained by changes in fossil fuel emissions (Bacastow, 1976; Gaudry, *et al.*, 1987). However, they can be explained by anomalous changes in ocean-atmosphere or land-atmosphere flux of carbon. El Niño events are associated with significant reduction in the flux of oceanic CO_2 from the equatorial Pacific, mainly due to reduced upwelling of CO_2 rich waters (Wong, *et al.*, 1993; Archer, *et al.*, 1996; Feely, *et al.*, 1997, 1999). Hot and arid conditions during El Niño events favor net respiration of biosphere in the tropics, which enhances the release of biospheric CO_2 (Tian, *et al.*, 1998; Malhi, *et al.*, 1998).

To identify the exact source of CO₂ anomalies, several high precision measurements of atmospheric CO₂ and its isotope ($\delta^{13}\text{C}$) were carried out from large number of atmospheric sampling stations of NOAA/CMDL cooperative air sampling network (Conway, *et al.*, 1994; Masarie, *et al.*, 2000). The trend of global rise of atmospheric CO₂ for the last two decades obtained from these measurements is shown in Fig. 4–6. It is evident from Fig. 4–6 that the periods of anomalously high CO₂ growth rates usually coincide with the El Niño events. From measurements of $^{13}\text{C}/^{12}\text{C}$ ratios ($\delta^{13}\text{C}$) it has been demonstrated that high growth rates of CO₂ in the atmosphere correlates with negative excursions of $\delta^{13}\text{C}$ by $\sim 0.1\text{‰}$

in tropospheric CO₂ (Keeling, *et al.*, 1995; Nakazawa, *et al.*, 1997). This supports the idea that release of ^{13}C -depleted CO₂ from the terrestrial biosphere mainly causes the anomalously high growth rates of CO₂ during the El Niño events. The initial reductions of CO₂ growth rates that are commonly observed in the early stages of El Niño events are attributed to the reduction in oceanic CO₂ flux.

Even though there are many reported evidences of correlation of atmospheric CO₂ concentration and $\delta^{13}\text{C}$ with El Niño/Southern Oscillation events, much less explored are the variations of $\Delta^{14}\text{C}$ of atmospheric CO₂ in response to these events. Several conditions during these events are conducive to an enhanced level of $\Delta^{14}\text{C}$ in the atmospheric CO₂. Since oceanic CO₂ is depleted in ^{14}C relative to that in atmosphere, reduction in regional oceanic CO₂ flux can increase the $\Delta^{14}\text{C}$ of atmospheric CO₂. In the post-bomb period, emission of biospheric CO₂ can also lead to enrichment of atmospheric CO₂ in ^{14}C . Thus during late 1990s, CO₂ liberated from fast cycling terrestrial organic matters was relatively enriched in ^{14}C compared to the

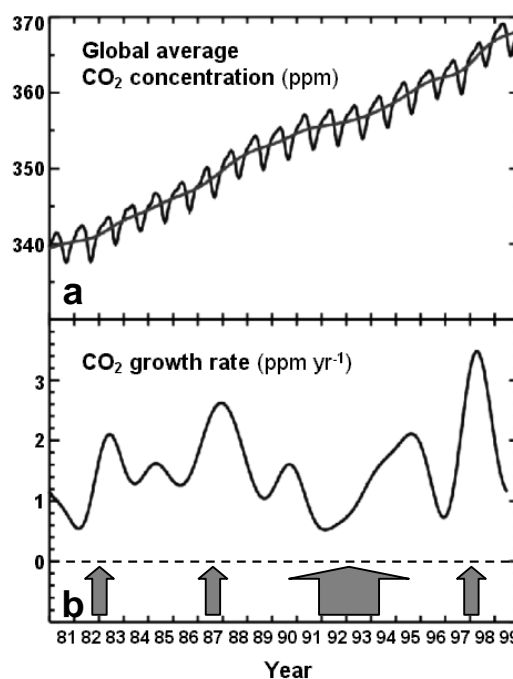


Figure 4–6 Global atmospheric carbon dioxide growth rate from NOAA–CMDL cooperative air sampling network (Masarie, *et al.*, 2000). (a) Monthly values of global average atmospheric CO₂ concentration, and the long-term trend. (b) Inter-annual variations of the CO₂ growth rate in the atmosphere. Filled arrows indicate the occurrences of major El Niño events.

atmosphere (Trumbore, 1997). Thus the El Niño events can increase the concentration of ^{14}C in the atmosphere through enhanced emission of biospheric CO_2 . The El Niño events are accompanied by anomalous atmospheric circulation patterns, with higher tropopause height and higher stratosphere-troposphere exchange (Gage and Reid, 1986), which can favor enhanced transport of stratospheric air with higher $\Delta^{14}\text{C}$ to the troposphere (Nakamura, *et al.*, 1992). All these phenomena, *e.g.*, reduction in supply of ^{14}C depleted CO_2 from oceans, reduced ocean-atmosphere $\Delta^{14}\text{C}$ gradient, release of ^{14}C enriched CO_2 from terrestrial biosphere and enhanced mixing with stratospheric air richer in $^{14}\text{C}/^{12}\text{C}$, together favor enhancement of $\Delta^{14}\text{C}$ in the tropospheric air during the El Niño events.

In Fig. 4–7, the residual $\Delta^{14}\text{C}$ (Table 4–2) over the northern Indian Ocean are compared with the classical Tahiti–Darwin Southern Oscillation index (SOI) and the bimonthly multi-variate ENSO index or MEI (*sec. 4.6.3*). The warm ENSO phases are indicated by high negative and positive values of SOI and MEI respectively.

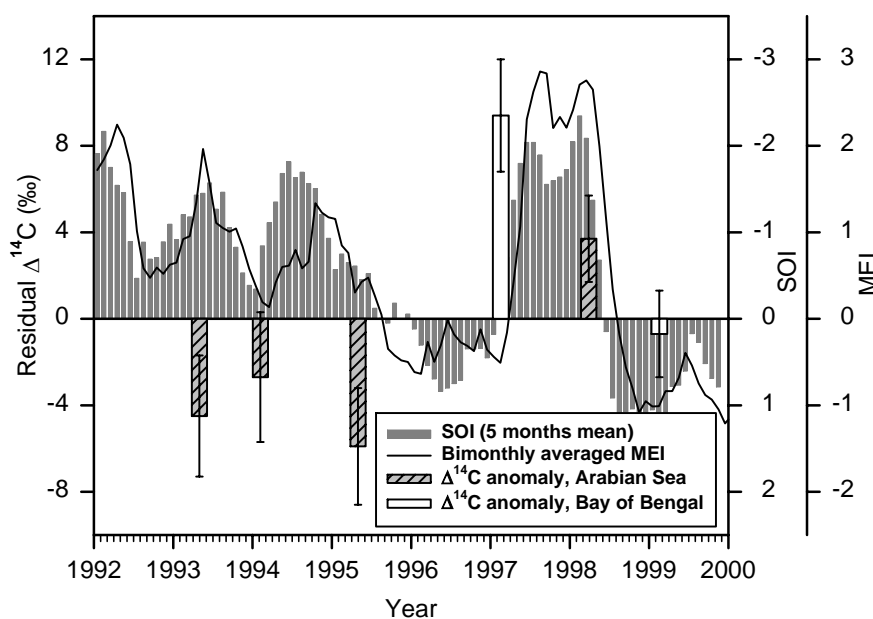


Figure 4–7 ^{14}C anomalies over the Arabian Sea (hatched bars) and the Bay of Bengal (open bars). Thin gray bars show the Tahiti–Darwin Southern Oscillation Index (SOI), averaged over 5 months. The curved line is the bimonthly averaged multi-variate ENSO index or MEI (Wolter, 2001). Negative SOI values and positive MEI values depict El Niño conditions.

It is important to note from Fig. 4–7, that the highest positive $\Delta^{14}\text{C}$ anomaly of 1997 was observed nearly 8 months prior to the peak development of El Niño condition during November 1997. However, no relationship is apparent with El Niño events and the ^{14}C measurements done over the Arabian Sea, between 1993 and 1995.

There are few reports on possible modulation of tropospheric $\Delta^{14}\text{C}$ by ENSO both for the pre- and post-nuclear era. It has been demonstrated that ENSO influences regional differences in tree ring ^{14}C from Washington State and Arizona, USA, during 1930 to 1955 (Jiricovic and Kalin, 1993). Periodicities in the 2 to 6.4yr range observed in the spectrum of annual high precision tree ring ^{14}C data (1511–1954 AD) from northwest Pacific coasts (Olympic Peninsula, Washington, USA), have been associated to ENSO related thermohaline circulation changes in the tropical Pacific (Stuiver and Braziunas, 1993b).

During the post bomb period, at the high latitudes of the northern hemisphere, slower decrease of tropospheric $\Delta^{14}\text{C}$ was observed over Abisko, Sweden ($68^{\circ}20.5'\text{N}$) and Svalbard, Spitsbergen ($78^{\circ}04'\text{N}$) during the El Niño years between 1982 and 1987 (Olsson, 1989). Strong modulation of tropospheric $\Delta^{14}\text{C}$ by the El Niño events was observed from atmospheric $\Delta^{14}\text{C}$ measurements from the equatorial Pacific coasts of Peru between 1991 and 1993 (Rozanski, *et al.*, 1995). A very regular quasi-biannual variation has been observed in recent high precision atmospheric $\Delta^{14}\text{C}$ records from the southern hemisphere, which might have possible association with the El Niño phenomenon (Levin, *et al.*, 1997). Significant interannual variability has been recorded in high precision $\Delta^{14}\text{C}$ measurements particularly at Cape Grim, Tasmania ($40^{\circ}41'\text{S}$), which seem to be linked to strong El Niño events (Levin *et al.*, 1998, 1999).

Is the observed ^{14}C –ENSO relationship real?

In spite of several evidences, no definite proof has yet been reported for a consistent $\Delta^{14}\text{C}$ –ENSO relationship on longer time scales. The difficulty mainly arises from the fact that, the ^{14}C -anomaly signals arising from ENSO related thermohaline circulation changes are rather small, only 1~2‰ in the pre-nuclear era, therefore no correlation was evident when individual El Niño events were compared with the tree-ring $\Delta^{14}\text{C}$ values (Stuiver and Braziunas, 1993b; Damon, 1995). A statistical analysis of the $\Delta^{14}\text{C}$ –ENSO relationship has been done in this study, using different $\Delta^{14}\text{C}$ datasets (tree-rings and atmospheric $\Delta^{14}\text{C}$ measurements) and suitable ENSO indices contemporary to the ^{14}C datasets.

4.5 Statistical coherence between ENSO and tropospheric $\Delta^{14}\text{C}$

To examine in detail the relationship of high-frequency $\Delta^{14}\text{C}$ variations in the atmosphere with ENSO, tropospheric $\Delta^{14}\text{C}$ data for both pre-bomb and post-bomb period have been analyzed in this study, to examine statistical coherence between tropospheric $\Delta^{14}\text{C}$ with suitable ENSO indices. Variability of tropospheric $\Delta^{14}\text{C}$ in the time window of 2 to 30yr has been analyzed here, focusing within the broad ENSO band, between 2 to 9yr.

4.5.1 Pre-bomb tropospheric $\Delta^{14}\text{C}$ data from Washington, U.S.A.

The pre-bomb tropospheric $\Delta^{14}\text{C}$ data are from single years high precision tree ring ^{14}C measurements in Douglas-fir tree (*Pseudotsuga menziesii*) from Olympic Peninsula (47°46'N, 124°06'W), Washington, U.S.A. (Stuiver, 1993; Stuiver, *et al.*, 1998b). The full record extends from 1511 to 1955 AD, and is shown in Fig. 4–9a. For single tree-ring $\Delta^{14}\text{C}$ measurements, the average 1σ error is $\pm 1.5\text{‰}$ (range from ± 0.8 to 2.6‰). The data shows strong secular variations resulting from solar modulation of galactic cosmic rays and reduction of $\Delta^{14}\text{C}$ between 1900 and 1950 due to input of ^{14}C -free fossil fuel CO_2 (Stuiver and Quay, 1981). The $\Delta^{14}\text{C}$ in this data range from 10‰ to -25‰ , with higher values during the periods of solar minima.

The raw tree ring $\Delta^{14}\text{C}$ data was first detrended by removing the secular trend, induced by solar modulation of the galactic cosmic rays and input of ^{14}C free CO_2 in atmosphere from fossil fuel burning between 1900 and 1950. This secular trend was obtained by smoothing the raw $\Delta^{14}\text{C}$ data using a FFT filter — retaining frequencies lower than $1/30\text{cycle}\cdot\text{year}^{-1}$ (*i.e.*, periods longer than 30yr). The raw data were then detrended by subtracting the smooth trend from it. The residual ^{14}C data show a variation of $\pm 6\text{‰}$ (Fig. 4–9b). To suppress the random high frequency noise, the residual data were smoothed by applying 2-years running mean.

4.5.2 Post-bomb tropospheric $\Delta^{14}\text{C}$ data from Wellington, New Zealand

Atmospheric $\Delta^{14}\text{C}$ measurements from Wellington (41°18'S, 174°48'E), New Zealand (Manning and Melhuish, 1994), has been chosen for the post-bomb $\Delta^{14}\text{C}$ data (Fig. 4–10a), for its proximity with the Pacific region influenced by El Niño events. The record extends from 1954 to 1993, with near monthly measurements of $\Delta^{14}\text{C}$. The average 1σ error is $\pm 4\text{‰}$ (range from ± 2.7 to 9.6‰). The raw data were detrended by subtracting the exponentially decreasing secular trend (Fig. 4–10b).

4.5.3 *El Niño/Southern Oscillation indices*

(a) *Niño-3 SST index*

The El Niño events are associated with above-normal sea surface temperature (SST) in the tropical Pacific region. The entire tropical Pacific region has been subdivided into certain zones, to characterize the regional influences of El Niño events (Fig. 4–8).

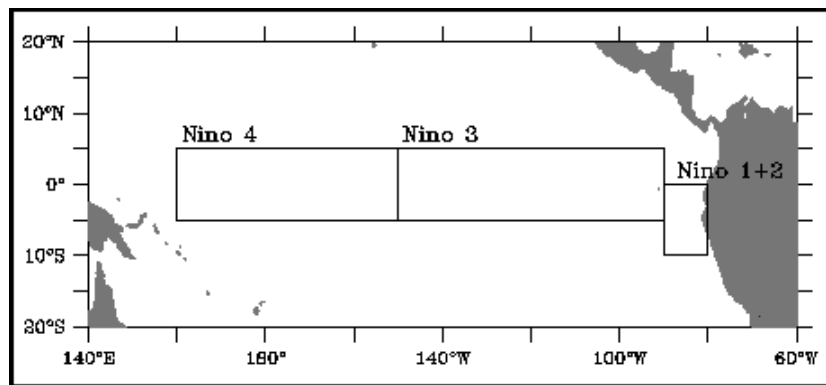


Figure 4–8 The Niño regions of the equatorial Pacific.

The Niño-3 SST index, a proxy for the ENSO events has been reconstructed for the period 1650–1950 AD (Mann, *et al.*, 2000). This index is based on a number of proxies in the tropical Pacific, and shown in Fig. 4–9c. Positive Niño-3 SST indices depict El Niño conditions, while the negative indices indicate La Niña.

(b) *Multivariate ENSO Index (MEI)*

El Niño/Southern Oscillation is a coupled ocean-atmosphere phenomenon, which causes global climate variability on interannual time scales. The Multivariate ENSO Index (MEI) is based on the six main observed variables over the tropical Pacific (Wolter and Timlin, 1998). These six variables are: sea-level pressure, zonal and meridional components of the surface wind, sea surface temperature, surface air temperature, and total cloud fraction of the sky. These variables are available for past several years from the Comprehensive Ocean Atmosphere Data Sets (COADS). The MEI has been calculated from these variables for every two months starting from 1950 till present (Wolter, 2001). Positive values of the MEI (>0.5) represent the warm phase of ENSO or El Niño, while negative values (<0.5) represent the cold phase or La Niña. The full data are available from NOAA-Climate Data Center (CDC), Boulder, Colorado, U.S.A. as bimonthly averaged values. The MEI time series is shown in Fig. 4–10c.

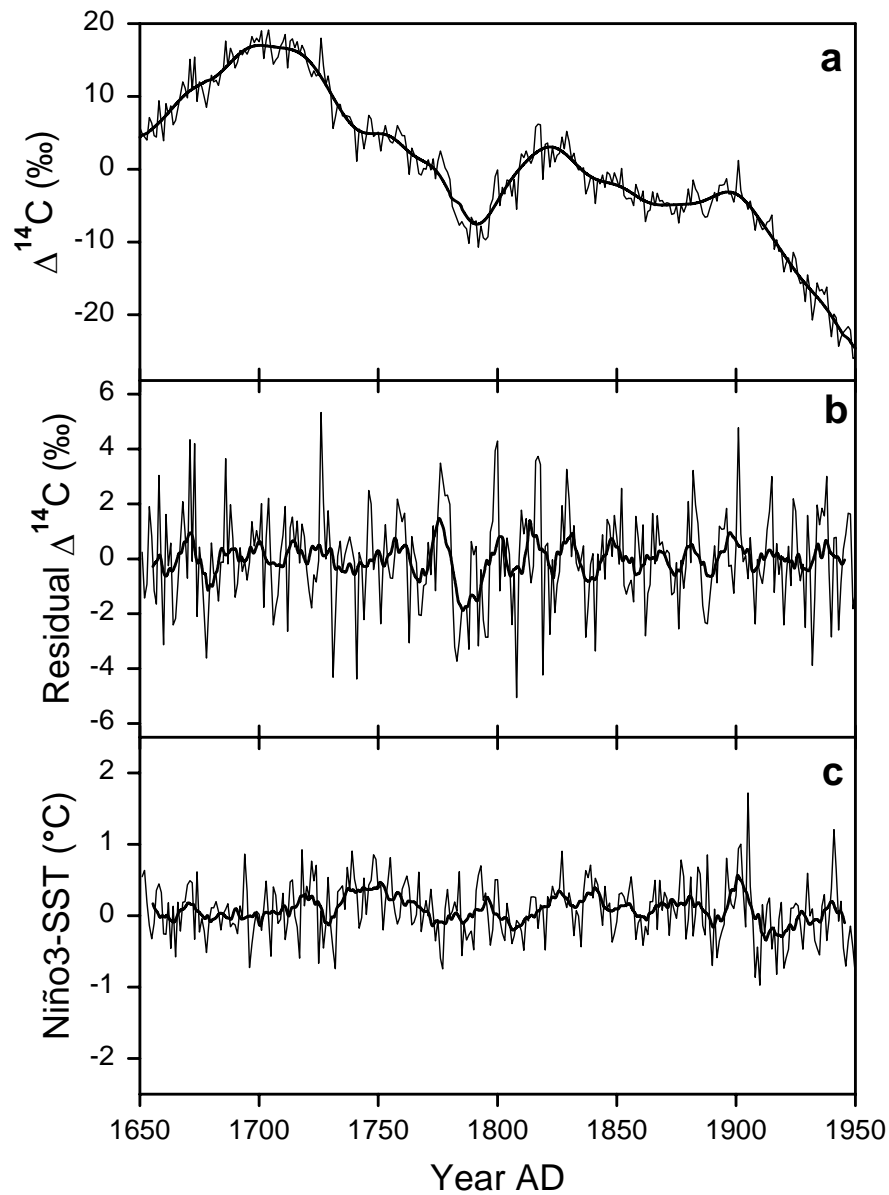


Figure 4-9 Tree-ring ^{14}C and El Niño strength during the pre-nuclear era. (a) High precision annual tree-ring $\Delta^{14}\text{C}$ from northwest Pacific coast, Washington, U.S.A. (Stuiver, et al., 1998b). The thick line is the secular trend, obtained by smoothing the raw data using a FFT filter. (b) Residual $\Delta^{14}\text{C}$ after removing the secular trend from the raw $\Delta^{14}\text{C}$ data. (c) Reconstructed Niño-3 SST index (Mann, et al., 2000). The thick lines in (b) & (c) are the 10years running means of the respective data. The residual tree-ring $\Delta^{14}\text{C}$ time series from Washington is compared with the reconstructed Niño-3 SST index, to search for coherency of the positive $\Delta^{14}\text{C}$ anomalies with positive Niño-3 SST indices, between 1650 and 1950.

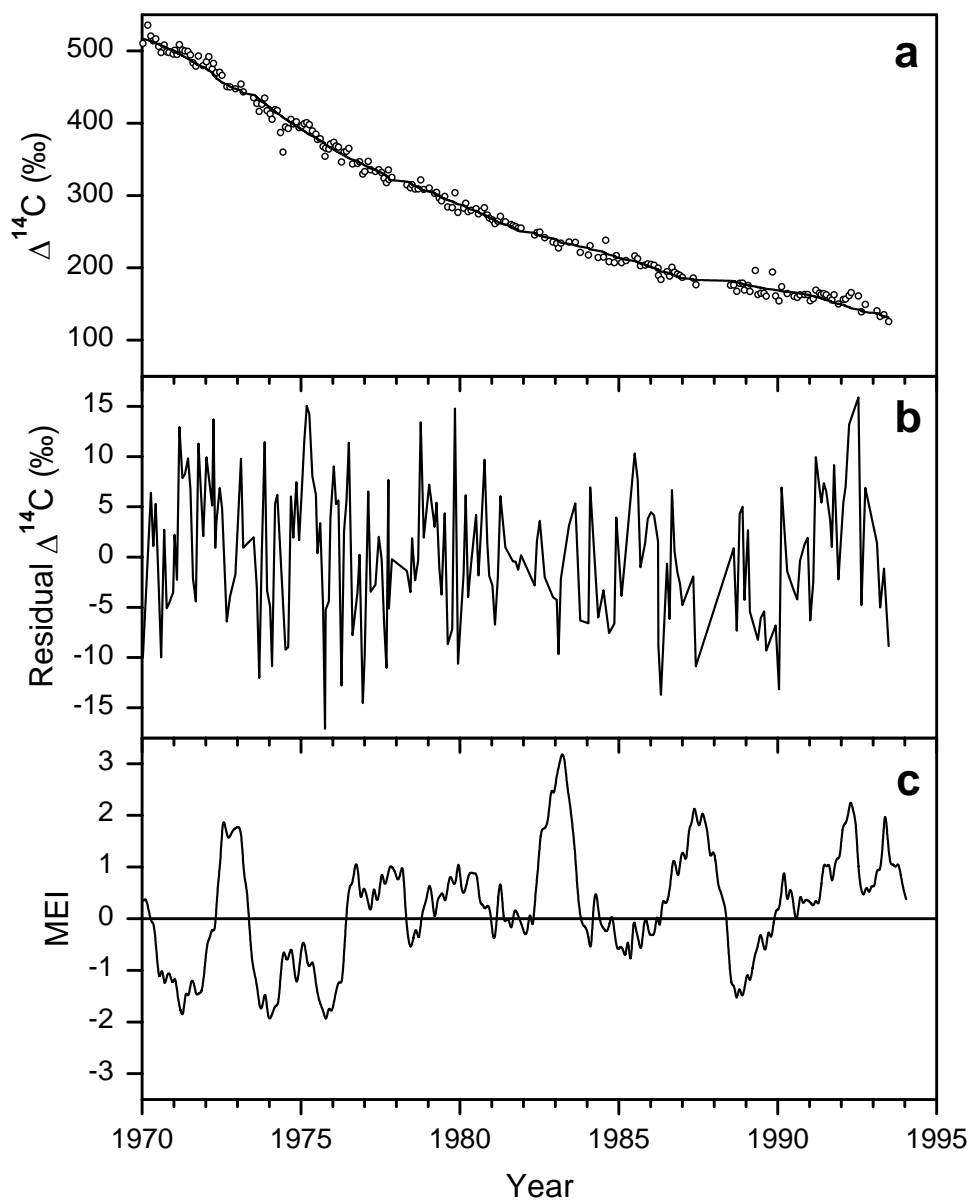


Figure 4-10 Tropospheric $\Delta^{14}\text{C}$ and El Niño strength in the post-nuclear era. (a) Bi-weekly to monthly $\Delta^{14}\text{C}$ from Wellington, New Zealand (Manning and Melhuish, 1994). The quasi-exponential secular trend, shown by the thick line was obtained by smoothing the raw $\Delta^{14}\text{C}$ data using a FFT filter. (b) Residual $\Delta^{14}\text{C}$ after removing the secular trend from the raw $\Delta^{14}\text{C}$ data. (c) Multi-variate ENSO index or MEI (Wolter, 2001). Positive MEI values depict El Niño conditions, while negative MEI indicate La Niña phase. The residual $\Delta^{14}\text{C}$ time series from Wellington is compared with the MEI, to search for coherency of positive $\Delta^{14}\text{C}$ anomalies with high MEI values, between 1970 and 1993.

4.5.4 Spectral and cross-spectral analyses of detrended $\Delta^{14}\text{C}$ and ENSO indices

The power spectra of detrended $\Delta^{14}\text{C}$ and the ENSO time series are obtained using the package REDFIT (Schulz and Mudelsee, 2001). Coherency and phase relations between the time series were obtained using the package SPECTRUM (Schulz and Stattegger, 1997). The program determines the Lomb–Scargle periodogram for unevenly spaced time series. The spectrum and the coherence are obtained by splitting the two time series into a number of equal and 50% overlapping segments, using Welch–I type spectral window.

Tree-ring $\Delta^{14}\text{C}$ and Niño-3 SST: Spectral analysis of the residual $\Delta^{14}\text{C}$ data for the period 1650–1950 AD after removing the secular trend (Fig. 4–9a), show significant cycles centered at 17, 13, 11.4 to 9.8, 6.6 to 5.6, 4.7 and 3.4 to 3.1yr (Fig. 4–11a). For the same period, the Niño-3 SST index shows significant cycles, centered at 14, 9.2, 6.6 to 4.8, 4.5 to 3.8, 3.5 and 2.8yr (Fig. 4–11b). Cross-spectral analysis of the residual $\Delta^{14}\text{C}$ and Niño-3 SST index for the period 1650–1950 AD revealed significant coherencies centered within 9.2 to 8.2, 6.9 to 6.2 and 3.8 to 3.6yr, with positive ^{14}C anomalies correlating to warm SST anomalies or El Niño (Fig. 4–11c). The phase lags are nearly zero at the frequencies of highest coherence, which indicate that these anomalies are mostly synchronous (Fig. 4–11d). However, within the total range of spectral resolution, the ^{14}C anomalies apparently lead Niño-3 SST by ~ 1 yr.

Wellington $\Delta^{14}\text{C}$ and MEI: Spectral analysis of detrended Wellington $\Delta^{14}\text{C}$ data show significant peaks centered within 5.8 to 4.5yr and 3.2 to 2.6yr, above the red noise level (Fig. 4–12a). According to Manning, *et al.* (1990), $\Delta^{14}\text{C}$ at Wellington exhibits an annual cycle, with maximum $\Delta^{14}\text{C}$ around July and minimum around February. However the analysis done in this work shows, annual cycle is much less significant than the interannual variations, indicated by shorter peak at $1\text{cycle}\cdot\text{year}^{-1}$. The MEI within the same period shows cycles of 5.4 to 3.1yr and 2.7 to 2.0yr (Fig. 4–12b). Cross-spectral analysis of the detrended monthly Wellington $\Delta^{14}\text{C}$ data with bimonthly multi-variate ENSO index (MEI) show significant coherency centered within period of 5.8 to 3.6yr, correlating positive ^{14}C anomaly with positive MEI values, *i.e.*, El Niño (Fig. 4–12c). As in tree-rings, the ^{14}C anomalies at Wellington are synchronous with positive MEI values, indicated by zero phase lag at frequency of highest coherence (Fig. 4–12d). Again, within the entire range of spectral resolution, the positive ^{14}C anomalies lead positive MEI values by ~ 1 yr on the average.

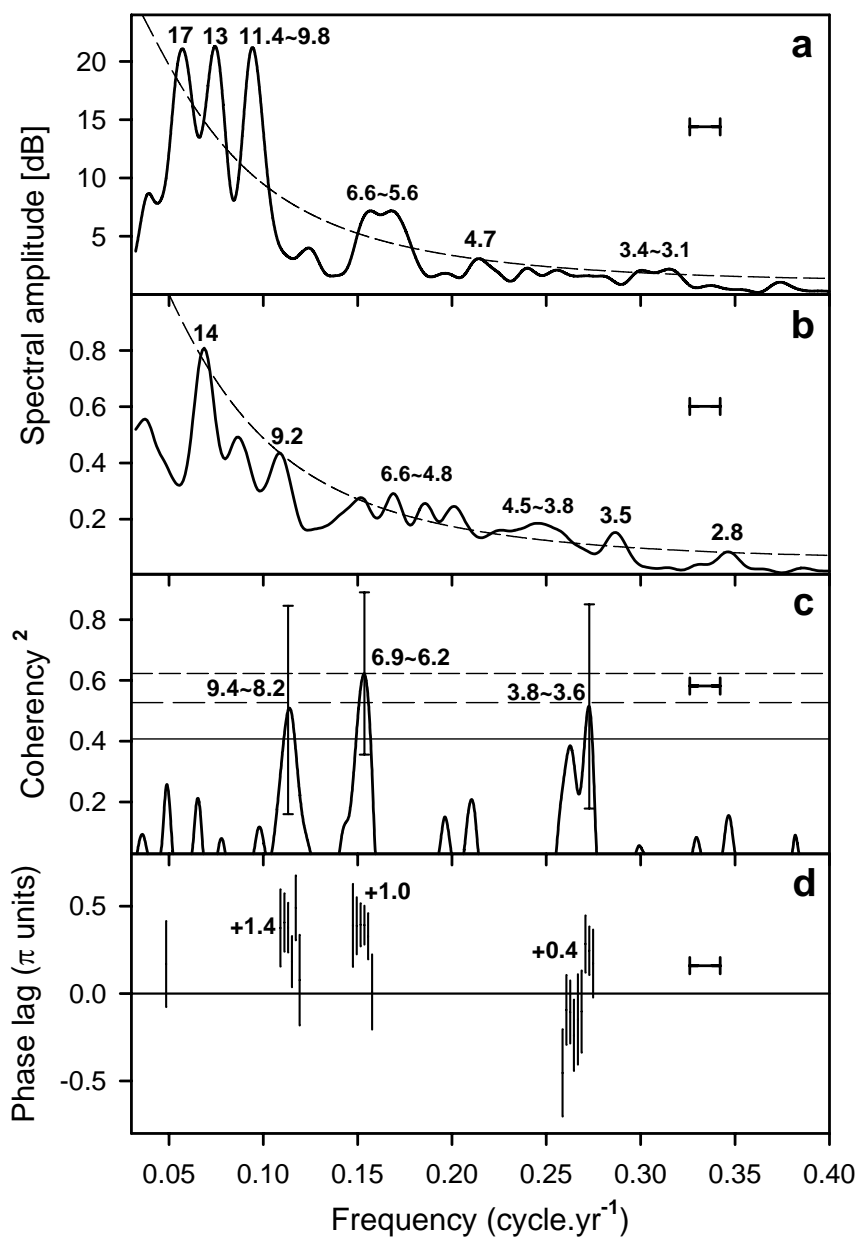


Figure 4-11 Spectral and cross-spectral analysis of the detrended Washington tree-ring $\Delta^{14}\text{C}$ and the Niño-3 SST index (1650–1950 AD). (a) Spectrum of residual $\Delta^{14}\text{C}$ and (b) Niño-3 SST data. The dashed line is the red noise background (upper 90% χ^2 , Schulz and Mudelsee, 2001). Peaks significant above the red noise background are labeled. The solid bar in all plots represents the 6dB bandwidth for spectral resolution. (c) Coherence between $\Delta^{14}\text{C}$ and Niño-3 SST (Schulz and Stahle, 1997). The squared coherence values indicate the fraction of variance of ^{14}C and SST that are linearly correlated. The horizontal lines from bottom to top are the 80%, 90% & 95% false alarm level. The periods of significant coherence are labeled. (d) The phase relationship between ^{14}C and SST anomalies. Positive phase lags indicate positive $\Delta^{14}\text{C}$ anomaly leads warm Niño-3 SST. Average phase lags (in years) over the window of spectral resolution centered at frequencies of highest coherence are labeled.

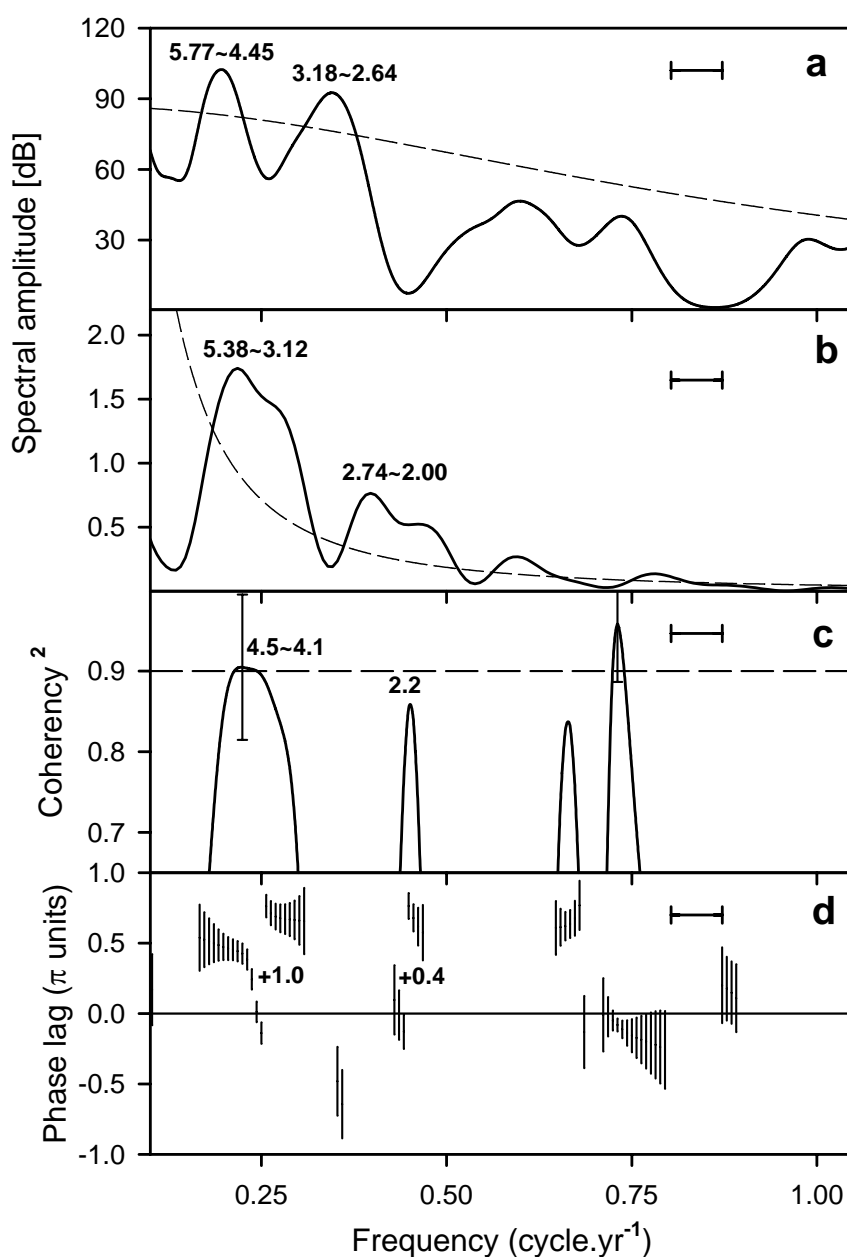


Figure 4–12 Spectral and cross-spectral analysis of the detrended Wellington $\Delta^{14}\text{C}$ and the MEI (1970–1993 AD). (a) Spectrum of detrended Wellington $\Delta^{14}\text{C}$ and (b) MEI data. The dashed line is the red noise background (upper 90% χ^2 , Schulz and Mudelsee, 2001). The peaks significant above the red noise background are labeled. The solid bar in all plots represents the 6dB bandwidth for spectral resolution. (c) Coherence between $\Delta^{14}\text{C}$ and MEI (Schulz and Stettger, 1997). The squared coherency values indicate the fraction of variance of ^{14}C and SST that are linearly correlated. The horizontal dashed line is the 80% false alarm level. The periods of significant coherence are labeled. (d) The phase relationship between ^{14}C and MEI. Positive phase lags indicate positive $\Delta^{14}\text{C}$ anomaly leads positive MEI (El Niño). Average phase lags (in years) over the window of spectral resolution centered at frequencies of highest coherence are labeled.

4.5.5 Discussion on coherence between tropospheric $\Delta^{14}\text{C}$ and ENSO

Stuiver and Braziunas (1993b) discussed the significant cycles between 2 to 17yr range in the Washington tree-ring ^{14}C record. The cycles in the 9.8 to 11.4yr range (with amplitude of $\sim 1.4\text{‰}$) corresponds to the Schwabe sunspot cycle of $\sim 11\text{yr}$. The longer cycles of 13 and 17yr are also possibly resulting from solar modulation. As mentioned before, the variance of $\Delta^{14}\text{C}$ in Washington tree-rings in the 2 to 6.4yr range with amplitude of $\sim 1\text{‰}$ have been attributed to ENSO related thermohaline circulation changes in the tropical Pacific (Stuiver and Braziunas, 1993b). However, the 2.10, 2.68, 3.54 and 5.68yr cycles in the same Washington $\Delta^{14}\text{C}$ data were interpreted as the 5th, 4th, 3rd and 2nd harmonics respectively of the Schwabe cycle, having fundamental period of 10.8yr (Peristykh and Damon, 1998). It is unlikely that the cycles shorter than $\sim 7\text{yr}$ are a result of ^{14}C production rate changes, given higher attenuation of the variance at these frequencies by the atmospheric carbon reservoir. In the post-bomb record, the interannual variability of Wellington $\Delta^{14}\text{C}$ has maximum amplitude of $\sim 15\text{‰}$ (Fig. 4–10b). The interannual variations are much stronger than the annual cycle, indicated by weaker power at $1\text{cycle}\cdot\text{year}^{-1}$ (Fig. 4–12b). Manning, *et al.*, (1990) reported an annual cycle in the Wellington $\Delta^{14}\text{C}$ data, whose peak-to-peak amplitude was $\sim 20\text{‰}$ in 1966, $\sim 3\text{‰}$ in 1980 and $\sim 5\text{‰}$ after 1980.

The significant coherencies between $\Delta^{14}\text{C}$ and the El Niño events shown in the Fig. 4–11c and 4–12c indicate that, ENSO related changes of the tropical CO_2 fluxes indeed influence tropospheric $\Delta^{14}\text{C}$ both in the pre-bomb as well as in the post-bomb era. A part of the variation of $\Delta^{14}\text{C}$, both during the pre-bomb and the post-bomb era is synchronous with the ENSO events, indicated by near zero phase lags at the periods of highest coherence (Fig. 4–11d and 4–12d). Some conclusions can be derived from the detailed features of the phase lags between $\Delta^{14}\text{C}$ and the ENSO indices. As can be seen in Figs. 4–11d and 4–12d, a part of the positive $\Delta^{14}\text{C}$ anomalies occur prior to the onset of the ENSO events (by approximately one year or less), indicated by the presence of positive phase lags of ^{14}C in both records. In the tree-ring $\Delta^{14}\text{C}$, positive phase lags are more prominent in the longer periods (8 to 9yr and 6 to 7yr). The longer periods of El Niño are normally associated with strong to very strong events (which are relatively rare). During such events, oceanic CO_2 flux from the equatorial Pacific probably drops much earlier, well before the main warm SST event which

continue in the following year. An early reduction of oceanic CO₂ flux can be recorded by Washington tree-rings, whose growth peaks during late spring. From the inversion of atmospheric concentration and stable isotopic composition, Rayner, *et al.*, (1999) demonstrated that interannual variability of the tropical CO₂ fluxes significantly correlate with southern oscillation index (SOI), with flux anomalies leading the SOI anomaly by 4 to 9 months. This is caused since negative CO₂ flux anomalies from oceans are synchronous or lead early months of the ENSO events by few months and positive anomalies from lands occur toward the end of these events. Thus, the lead of $\Delta^{14}\text{C}$ anomaly relative to the ENSO indices points to the reduction of oceanic CO₂ flux as the main source of the observed positive ¹⁴C anomaly in the atmosphere. It is important to note here, that the observed modulation of $\Delta^{14}\text{C}$ by the El Niño events is mainly due to switching on and off of the tropical CO₂ flux from the Pacific, as also observed earlier by Rozanski, *et al.*, (1995). The ENSO events are also associated with higher $\Delta^{14}\text{C}$ values (by about 40‰) in the surface ocean DIC, as observed from coral ¹⁴C measurements, due to reduction in upwelling of deeper ¹⁴C depleted water and advection of water from the sub-tropics with higher ¹⁴C (Druffel, 1987; Brown, *et al.*, 1993; Guilderson, *et al.*, 1998, 1999, 2000b). Increase of $\Delta^{14}\text{C}$ in oceanic DIC may result in higher atmospheric $\Delta^{14}\text{C}$, but with a delayed response of ~2yrs, considering the equilibration time of CO₂ between the atmosphere and ocean.

Emissions of biospheric CO₂ during the El Niño events during the post-bomb period might have played a major role to cause interannual $\Delta^{14}\text{C}$ variations in the atmosphere. However, this is not apparent from the phase relations shown by the Wellington $\Delta^{14}\text{C}$ data (Fig. 4–12d), where $\Delta^{14}\text{C}$ leads the ENSO indices by <1yr. Moreover, during the very strong El Niño event of 1997-1998, the positive $\Delta^{14}\text{C}$ anomaly was observed over the Bay of Bengal during February 1997, about 9 months ahead of the peak event which took place around November 1997. If the biospheric CO₂ flux is responsible to cause the interannual $\Delta^{14}\text{C}$ variations, the positive $\Delta^{14}\text{C}$ anomalies are expected to lag the MEI indices, since these fluxes mainly occur in the late or matured phases of the El Niño events (Yang and Wang, 2000). Anomalous stratosphere-troposphere exchange could be a possible candidate for the observed anomaly. The trend of fossil fuel consumption doesn't show any decrease during 1996 or 1997 (Marland, *et al.*, 2000), which can explain the observed positive anomaly of $\Delta^{14}\text{C}$ over the northern Indian Ocean.

Detailed analysis of monthly high precision $\Delta^{14}\text{C}$ records for longer period from various tropical sampling stations will help to identify the exact origin of $\Delta^{14}\text{C}$ variations in the atmosphere during El Niño. The number of annual tree-ring $\Delta^{14}\text{C}$ records and direct atmospheric measurements from tropical regions are too meager, to provide spatially consistent proof of atmospheric $\Delta^{14}\text{C}$ modulation by ENSO events.

4.6 Conclusions

The spatial and temporal variations of $\Delta^{14}\text{C}$ values observed over the northern Indian Ocean, between 1993 and 1999 show:

- (a) The $\Delta^{14}\text{C}$ of CO_2 in the air over the northern Indian Ocean were: $109 \pm 3\%$ in 1997 over the Bay of Bengal, $97 \pm 2\%$ in 1998 over the Arabian Sea and $88 \pm 2\%$ in 1999 over the Bay Bengal.
- (b) During the 1990's $\Delta^{14}\text{C}$ has been decreasing at the rate of $5\%.\text{yr}^{-1}$ on an average. The decrease corresponds to average e-folding time of about 17yr for the removal of tropospheric ^{14}C over this region.
- (c) $\Delta^{14}\text{C}$ in air overlying the Arabian Sea appears to be lower than that over the Bay of Bengal (by about 5%, comparing the $\Delta^{14}\text{C}$ values of non-ENSO years 1995 and 1999). This is due to the fact that the Arabian Sea is a perennial source of CO_2 to the atmosphere. Evasion of ^{14}C -depleted CO_2 from the Arabian Sea through upwelling causes depletion of $\Delta^{14}\text{C}$ in the atmosphere overlying this basin.
- (d) The interannual variations of $\Delta^{14}\text{C}$ over this region apparently correlate with the onset of warm phase of the El Niño/Southern Oscillation events.

Spectra of atmospheric $\Delta^{14}\text{C}$ variations both for the pre-bomb and the post-bomb periods show variations at ENSO time scales. Cross-spectral analyses of the high-frequency atmospheric $\Delta^{14}\text{C}$ variations for past three centuries before 1950 and for the two decades after 1970 show significant coherency in the major ENSO bands, with positive ^{14}C anomaly correlating with and leading the El Niño events by approximately one year. This suggests modulation of tropospheric $\Delta^{14}\text{C}$ by the ENSO events, with enrichment of CO_2 in ^{14}C during the warm phases of ENSO (El Niño).

Chapter 5

^{14}C in the Northern Indian Ocean: Two Decades after GEOSECS

5.1 Hydrographic features of the northern Indian Ocean

The hydrography of the northern Indian Ocean basin have been described in details by several workers, and various water masses have been identified, based on their temperature, salinity and nutrient contents (Emery and Meincke, 1986; Warren, 1992; You and Tomczak, 1993; You, 1997). The top 500m of the basin is made of a number of water masses which have been identified based on their temperature, salinity and nutrient characteristics. The potential temperature (θ) and salinity (s) plots of the northern Indian Ocean stations described in this study are shown in Fig. 5–1, where the θ - s ranges of various water masses, as identified by the above workers are also shown. These are: (i) BBW–Bengal Bay water, the low salinity surface water in the Bay of Bengal; (ii) ASW–Arabian Sea water, the high salinity surface water in the Arabian Sea; (iii) IEW–Indian equatorial water, formed in the western equatorial region; (iv) NICW–North Indian Central water, thermocline water below the surface in the Bay of Bengal; (v) AAMW–Australasian Mediterranean water, which flows in through the Indonesian passage; (vi) ICW–Indian central water, sub tropical surface water formed at 40-45°S latitudes; (vii) PGW and RSW–Persian Gulf and Red Sea water, the high salinity and low oxygen water masses which are prominent in the northwestern Indian Ocean; (viii) AABW–Antarctic bottom water, the cold and oxygen rich deepest water mass in this region, originating from Antarctica.

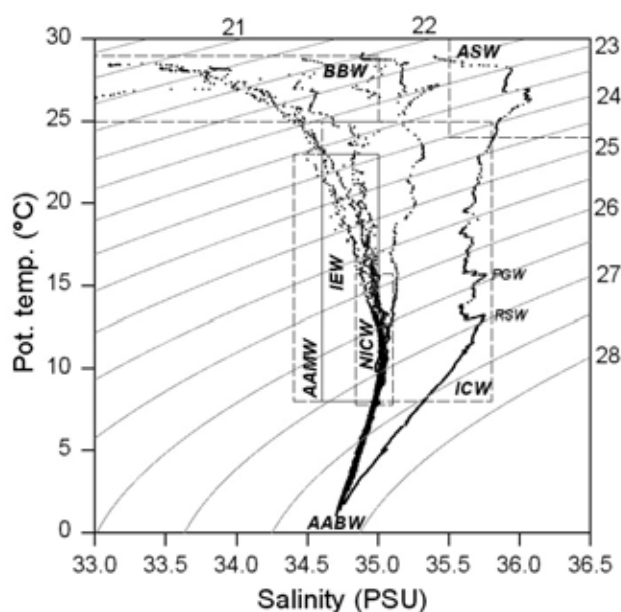


Figure 5–1 θ - S profiles of the seawater sampling stations in the northern Indian Ocean. The σ_θ contours are labeled at the top and right axes. The θ - S ranges of the principal water masses are shown by dashed rectangles.

Goyet, *et al.*, (1999) called the IEW, NICW as IIW (Indian intermediate water) and BBIW (Bay of Bengal intermediate water), and identified two deep-water masses in this region as DIW (deep Indian water) and BW (bottom water). As can be seen in Fig. 5–1, the θ - s plot for the Arabian Sea station near the Gulf of Aden (far right curve) is distinctly different from all other stations, which are mainly in the Bay of Bengal and one in the equatorial Indian Ocean. Steeper isopycnal gradient is evident in the Bay of Bengal than in the Arabian Sea.

The large differences in the hydrographic properties in the northern Indian Ocean would result in complex behavior of the movement of tracers within this basin. Modeling the temporal variations of ^{14}C in the northern Indian Ocean is difficult due to water inputs from the Red Sea and the Indonesian throughflow region having different ^{14}C contents, and also due to the changing monsoonal circulation patterns.

5.2 Distribution of ^{14}C in the northern Indian Ocean two decades after the GEOSECS

The ^{14}C measurements made in the Arabian Sea and the Bay of Bengal during the late 1990s offer a way to assess the temporal changes in the inventories of bomb- ^{14}C and its penetration into the ocean, in two decades since the GEOSECS expeditions conducted during 1977–1978. The ^{14}C depth profiles, measured at seven stations in the northern Indian Ocean, six stations in the Bay of Bengal and one in the Arabian Sea (near the Red Sea mouth, in the Gulf of Aden) obtained during the cruises conducted between 1997 and 1999, will be described here.

To assess the temporal changes of bomb- ^{14}C , data on the steady state or pre-nuclear $\Delta^{14}\text{C}$ profiles are required. In the absence of the measurements of pre-nuclear $\Delta^{14}\text{C}$ profiles, they can be reconstructed based on the pre-nuclear surface $\Delta^{14}\text{C}$ (from marine shells) and the profiles of bomb produced ^3H or dissolved silica (Broecker, *et al.*, 1985, 1995). In this work, the pre-nuclear $\Delta^{14}\text{C}$ profiles for different stations are reconstructed from the measured SiO_2 data, based on the empirical linear relationship for the global ocean between the natural $\Delta^{14}\text{C}$ and SiO_2 ($\Delta^{14}\text{C}_{\text{natural}} = -70 - \text{SiO}_2$), established by Broecker, *et al.*, (1995). Here $\Delta^{14}\text{C}$ is expressed in permil (‰) and SiO_2 in micromole per kg ($\mu\text{mol.kg}^{-1}$). The procedure of reconstructing the pre-nuclear $\Delta^{14}\text{C}$ profile is explained in Appendix–C. The above linear relationship has been derived from the $\Delta^{14}\text{C}$ – SiO_2 data of GEOSECS samples deeper than 1000m,

which are uncontaminated with bomb- ^{14}C and tritium. Deep waters originating from Antarctic circum-polar regions have relatively higher $\Delta^{14}\text{C}$ and therefore deviate from the above linear relationship. From the GEOSECS deep-water samples of the Arabian Sea and the Bay of Bengal with $\text{SiO}_2 > 50\mu\text{mol.kg}^{-1}$, Bhushan, *et al.*, (2000) obtained a relation $\Delta^{14}\text{C}_{\text{natural}} = -80 - 0.83\text{SiO}_2$. The pre-nuclear $\Delta^{14}\text{C}$ profiles based on this relation and those derived from Broecker, *et al.*, (1995) are consistent within $\pm 10\%$. The estimated uncertainty of reconstructing the pre-nuclear $\Delta^{14}\text{C}$ using the linear relation of Broecker, *et al.*, (1995) is also $\pm 10\%$ (Peng, *et al.*, 1998). Therefore, reconstruction of pre-nuclear $\Delta^{14}\text{C}$ for the northern Indian Ocean using the relation ($\Delta^{14}\text{C}_{\text{natural}} = -80 - 0.83\text{SiO}_2$) will not be significantly different from that derived using the relation of Broecker, *et al.*, (1995). Hence, all the pre-nuclear profiles have been calculated from the relation ($\Delta^{14}\text{C}_{\text{natural}} = -70 - \text{SiO}_2$).

The pre-nuclear surface $\Delta^{14}\text{C}$ values used in this study for different regions are based on the $\Delta^{14}\text{C}$ measurements of pre-nuclear shells (*sec.* 3.5), rounded off to nearest 5%. The surface SiO_2 values are adjusted to match the reconstructed pre-nuclear surface $\Delta^{14}\text{C}$ with the values estimated from shells. The pre-nuclear surface $\Delta^{14}\text{C}$ values adopted for different regions of the northern Indian Ocean are given in Table 5–1. Locations nearest to the region, from where pre-nuclear shell or coral samples were measured for $\Delta^{14}\text{C}$ are also mentioned.

Table 5–1:
Pre-nuclear surface $\Delta^{14}\text{C}$ values adopted for the northern Indian Ocean

Region	Surface $\Delta^{14}\text{C}_{\text{natural}}$
Northern Bay of Bengal (<i>Chilika Lake</i>)	–50‰
Central Bay of Bengal and Andaman Sea (<i>Stewart Id.</i>)	–55‰
Southern Bay of Bengal (<i>Rameswaram</i>)	–60‰
Equatorial Indian Ocean (<i>Rameswaram</i>)	–60‰
Southern Arabian Sea (<i>Rameswaram</i>)	–60‰
Central Arabian Sea (<i>Red Sea coral, [Cember, 1989]</i>)	–70‰
Northern Arabian Sea (<i>Dwarka and Port Okha</i>)	–80‰

The measured $\Delta^{14}\text{C}$ profiles are shown in Figs. 5–2 to 5–7. The sampled depths are indicated in the θ -S plots, shown in top graphs for each station (open circles), to compare the distributions of ^{14}C in different water masses. The measured $\Delta^{14}\text{C}$ profiles are shown in the bottom graphs (filled circles with $\pm 1\sigma$ errors). The reconstructed pre-nuclear $\Delta^{14}\text{C}$ profiles for these stations are also shown as dashed lines in the bottom graphs.

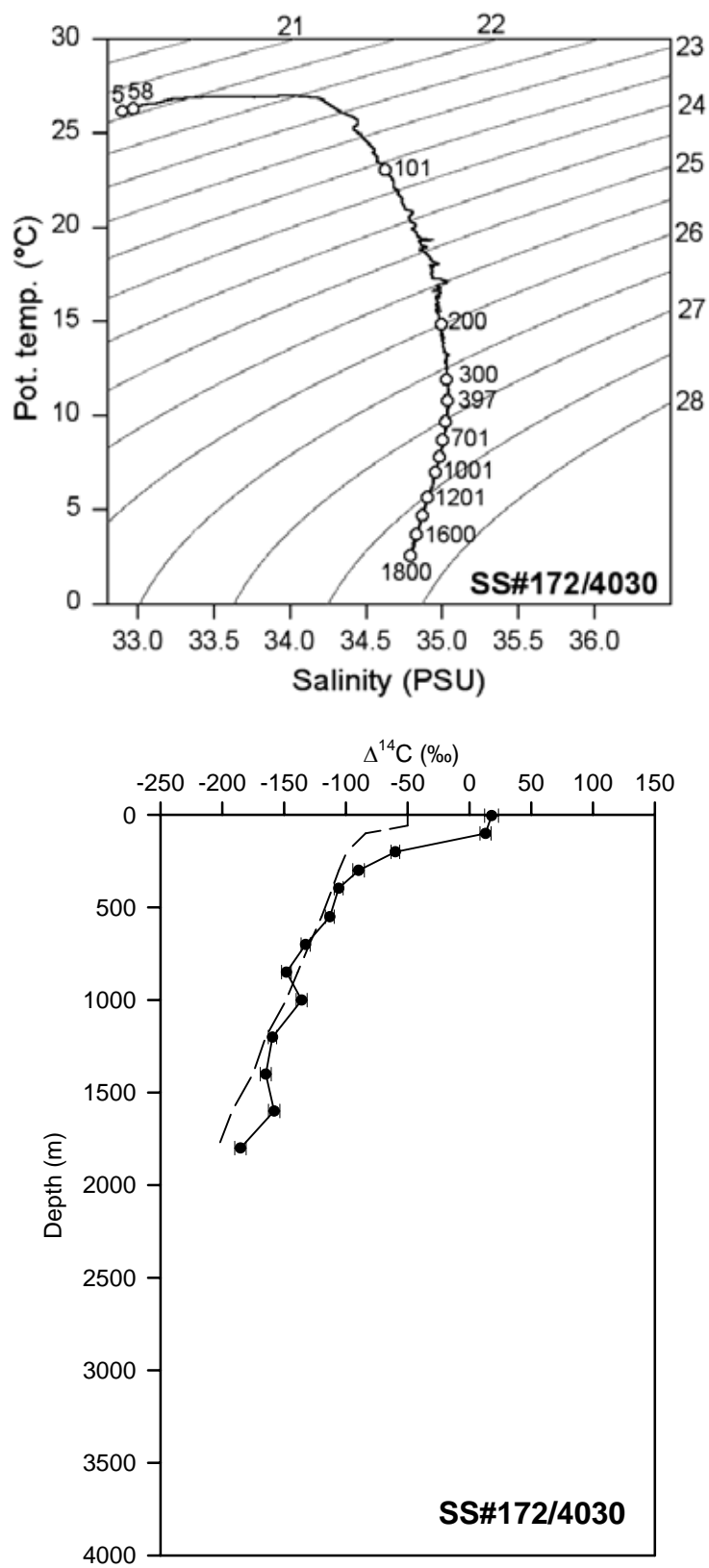


Figure 5-2 θ - S and radiocarbon profiles for the northern Bay of Bengal station SS#172/4030. The surface $\Delta^{14}\text{C}$ for this station is -18‰ , least when compared with all other stations of the Bay of Bengal.

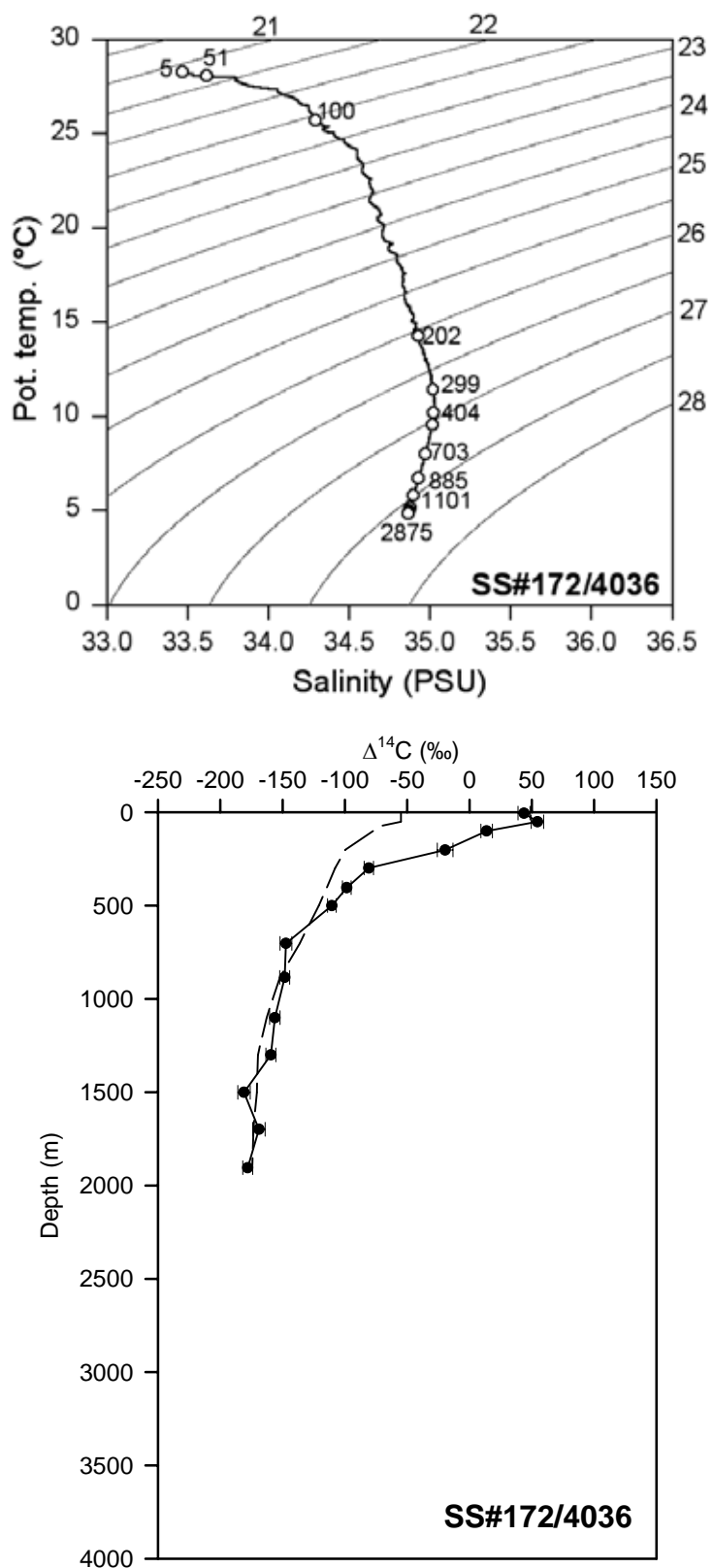


Figure 5-3 θ -S and radiocarbon profiles for the Andaman Basin station (north) SS#172/4036. Note the distinct subsurface maxima of $\Delta^{14}\text{C}$, which is observed in all stations of the Bay of Bengal during 1997 and 1999, except at SS#172/4030 (see text for discussion).

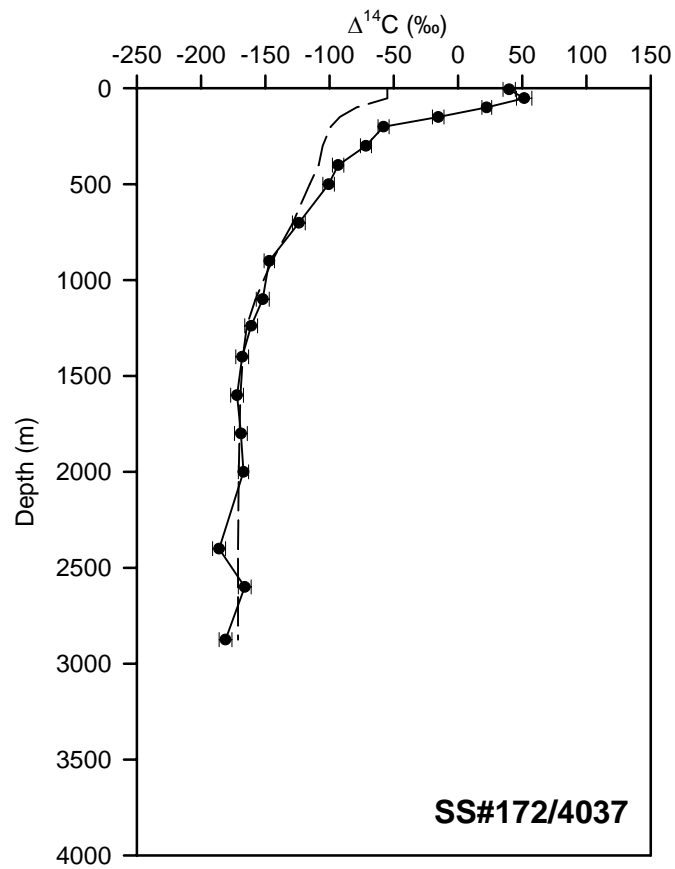
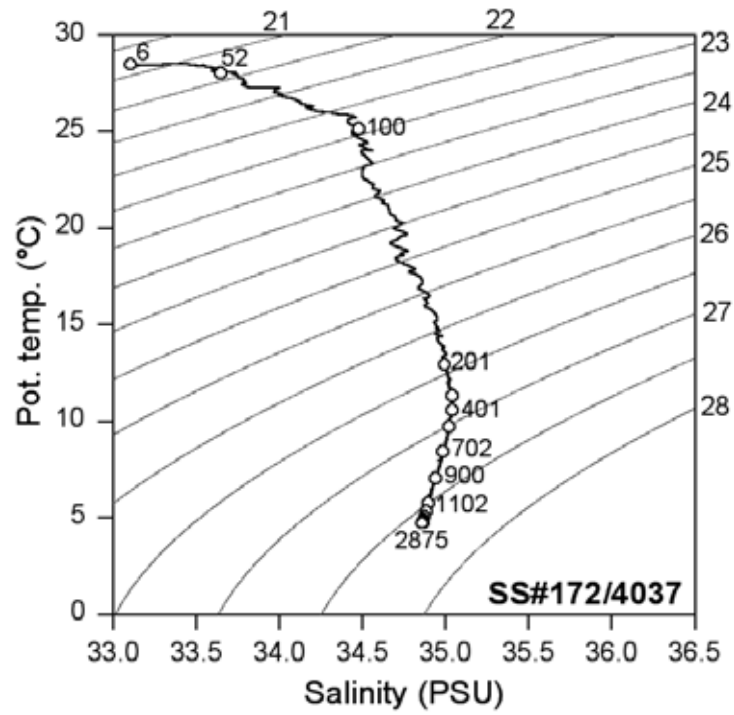


Figure 5-4 θ - S and radiocarbon profiles for the Andaman Basin station (south) SS#172/4037. Note near linear $\Delta^{14}\text{C}$ profile below ~1500m (see text for discussion).

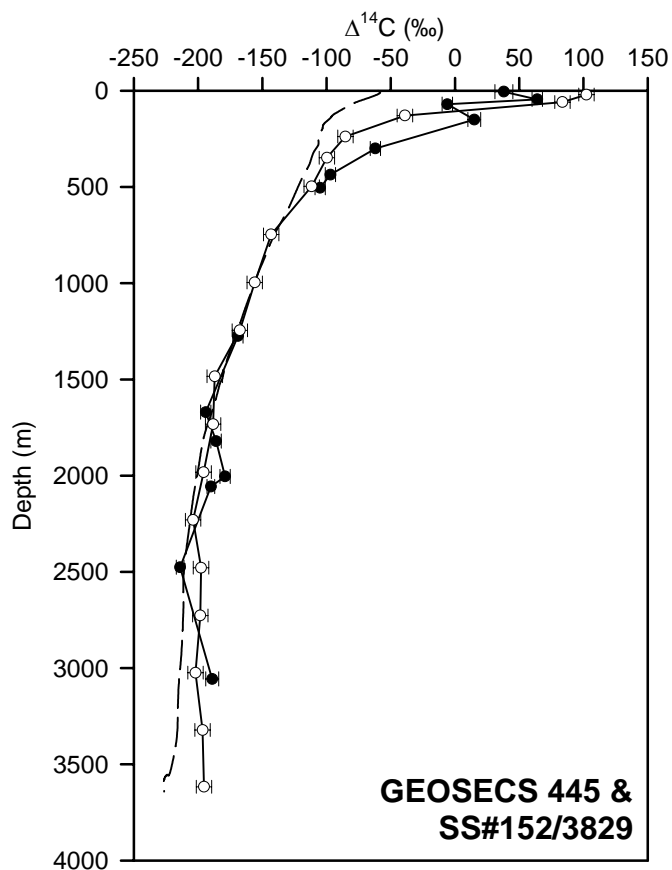
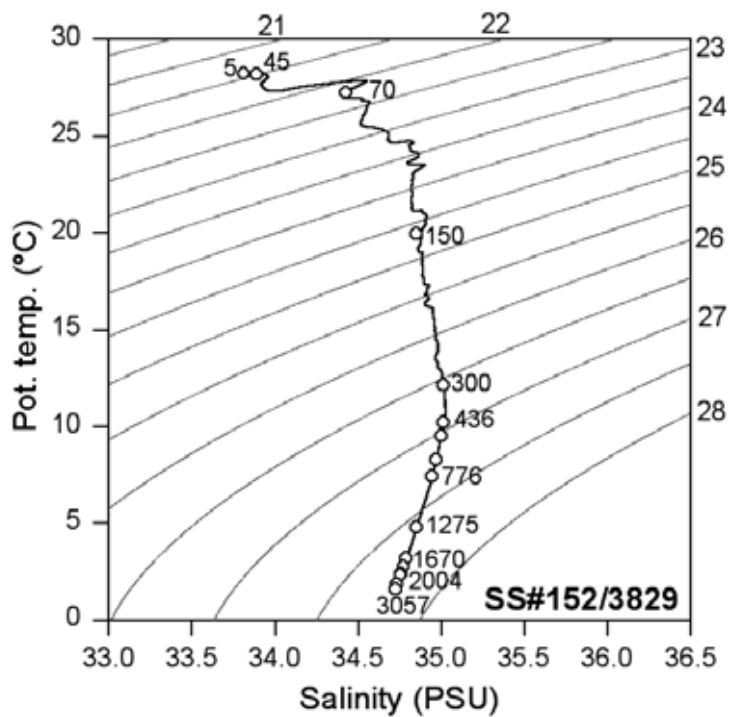


Figure 5-5 θ - S and radiocarbon profiles for the southern Bay of Bengal stations SS#152/3829 and GEOSECS 445. Open symbols: GEOSECS 445 and solid symbols: SS#152/3829. Note the deviation of measured $\Delta^{14}\text{C}$ profiles from the estimated pre-nuclear profiles below 2500m (see text for discussion).

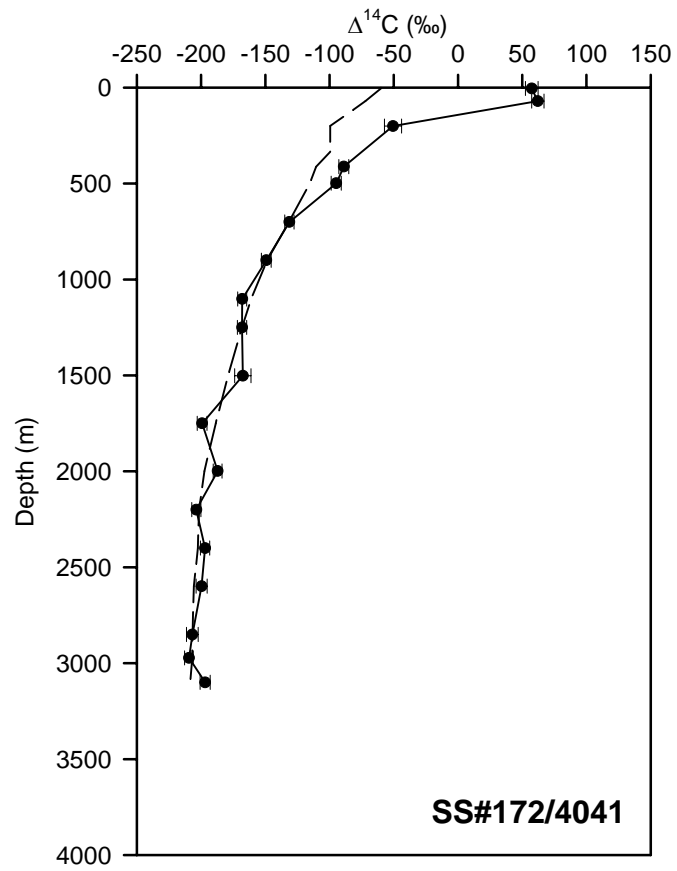
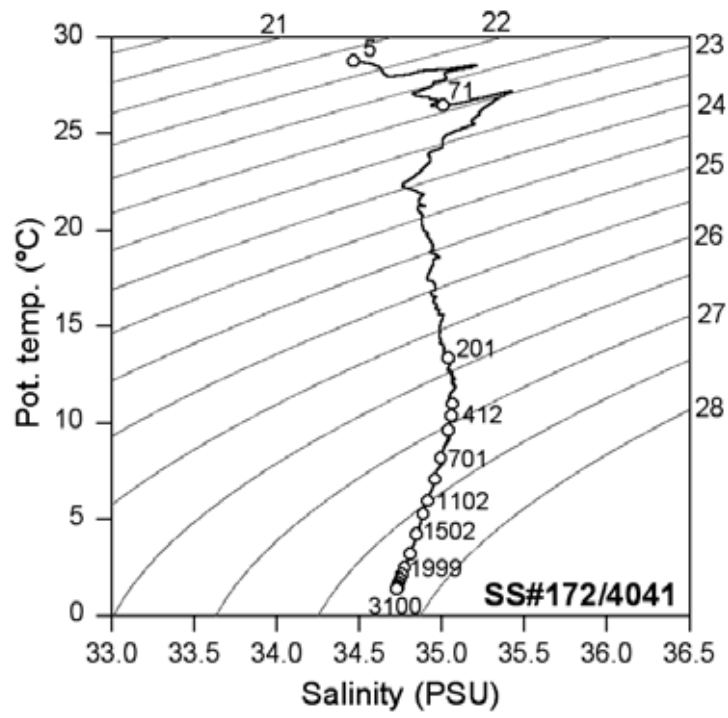


Figure 5-6 θ -S and radiocarbon profiles for the southern Bay of Bengal station SS#172/4041.

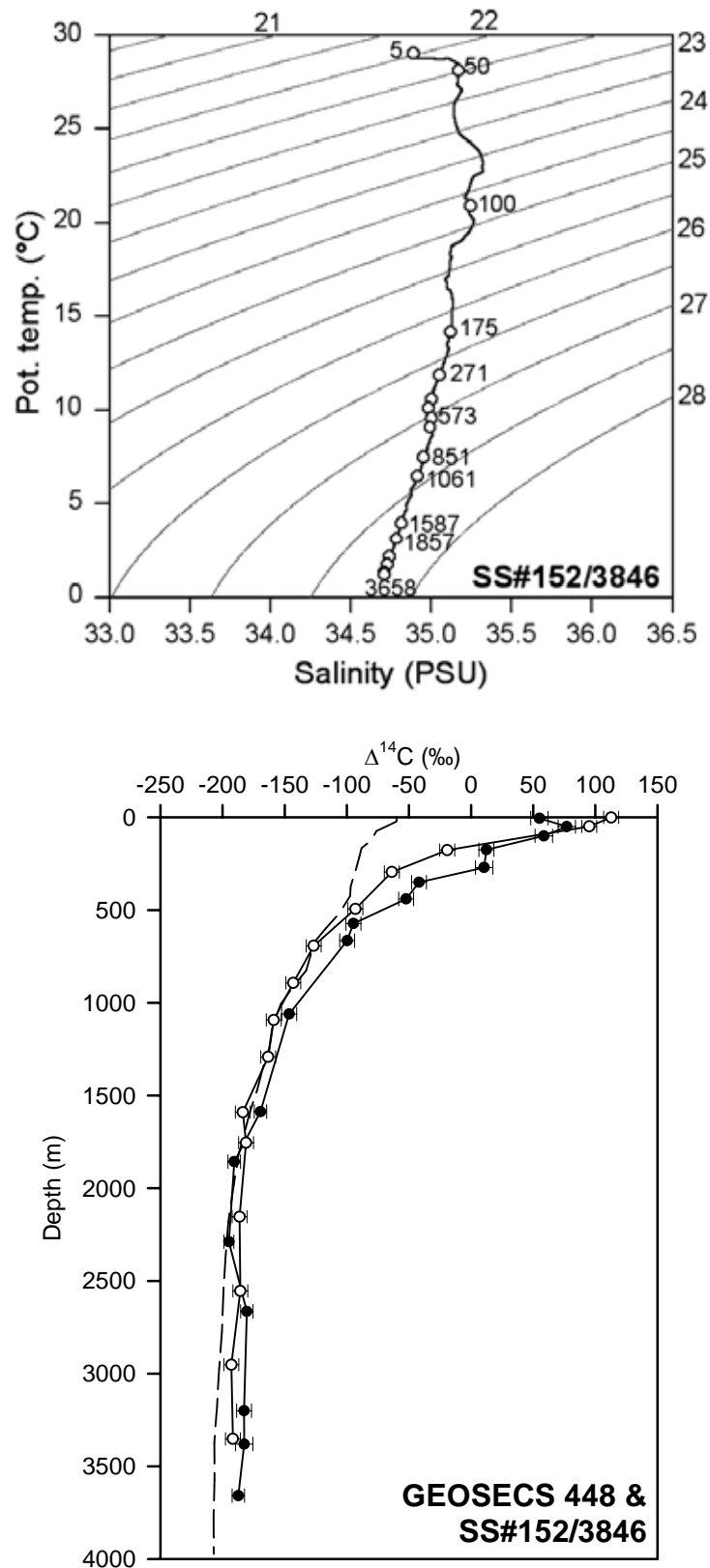


Figure 5-7 θ -S and radiocarbon profiles for the equatorial Indian Ocean stations south of Sri Lanka. Solid symbols: SS#152/3846 and open symbols: GEOSECS 448. The mean $\Delta^{14}\text{C}$ value below 2500m is -183‰ , and the minima of $\Delta^{14}\text{C}$ occurs between 1500-2500m, at -193‰ (see text for discussion).

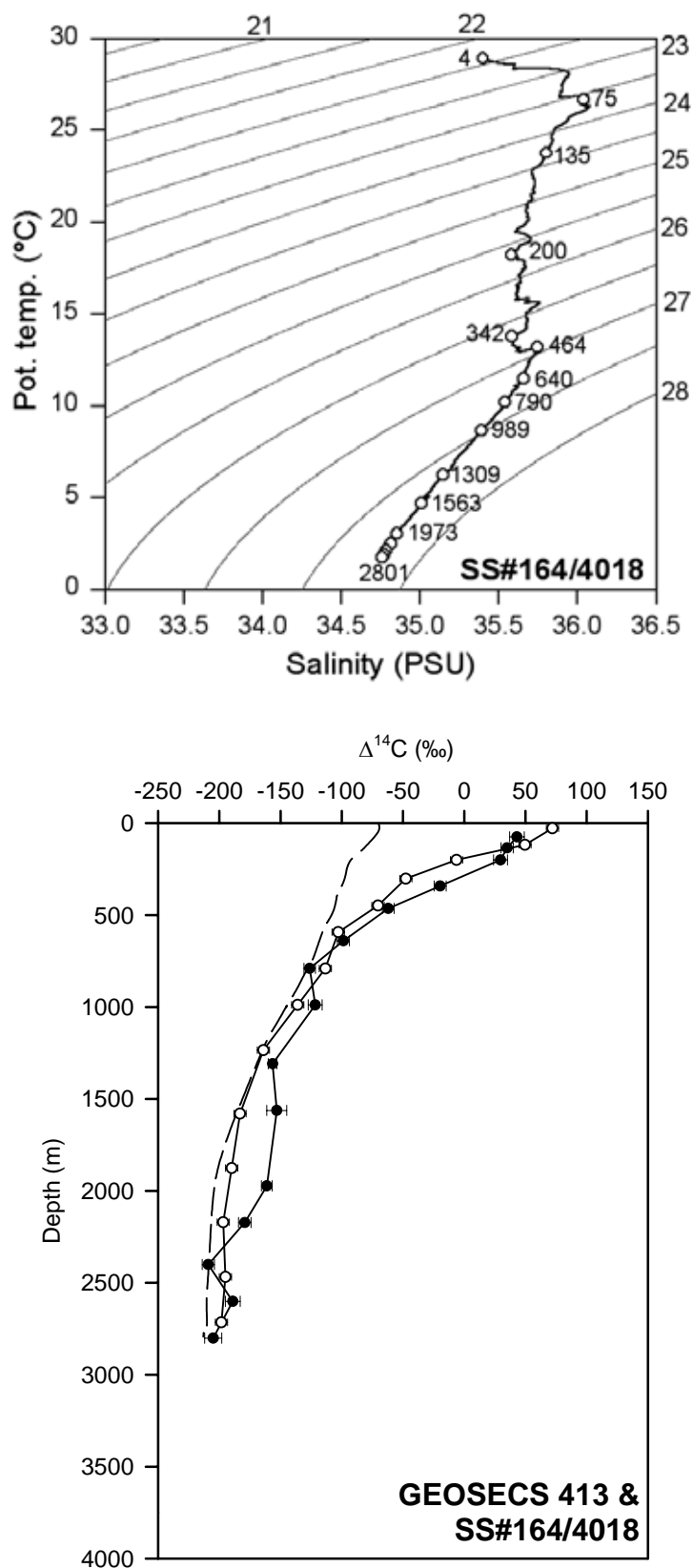


Figure 5-8 θ - S and radiocarbon profiles in the western Arabian Sea near the Red Sea mouth. Solid symbols: SS#164/4018 and open symbols: GEOSECS 413. Distinct change in $\Delta^{14}\text{C}$ is observed in the intermediate waters below 1500m and above 2500m, possibly due to increased inflow of sinking Red Sea waters with higher $\Delta^{14}\text{C}$ at these depths (see text for discussion).

Significant decrease in the $\Delta^{14}\text{C}$ values have been observed in the surface Bay of Bengal in two decades after the GEOSECS expedition of 1977-'78 (Fig. 5–9). During 1997 and 1999, the $\Delta^{14}\text{C}$ values of the surface waters (at ~5m) ranged from 57‰ in the southern Bay of Bengal (SS#172/4041) to a minimum of only 18‰ in the northern Bay of Bengal (SS#172/4030). The mean surface $\Delta^{14}\text{C}$ values for the Bay of Bengal stations between 9°N to 20°N are about 40‰; while for the surface equatorial Indian Ocean it is 55‰ (SS#152/3846). These values are lower by 60~80‰ than those measured during 1978, if the data at the GEOSECS stations 445 and 448 are compared. The decrease in the surface $\Delta^{14}\text{C}$ values in the Arabian Sea is only half this magnitude (~30‰). During the GEOSECS, significant contrast was seen between the surface $\Delta^{14}\text{C}$ values of the Arabian Sea (59 to 95‰) and the Bay of Bengal (107 to 117‰). This difference became insignificant after two decades, when the surface Arabian Sea recorded $\Delta^{14}\text{C}$ values of 40 to 58‰ during 1994 and 1995, compared to 40 to 57‰ in the Andaman Sea and the southern Bay of Bengal during 1997 and 1999.

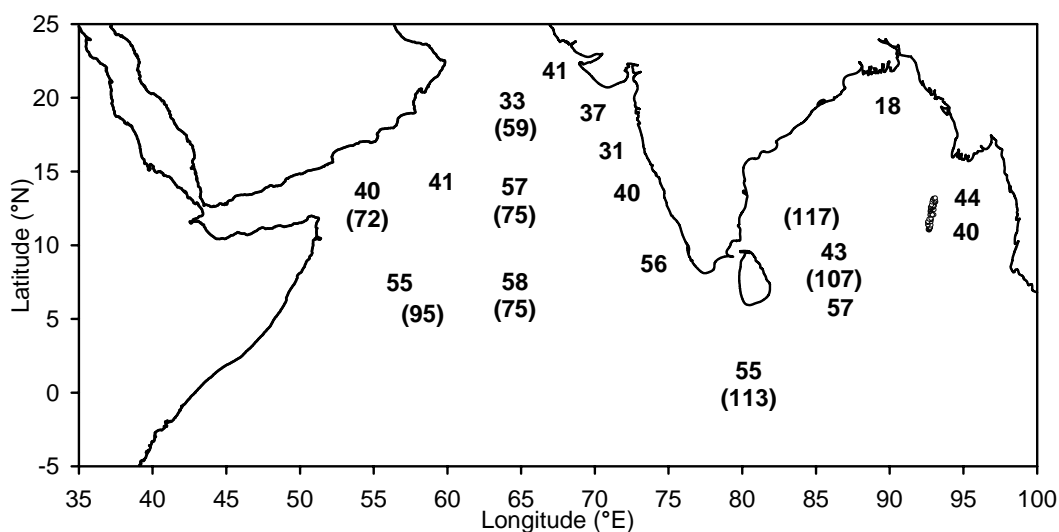


Figure 5–9 Distribution of $\Delta^{14}\text{C}$ (in ‰) in the surface northern Indian Ocean during late 1990s. The values in parentheses show the surface $\Delta^{14}\text{C}$ during 1977–1978 at the GEOSECS stations.

The reduction in the surface $\Delta^{14}\text{C}$ values can be partly attributed to the lowering of the atmospheric $\Delta^{14}\text{C}$ from ~300‰ during 1978 to ~90‰ in late 1990s and transfer of ^{14}C -enriched waters from the surface to the deeper layers through mixing. The later process appears to play a major role in the northern Indian Ocean as evidenced from the changes in their mean penetration depths.

In all stations of the Bay of Bengal, a distinct maxima of $\Delta^{14}\text{C}$ was seen at depths of 70~100m, with $\Delta^{14}\text{C}$ values of about 60~70‰. This subsurface ‘maxima’ were developed due to gradual downward transfer of the surface bomb- ^{14}C transient to deeper levels, and subsequent equilibration of the surface water with atmospheric CO_2 with lower $\Delta^{14}\text{C}$ values. This feature is not seen in the northern Bay of Bengal (SS#172/4030) probably because of rapid replenishment of the surface waters resulting from voluminous fresh water discharge. Such a subsurface maxima could not be resolved in the Arabian Sea ^{14}C profiles obtained during 1994–1995 due to coarser sampling resolution. Even with finer sampling resolution, it is unlikely that one can observe this feature in the Arabian Sea. The isopycnal gradient of the surface waters is much less in the Arabian Sea than in the Bay of Bengal, which will aid in mixing of waters and hence more rapid transfer of ^{14}C -enriched waters from the surface to deeper levels, thus preventing formation of any distinct subsurface $\Delta^{14}\text{C}$ maxima in the Arabian Sea.

From the GEOSECS measurements, no significant changes in the deep-water $\Delta^{14}\text{C}$ values of the northern Indian Ocean stations are seen from the present study, except for the station SS#164/4018, near the Gulf of Aden. The intermediate water between 1200 to 2200m depths in this station has shown an increase of $\Delta^{14}\text{C}$ by ~40‰ from the values measured during 1977 (at GEOSECS 413). This increase is most likely due to gradual sinking of more saline and dense Red Sea surface water (RSW), with higher $\Delta^{14}\text{C}$ to deeper depths. The mixing proportion of RSW between 1200 and 2200m depths near the location of SS#164/4018 is 5 to 20%, as seen from multi parametric water mass analyses in the northern Indian Ocean (Goyet, *et al.*, 1999).

In the deep waters at the equatorial Indian Ocean and the southern Bay of Bengal, the measured $\Delta^{14}\text{C}$ values below 2500m are higher than the estimated pre-nuclear $\Delta^{14}\text{C}$ profile (from silica) by about 20‰ (Fig. 5–5 and 5–7). Presence of Antarctic bottom water with higher silica content at these depths causes this deviation. The scatter plot of $\Delta^{14}\text{C}$ versus silica for global ocean waters deeper than 1000m (Broecker, *et al.*, 1995), also show significant deviation from the linearity at the high silica end, caused by circum-polar waters. However, this feature is not seen at the station SS#172/4041.

5.3 Bomb-¹⁴C in the northern Indian Ocean

The inventories and mean penetration depths of bomb ¹⁴C were determined from the column-integrated bomb-¹⁴C, ΣCO₂ and the surface ¹⁴C excess, following the procedures outlined in Broecker, *et al.*, (1985). The detailed procedures of determining bomb-¹⁴C inventory are discussed in Appendix–C. The inventories for the GEOSECS stations and for the Arabian Sea stations occupied during 1994 and 1995 (Bhushan, *et al.*, 2000) are recalculated using the pre-nuclear surface ocean Δ¹⁴C values obtained from this work (Table 5–1). The results are shown in Table 5–2. No significant changes are noticed in the recalculated values of bomb-¹⁴C inventories and mean penetration depths, from the earlier published values (Bhushan, *et al.*, 2000).

Table 5–2:
Inventory and mean penetration depths of bomb-¹⁴C in the northern Indian Ocean

Station	Location (Lat°N;Long.°E)	Sampling date (month/year)	Surface ΔΔ ¹⁴ C (‰)	Mean* penetration depth (m)		Specific bomb- ¹⁴ C inventory (10 ⁹ atoms.cm ⁻²)	
				A	B	A	B
Arabian Sea							
GEOSECS 413	13.35; 53.27	12/1977	142	333	—	7.3	—
GEOSECS 416	19.75; 64.62	12/1977	139	284	297	6.3	6.2
GEOSECS 417	12.97; 64.47	01/1978	145	231	220	5.2	5.0
GEOSECS 418	6.18; 64.42	01/1978	135	293	269	6.1	6.0
GEOSECS 419	3.95; 56.80	01/1978	155	207	—	4.8	—
SS#118/E-8	15.30; 71.50	03/1994	101	225	218	3.5	3.5
SS#118/F-6	17.90; 70.30	03/1994	117	286	302	5.2	5.2
SS#118/H-12	19.75; 64.62	03/1994	113	318	337	5.9	5.9
SS#132/3269	12.80; 71.60	04/1995	110	275	287	4.8	5.1
SS#132/3271	12.97; 64.47	04/1995	127	337	321	6.9	6.6
SS#132/3272	13.20; 58.30	05/1995	111	369	329	6.4	5.8
SS#132/3273	5.70; 56.20	05/1995	115	441	387	8.0	7.7
SS#132/3274	6.18; 64.42	05/1995	118	346	314	6.4	6.3
SS#132/3275	8.00; 74.00	05/1995	127	253	250	5.0	5.0
SS#164/4018	13.35; 53.27	04/1998	110	461	—	8.0	—
Bay of Bengal							
GEOSECS 445	8.50; 86.02	03/1978	162	153	—	3.7	—
GEOSECS 446	12.50; 84.50	03/1978	172	183	—	4.5	—
GEOSECS 448	0.00; 80.10	03/1978	173	194	—	5.0	—
SS#152/3829	8.30; 86.02	02/1997	98	360	—	5.5	—
SS#152/3846	0.00; 80.00	02/1997	115	533	—	9.5	—
SS#172/4030	18.98; 89.53	02/1999	68	299	—	3.1	—
SS#172/4036	13.06; 94.09	02/1999	99	280	—	4.2	—
SS#172/4037	10.80; 94.76	02/1999	95	296	—	4.3	—
SS#172/4041	5.00; 86.00	02/1999	117	250	—	4.5	—

*A: Values determined in this work. B: As reported in Bhushan, *et al.* (2000).

5.3.1 Changes in the inventories and penetration depths of bomb- ^{14}C in the northern Indian Ocean

The spatial and temporal variations of the inventory and penetration depths of bomb- ^{14}C are discussed in this section. The snapshot distributions of bomb- ^{14}C in the northern Indian Ocean as observed during 1977–1978 (GEOSECS), 1994–1995 (Bhushan, *et al.*, 2000) and 1997–1999 (this work) are shown in the Figs. 5–10, 5–11 and 5–12.

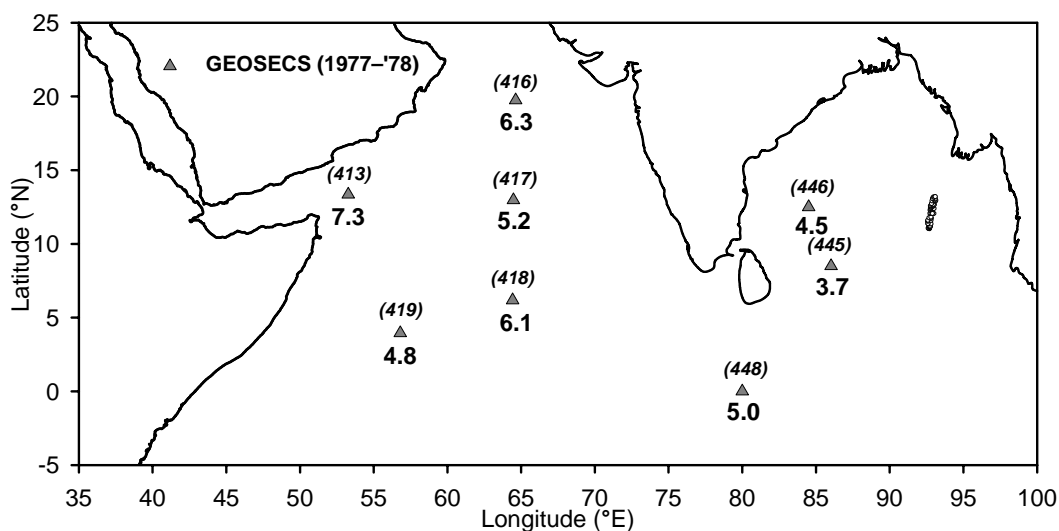


Figure 5–10 Distributions of bomb- ^{14}C inventories ($10^9 \text{ atoms.cm}^{-2}$) in the northern Indian Ocean during the GEOSECS expedition of 1977–1978. The inventories are recalculated from the GEOSECS Indian Ocean ^{14}C results of Stuiver and Östlund (1983). GEOSECS station numbers are given in parentheses.

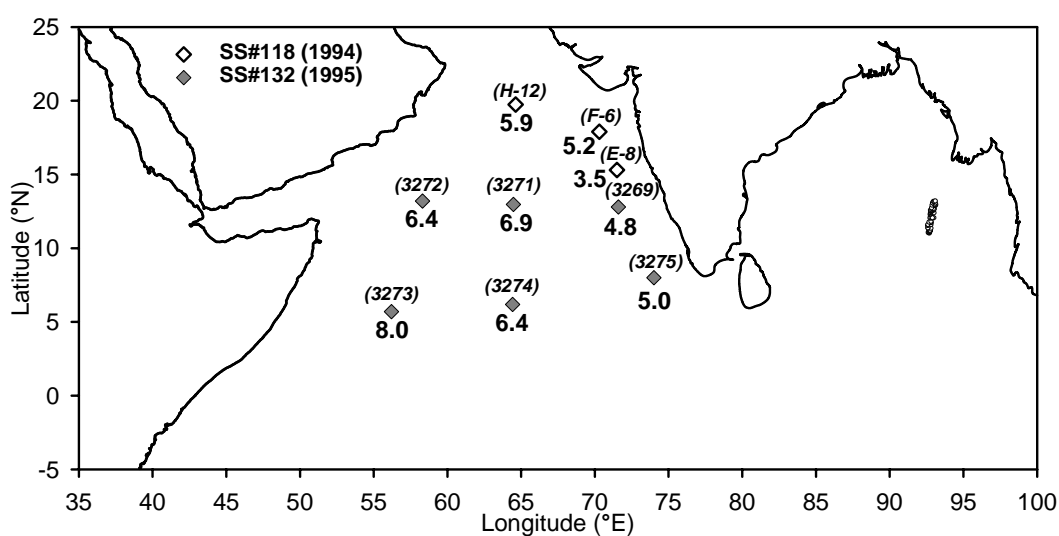


Figure 5–11 Distributions of bomb- ^{14}C inventories ($10^9 \text{ atoms.cm}^{-2}$) in the Arabian Sea during 1994–1995. The inventories (in bold) are recalculated from the Arabian Sea ^{14}C results of Bhushan *et al.* (2000). Station numbers are given in parentheses.

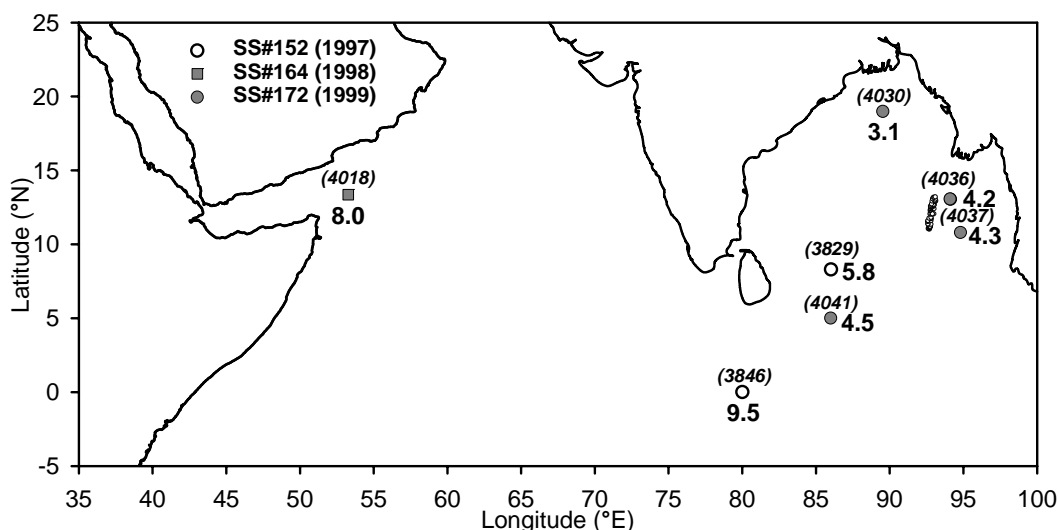


Figure 5–12 Distributions of bomb- ^{14}C inventories (10^9atoms.cm^{-2}) in the equatorial Indian Ocean and Bay of Bengal during 1997 and 1999, and in the Red Sea mouth during 1998. Station numbers are given in parentheses.

Between 1977–1978 and late 1990s, the bomb- ^{14}C inventories has increased by less than 10% on the average for most stations in the northern Indian Ocean, excluding the stations near the equatorial Indian Ocean, *e.g.*, SS#132/3273 (near GEOSECS 419) and SS#152/3846 (reoccupation of GEOSECS 448), where bomb- ^{14}C inventory has increased by ~80%. The mean ^{14}C penetration depths also have been more than doubled at these stations. In the equatorial Indian Ocean station SS#152/3846, the largest increase of bomb- ^{14}C has been observed for depths between 200m and 1000m (Fig. 5–7). Major portion of this bomb- ^{14}C is above 500m. During the French INDIGO expedition in 1985–1987, from the reoccupation of GEOSECS equatorial Indian Ocean stations between 4°N and 6°S , it has been shown that bomb- ^{14}C inventory has increased by ~90% and its penetration has increased by ~80%. This increase has been attributed to the westward flowing waters with high concentration of bomb tracers, due to the entry of ^{14}C -enriched Pacific waters through the passages in the Indonesian archipelago, or mixing with the Mode water from the southern gyre of the Indian Ocean (Bard, *et al.*, 1988, 1989). Evidence of influx of Pacific water through the Indonesian archipelago has been demonstrated from GEOSECS surface tritium distribution (Fine, 1985), and high concentration of ^{90}Sr in banded corals from the western Indian Ocean (Toggweiler and Trumbore, 1985). These processes also must have been operative for the higher increase of bomb- ^{14}C inventory at stations SS#132/3273 and SS#152/3846. The inventory at SS#172/4041 (near GEOSECS 445) which doesn't fall in the path of the throughflow water for its NW–SE trend, has not changed much since 1978, although it is at the same latitude (5°N) as SS#132/3273.

The average value of the mean penetration depth during 1977–1978 for the five Arabian Sea GEOSECS stations (413, 416, 417, 418 and 419) was 270m. During 1994–1998, this has increased by ~40%, to 381m on the average (considering only the reoccupation or nearby stations). In the Bay of Bengal, the mean penetration depth has increased by ~80%, from 168m in 1978 (for the two GEOSECS stations 445 and 446), to 297m during 1997 and 1999 (average of five stations). Thus the relative increase of mean penetration depths in two decades is much higher for the Bay of Bengal than that for the Arabian Sea, although the actual depth of penetration of bomb-¹⁴C is always higher in the Arabian Sea than in the Bay of Bengal. This could be due slower rate of penetration of bomb-¹⁴C in the Bay of Bengal during the GEOSECS times, when due to strong isopycnal gradient, bomb-¹⁴C was mainly accumulated within the top ~200m of water column. This also explains higher surface $\Delta^{14}\text{C}$ in the Bay of Bengal than in the Arabian Sea during the GEOSECS. The downward transfer of bomb-¹⁴C would have become faster after it crossed the surface barrier of isopycnal gradient, thus causing relatively large increase in the penetration depths of bomb-¹⁴C after GEOSECS.

For most stations in the northern Indian Ocean, small change in bomb-¹⁴C inventories, significant increase in the mean penetration depths and lowering of the surface $\Delta^{14}\text{C}$ values indicate the temporal variation of bomb-¹⁴C in two decades is mainly through downward transfer through mixing with deeper waters.

The ratio of the average values of the mean penetration depths for all stations of the northern Indian Ocean (excluding stations GEOSECS 419 & 448, SS#132/3273 and SS#152/3846) during 1977–1978 and that during 1994 and 1999 is 224/339 or 0.660. In a diffusive process, the characteristic mixing depth is proportional to the square root of mixing time if the lateral transport processes are neglected (Stuiver, 1980; Peng, *et al*, 1998). Since the atmospheric $\Delta^{14}\text{C}$ reached its peak during 1963, the initial time for mixing is taken as 1963. The square root of the ratios of the mixing times since 1963 between GEOSECS and the northern Indian Ocean cruises between 1994 and 1999 is $\sqrt{(15/33)}$, or 0.674. This is close to the mixing depth ratio (0.660) calculated for bomb-¹⁴C. Thus diffusive mixing process appears to play a major role in the temporal variations of bomb-¹⁴C distribution in the northern Indian Ocean (north of 0°), excluding the equatorial Indian Ocean, where lateral transport processes are also important.

5.3.2 Comparison of the observed changes of bomb-¹⁴C inventories with model simulated bomb-¹⁴C distributions

Toggweiler, *et al.*, (1989b) simulated the penetration of bomb-produced ¹⁴C in the world ocean using the Geophysical Fluid Dynamics Laboratory's (GFDL) primitive equation ocean general circulation model. Changes in the inventories of bomb-¹⁴C have been simulated using this model, for the entire world ocean. The model predicted changes in inventory from 1981 and 1990 are shown in Fig. 5–13.

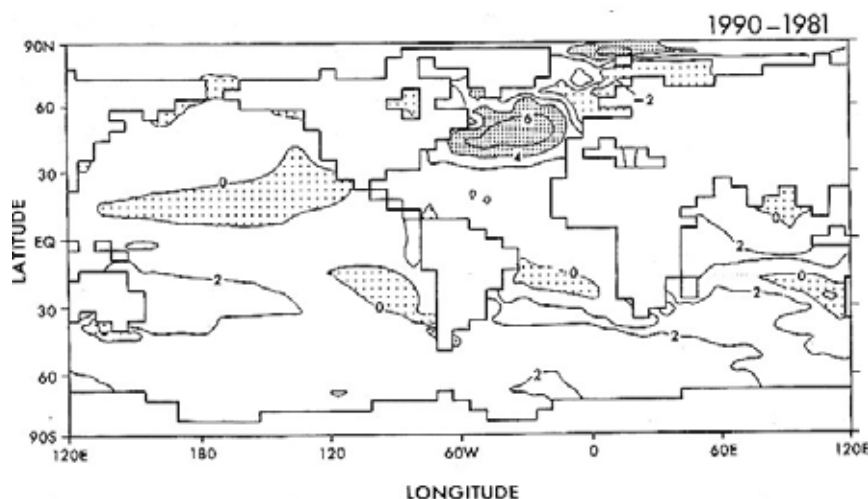


Figure 5–13 Predicted changes in bomb-¹⁴C inventories for the world ocean (in $10^9 \text{ atoms.cm}^{-2}$) between 1981 and 1990, using the Geophysical Fluid Dynamics Laboratory (GFDL) world ocean model (Toggweiler, *et al.*, 1989b).

In this study the comparison of changes in bomb-¹⁴C inventories are done between 1970s and late 1990s, the predicted changes between 1990 and 1981 should be considered as the lower limit. For the decade 1981 to 1990, the model predicts increase in bomb-¹⁴C inventories from 0 to $2 \times 10^9 \text{ atoms.cm}^{-2}$ for the Arabian Sea and the equatorial Indian Ocean, while no change has been predicted for the Bay of Bengal. The average bomb-¹⁴C inventory for the GEOSECS stations 416, 417 and 418 during 1977 was $5.9 \times 10^9 \text{ atoms.cm}^{-2}$, which rose to $6.4 \times 10^9 \text{ atoms.cm}^{-2}$ during 1994 and 1995. Average bomb-¹⁴C inventory in the Bay of Bengal during 1978 was $4.1 \times 10^9 \text{ atoms.cm}^{-2}$; while during 1997 and 1999 it rose to $4.4 \times 10^9 \text{ atoms.cm}^{-2}$, consistent with the model prediction. Major discrepancy seen at the equatorial Indian Ocean, where the inventory increased by $4.5 \times 10^9 \text{ atoms.cm}^{-2}$ between 1978 and 1997, which is more than twice the model predicted rise between 1981 and 1990. Thus, the observed ¹⁴C values in the northern Indian Ocean obtained from this work and from Bhushan *et al.*, (2000) agrees with the GFDL model simulated values, except at the equatorial Indian Ocean.

5.4 Air-sea exchange rate of CO₂ based on bomb-¹⁴C inventories

Air-sea exchange rates of CO₂ have been calculated for all stations based on the bomb ¹⁴C inventories, following the procedure of Stuiver, (1980). The detailed method is explained in Appendix–C. This method is based on the assumption, that the net amount of bomb-¹⁴C gone into the ocean is proportional to the integrated atmosphere-ocean $\Delta^{14}\text{C}$ gradient and the regional air-sea exchange rate of CO₂. Another assumption of this procedure is that the changes in the inventory of bomb-¹⁴C only result from air-sea exchange of CO₂ and vertical diffusive mixing, and the invasion of CO₂ from air to sea is equal to its evasion out of the sea. However, this assumption may not be valid for some locations, *e.g.*, SS#172/4030 and SS#152/3846 where lateral transport plays a significant role in deciding the ¹⁴C inventory.

5.4.1 Distribution of air-sea CO₂ exchange rates over the northern Indian Ocean

Bhushan *et al.*, (2000) had reported the air-sea CO₂ exchange rates for the Arabian Sea from the GEOSECS ¹⁴C measurements and from the measurements made during 1994 and 1995. In that study, tropospheric $\Delta^{14}\text{C}$ history for the northern hemisphere was used, which has peak $\Delta^{14}\text{C}$ of ~1000‰ in 1964 (Fig. 1–1). As far as tropical oceanic regions are concerned, it is more appropriate to use the tropospheric $\Delta^{14}\text{C}$ trend for the tropical regions, where the peak $\Delta^{14}\text{C}$ was ~750‰ in 1964. Also in Bhushan *et al.*, (2000), the mixed layer $\Delta^{14}\text{C}$ trend was derived from a Gulf of Kutch coral, which recorded peak $\Delta^{14}\text{C}$ of 170‰ in 1968 (Chakraborty, *et al.*, 1994). For the reasons explained in *sec. 3.5.1*, the mixed-layer $\Delta^{14}\text{C}$ trend recorded in the Gulf of Kutch may not be representative for the open northern Indian Ocean. If the $\Delta^{14}\text{C}$ trend from the Gulf of Kutch coral is used then, the integrated mixed-layer $\Delta^{14}\text{C}$ value would be an overestimate, due to the over all higher $\Delta^{14}\text{C}$ values in the Gulf of Kutch than the contemporary open northern Indian Ocean waters. However, since for determining the ¹⁴C input, it is the atmosphere-ocean gradient of $\Delta^{14}\text{C}$ that is integrated, the effect of using higher $\Delta^{14}\text{C}$ values for both the atmosphere and the ocean mixed layer is likely to cancel each other. The ¹⁴C based air-sea CO₂ exchange rates for the northern Indian Ocean stations are given in Table 5–3. As compared to the values reported in Bhushan, *et al.*, (2000), the exchange rates recalculated in this study are higher by ~9% on an average for all but one station in the Arabian Sea (the recalculated values are higher by –1 to 17% for different stations).

Table 5-3:
Bomb-¹⁴C based air-sea CO₂ exchange rates over the northern Indian Ocean

Station	Location (Lat°N;Long.°E)	Date (month/year)	Air-sea CO ₂ exchange rate F_{12} (mol.m ⁻² .yr ⁻¹)	
			This study	Earlier report*
<i>Arabian Sea</i>				
GEOSECS 413	13.35; 53.27	12/1977	17.9	—
GEOSECS 416	19.75; 64.62	12/1977	15.4	13.9
GEOSECS 417	12.97; 64.47	01/1978	12.7	11.0
GEOSECS 418	6.18; 64.42	01/1978	15.0	13.7
GEOSECS 419	3.95; 56.80	01/1978	11.8	—
SS#118/E-8	15.30; 71.50	03/1994	7.5	7.0
SS#118/F-6	17.90; 70.30	03/1994	11.1	10.4
SS#118/H-12	19.75; 64.62	03/1994	12.6	11.8
SS#132/3269	12.80; 71.60	04/1995	10.3	10.4
SS#132/3271	12.97; 64.47	04/1995	14.8	13.2
SS#132/3272	13.20; 58.30	05/1995	13.7	11.7
SS#132/3273	5.70; 56.20	05/1995	17.1	16.0
SS#132/3274	6.18; 64.42	05/1995	13.7	12.4
SS#132/3275	8.00; 74.00	05/1995	10.7	10.2
SS#164/4018	13.35; 53.27	04/1998	17.2	—
<i>Bay of Bengal</i>				
GEOSECS 445	8.50; 86.02	03/1978	9.0	—
GEOSECS 446	12.50; 84.50	03/1978	10.9	—
GEOSECS 448	0.00; 80.10	03/1978	12.1	—
SS#152/3829	8.30; 86.02	02/1997	11.8	—
SS#152/3846	0.00; 80.00	02/1997	20.4	—
SS#172/4030	18.98; 89.53	02/1999	6.7	—
SS#172/4036	13.06; 94.09	02/1999	9.1	—
SS#172/4037	10.80; 94.76	02/1999	9.3	—
SS#172/4041	5.00; 86.00	02/1999	9.7	—

*Exchange rates as reported for these stations by Bhushan, et al., (2000).

The air-sea CO₂ exchange rates in the northern Indian Ocean calculated from the bomb-¹⁴C inventories range from ~7mol.m⁻².yr⁻¹ (in the northern Bay of Bengal) to 20mol.m⁻².yr⁻¹ (in the equatorial Indian Ocean). High CO₂ exchange rates of ~17mol.m⁻².yr⁻¹ are measured in the western Arabian Sea, off Oman and near the Gulf of Aden. As discussed later, the high exchange rate obtained at the equator (and also possibly at SS#132/3273) is an artifact of lateral advection of ¹⁴C-enriched waters from the Pacific into this area from the Indonesian archipelago.

5.4.2 Comparison of bomb-¹⁴C derived air-sea CO₂ exchange rates with the climatological wind speed data

One of the main controlling factors that govern the process of air-sea exchange of gases is the intensity of surface wind speed. The bomb-¹⁴C derived air-sea CO₂ exchange rates over the northern Indian Ocean as obtained during the late 1990s are compared here with the long-term climatological wind speed data obtained from NCEP Reanalysis Project (Kalnay, *et al*, 1996). The comparison is illustrated in Fig. 5–14. It is evident that the measured exchange rates are roughly proportional to the long-term average wind speeds. Highest wind speeds (8 to 10m.sec⁻¹) are observed over the western Arabian Sea near Oman, where the measured exchange rates are also the highest. Whereas, lowest exchange rates have been obtained at the stations in the eastern Arabian Sea, the northern Bay of Bengal and the Andaman Sea, all of which fall in the low wind speed regime (5 to 6m.sec⁻¹).

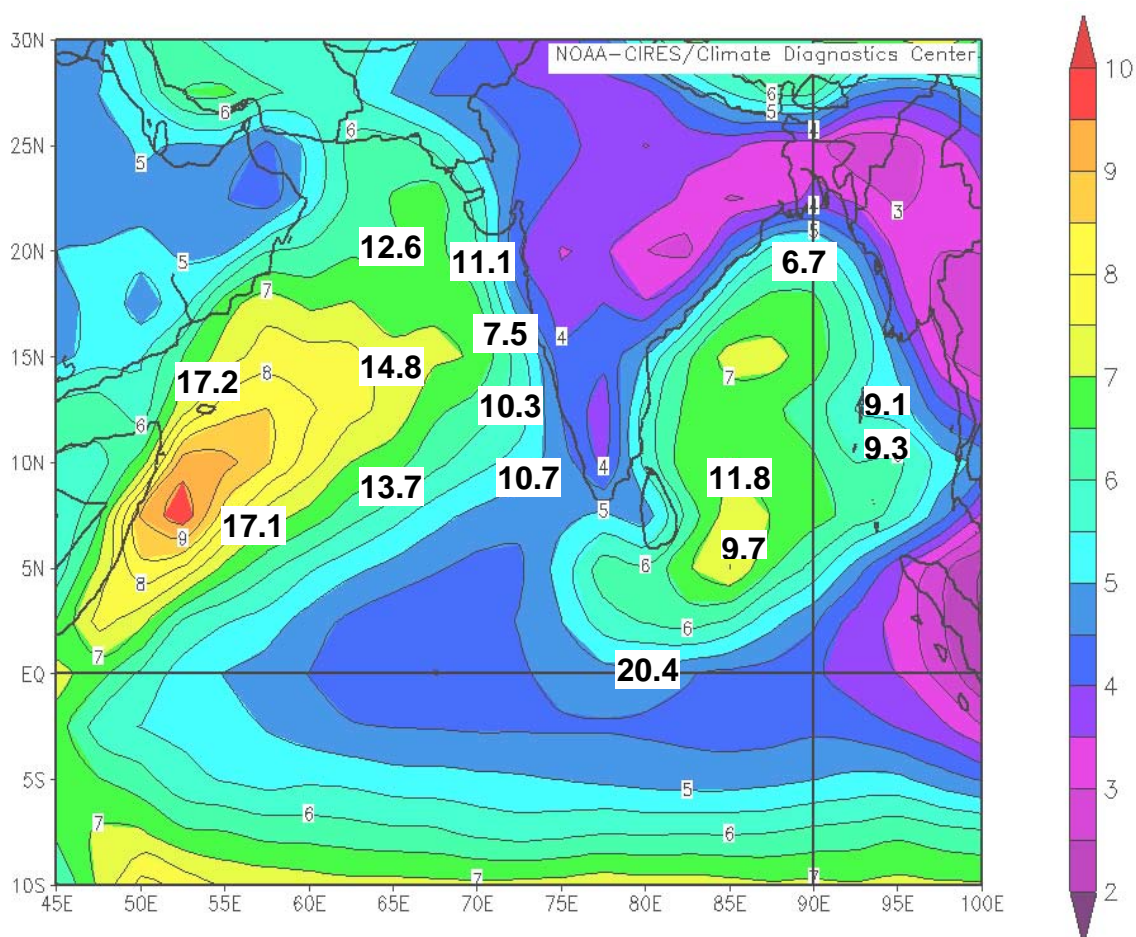


Figure 5–14 Contours of long-term mean scalar wind speed (labeled in m.sec⁻¹) at the surface over the northern Indian Ocean region and bomb-¹⁴C based air-sea CO₂ exchange rates (in mol.m⁻².yr⁻¹). The wind speed contours are drawn from NCEP-Reanalysis Project long-term scalar wind speed data for the period 1968 to 2000 (Kalnay, *et al*, 1996). GrADS image of the wind speed contours obtained from NOAA-CIRES Climate Diagnostics Center, Boulder, CO., USA <<http://www.cdc.noaa.gov/Composites>>.

The measured air-sea CO₂ exchange rates are plotted with the long-term wind speed in Fig. 5–15. All points for the northern Indian Ocean station fall on a roughly linear trend, for wind speeds ranging from 5 to 8 m.sec⁻¹. From the GEOSECS ¹⁴C measurements, Broecker, *et al.*, (1985) reported mean exchange rate of 20 mol.m⁻².yr⁻¹ for the global ocean, for a global average surface wind speed of 7.4 m.sec⁻¹. From ¹⁴C measurements in corals from the Red Sea, an invasion flux of 8±2 mol.m⁻².yr⁻¹ has been obtained, for a mean wind speed 4.7 m.sec⁻¹ (Cember, 1989). As evident from Fig. 5–15, the CO₂ exchange rates calculated from the Red Sea coral, northern Indian Ocean measurements from this study and the global mean value obtained from GEOSECS ¹⁴C data (Broecker, *et al.*, 1985), all follow an approximately common trend. Also shown in this plot, are the empirical linear, quadratic and cubic relationships established between long-term average wind speed and CO₂ exchange rates (Wanninkhof, *et al.*, 1985; Wanninkhof, 1992; Wanninkhof and McGillis, 1999). The cubic relationship appears to fit better with the bomb-¹⁴C derived CO₂ exchange rates in the northern Indian Ocean.

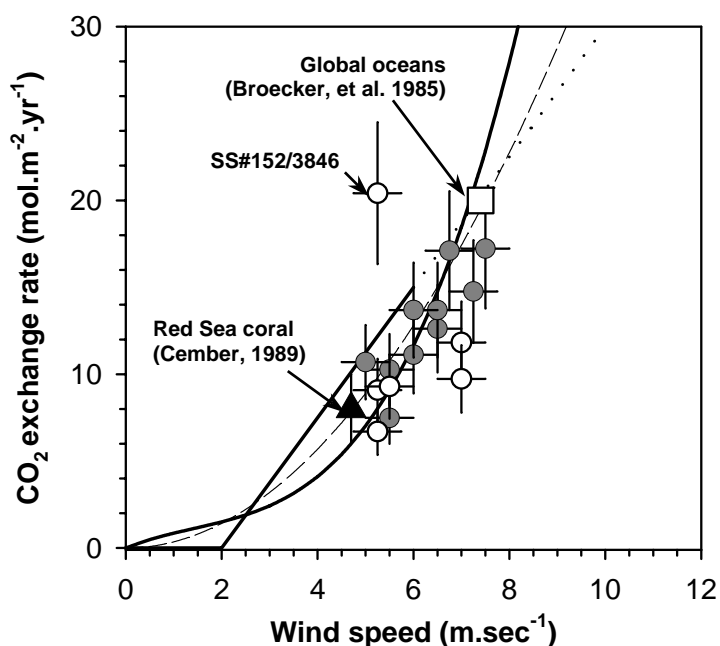


Figure 5–15 Dependence of ¹⁴C derived CO₂ exchange rates with long-term mean scalar wind speed. The filled and open circles denote bomb-¹⁴C based exchange rates measured at the Arabian Sea and the Bay of Bengal stations respectively, between 1994 and 1999. The open square is the bomb-¹⁴C derived global average CO₂ exchange rate, obtained from GEOSECS ¹⁴C measurements (Broecker, *et al.*, 1985). The filled triangle is the value obtained from ¹⁴C in Red Sea coral (Cember, 1989). The CO₂ exchange rates are obtained from the gas transfer rates from the CO₂ solubility function of Weiss (1974). The gas transfer rates are calculated from the empirical relationships with wind-speed and are shown by (i) solid straight line extrapolated with dotted line (SF₆ experiment in lake, Wanninkhof, *et al.*, 1985), (ii) dashed curved line (quadratic relationship for long-term average winds, Wanninkhof, 1992) and (iii) solid curved line (cubic relationship for long-term average winds, Wanninkhof & McGillis, 1999).

In Fig. 5–15, the value obtained for the equatorial Indian Ocean station SS#152–3846 during 1997, is a clear outlier from the general polynomial trend. It is interesting to note here, that using the bomb- ^{14}C inventory measured at this station during 1978 (GEOSECS 448) and the local long-term wind speed of $\sim 5\text{m}\cdot\text{sec}^{-1}$, one gets an exchange rate of $12.1\text{mol}\cdot\text{m}^{-2}\cdot\text{yr}^{-1}$, which fits better with the general trend. As discussed in *sec.* 5.3.1, significant change in bomb- ^{14}C at this location is due to lateral advection of waters from the Pacific. Assuming lateral advection a steady state process, the fact that the inventory of GEOSECS 448 matches the regional wind speed indicates, that the $\Delta^{14}\text{C}$ of the water that is flowing in to this region has steadily increased in the last two decades since 1978. This increase is in response to the bomb transient, with a delay introduced by the transport processes. Thus, in the equatorial Indian Ocean, between 1978 and 1997, a major portion of the increment in the bomb- ^{14}C inventory is through lateral advection of ^{14}C -enriched waters, rather than through air-sea CO_2 exchange.

5.4.3 Estimate of net sea-air flux of CO_2 from the northern Indian Ocean

Once the rate of air-sea CO_2 exchange (I) is known, it is possible to compute net transfer rate of atmospheric CO_2 across the ocean surface, from the difference of the partial pressure of CO_2 ($p\text{CO}_2$) in the surface ocean and that in the atmosphere (Wanninkhof, 1992). The net transfer rate of CO_2 (F) is given by,

$$F = I \times (p\text{CO}_{2\text{sea}} - p\text{CO}_{2\text{air}}) / p\text{CO}_{2\text{air}} = I \times \Delta p\text{CO}_2 / p\text{CO}_{2\text{air}}$$

In this case, the sign of F (or direction of flux) is *positive upwards*. Thus the net flux of CO_2 will be from sea to air, in regions where $\Delta p\text{CO}_2$ is positive. This condition is common in most tropical oceanic areas due to equatorial upwelling, which brings deeper CO_2 rich waters to the surface. The exchange rates calculated from bomb- ^{14}C inventories are the long-term averaged values. Thus, if average ocean-atmosphere $p\text{CO}_2$ gradient ($\Delta p\text{CO}_2$) over a given oceanic region is known, it is possible to compute the net transfer rate of CO_2 from a knowledge of the exchange rates.

Both in the Arabian Sea and the Bay of Bengal, large seasonal variations of $p\text{CO}_2$ in the surface waters are seen due to strong seasonality of wind induced upwelling and nutrient inputs through large amount of river discharge (Kumar, *et al.*, 1992). Surface $p\text{CO}_2$ over the Arabian Sea is found to be higher than that in the

atmosphere throughout the year, thus making this basin a perennial source of CO₂ to the atmosphere (George, *et al.*, 1994; Sarma, *et al.*, 1998; Goyet, *et al.*, 1998). Surface Bay of Bengal on the other hand acts as a sink of atmospheric CO₂ due to significant lowering of the surface water pCO₂ relative to the atmosphere (often exceeding 100 μ atm), due to large amount of fresh water input and sequestering of CO₂ through intense biological pumping resulting from large nutrient supply (Kumar, *et al.*, 1996).

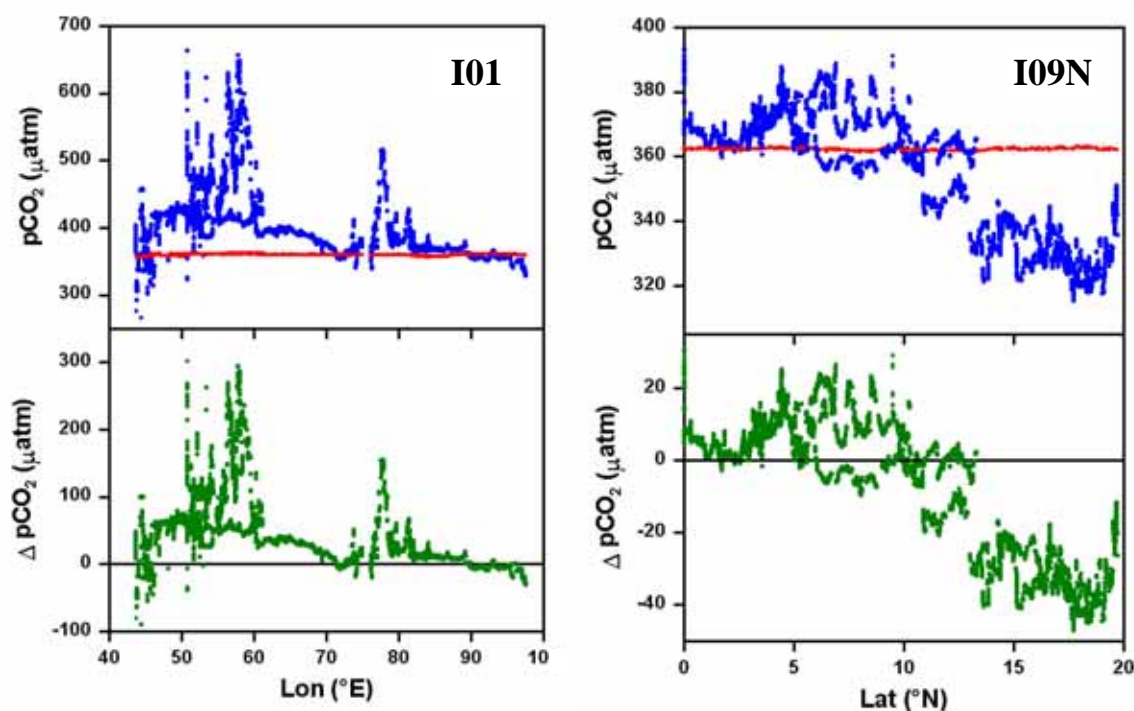


Figure 5-16 Underway pCO₂ in surface seawater (blue) and in the atmosphere (red) measured along WOCE sections I01 and I09N in the northern Indian Ocean (Sabine and Key, 1997). The ocean-atmosphere gradients of pCO₂ or Δ pCO₂ are shown in the bottom graphs (green). Cruise I01 was during Aug–Oct, 1995 (SW monsoon), and I09N during Feb–Mar, 1995 (inter monsoon).

The contrasting ocean-atmosphere pCO₂ gradients for the Arabian Sea and the Bay of Bengal is clearly evident from the underway pCO₂ measurements obtained during the WOCE expeditions in 1995 (Fig. 5-16). During Aug-Oct 1995, surface pCO₂ was higher than that in the atmosphere by up to 300 μ atm in the western Arabian Sea. In the northern Bay of Bengal (north of 10°N) pCO₂ was lower by 40 μ atm than the atmospheric value during Jan-Mar 1995.

Data on the distribution of pCO₂ over the northern Indian Ocean, for different times of the year and with adequate spatial coverage is meager, making difficult the task of ascertaining the average pCO₂ for the entire region. In this study, from the

reported pCO₂ values at various locations for different seasons, annual mean pCO₂ for the northern Indian Ocean regions have been compiled from Kumar, *et al.*, (1996), Goyet, (1997), Sabine and Key, (1997), Sarma, *et al.*, (1998, 2000). The surface ocean pCO₂ values for the Arabian Sea and the Bay of Bengal, compiled mainly from the cruises of JGOFS and WOCE are given in Table 5–4.

Table 5–4:
Compilation of surface water pCO₂ in the northern Indian Ocean (1991–1995)

Region (range of Lat., Long.)	Month / Season*	pCO ₂ μ atm (Range & mean [†])	Ref. [‡] No.
Arabian Sea			
W. Arabian Sea (14~21°N; 57~65°E)	Feb (1995)	338 – 386 (360.0)	1
Central Arabian Sea (11~21°N; 64°E)	NE monsoon (1995)	351 – 433	2,3
–do–	Inter monsoon (1994)	379 – 478	2,3
–do–	SW monsoon (1995)	385 – 432	2,3
E. Arabian Sea (14~21°N; 57~65°E)	NE monsoon (1995)	375 – 446	2,3
–do–	Inter monsoon (1994)	416 – 427	2,3
S. Arabian Sea (5~22°N; 43~80°E)	Sep (1995)	266 – 663 (411.0)	4
Bay of Bengal			
S. Bay of Bengal (0~15°N; 80~93°E)	Feb (1995)	321 – 393 (362.5)	4
S. Bay of Bengal (10~15°N; 80~85°E)	Mar-Apr (1991)	325 – 375	5
–do–	Nov-Dec (1991)	325 – 350	5
S. Bay of Bengal (4~10°N; 80~97°E)	Oct (1995)	329 – 427 (366.6)	4
N. Bay of Bengal (15~20°N; 90~92°E)	Feb-Mar (1995)	315 – 351 (329.4)	4
N. Bay of Bengal (15~20°N; 82~87°E)	Mar-Apr (1991)	275 – 325	5
–do–	Nov-Dec (1991)	250 – 350	5

*NE monsoon: Feb-Mar; Inter monsoon: Apr-May; SW monsoon: Jun-Aug.

[†]Means are given, where very large number of underway pCO₂ measurements are available.

[‡]Surface water pCO₂ data are compiled from the following sources:

[1] Goyet, (1997); [2] Sarma, *et al.*, (1998); [3] Sarma, *et al.*, (2000); [4] Sabine and Key, (1997); [5] Kumar, *et al.*, (1996).

The annual average pCO₂ in the surface water of the whole Arabian Sea (0° to 25°N and 45°E to 80°E) is estimated to 412 μ atm. The Bay of Bengal (0° to 23°N and 80°E to 98°E) has been divided into two parts: the area north of 15°N (northern Bay of Bengal) with estimated mean pCO₂ of 330 μ atm, and between 0°N to 15°N

(southern Bay of Bengal) with mean $p\text{CO}_2$ of $358\mu\text{atm}$. Assuming the $p\text{CO}_2$ of the atmosphere in the late 1990s as $360\mu\text{atm}$, the net flux of CO_2 from different northern Indian Ocean regions within the above mentioned area are calculated from the regional average exchange rates and the ocean-atmosphere $p\text{CO}_2$ gradients ($\Delta p\text{CO}_2$). The results are given in Table 5–5.

Table 5–5:
Estimates of sea to air flux of CO_2 from the northern Indian Ocean

Region	Approx. area (10^6km^2)	Mean $p\text{CO}_2$ (μatm)	Air-sea CO_2 exchange rate ($\text{mol.m}^{-2}.\text{yr}^{-1}$)	Net annual flux of CO_2 ($\text{mol.m}^{-2}.\text{yr}^{-1}$)	Net regional flux of CO_2 (TgC.yr^{-1})
Arabian Sea (0° – 25°N , 45°E – 80°E)	7.158	412	14	2.02	173.5
N. Bay of Bengal (15°N – 23°N , 80°E – 98°E)	0.799	330	9	–0.75	–7.2
S. Bay of Bengal (0° – 15°N , 80°E – 98°E)	3.031	358	10	–0.06	–2.2

This estimate shows, the net annual flux of CO_2 from the northern Indian Ocean region (between 0° to 25°N) is $\sim 164\text{TgC.yr}^{-1}$. The source of this flux is entirely located in the Arabian Sea, with annual sea-air flux of $\sim 174\text{TgC.yr}^{-1}$. Sarma, *et al.*, (1998) estimated annual flux of $\sim 45\text{TgC.yr}^{-1}$ from an area $\sim 1.6 \times 10^6\text{km}^2$ in the eastern Arabian Sea. The Bay of Bengal as a whole is acting as a sink of atmospheric CO_2 , where the sink is mainly located in its northern part. The net estimated uptake rate of CO_2 by the Bay of Bengal is $\sim 9\text{TgC.yr}^{-1}$.

Louanchi, *et al.*, (1996) estimated annual flux of 169TgC.yr^{-1} for the northern Indian Ocean between 10°S and 18°N , using a one-dimensional model and incorporating the effects of physical and biogeochemical processes. The present estimated flux of $\sim 164\text{TgC.yr}^{-1}$ from 0° to 25°N agrees well with this modeled value.

5.5 ^{14}C in the deep waters of the northern Indian Ocean

From the GEOSECS ^{14}C measurements in the northern Indian Ocean, it has been shown the minimal $\Delta^{14}\text{C}$ ranging from -190‰ and -200‰ occur between 2000m and 2500m depths (Stuiver and Östlund, 1983, Srinivasan, *et al.*, 2000). The bottom waters below 2500m have higher $\Delta^{14}\text{C}$ values of about -183‰ . In the profiles measured in this work, this feature is most prominent in the equatorial Indian Ocean station SS#152/3846 (Fig. 5–7). A general northward decrease in the Indian Ocean deep water (2000~4000m) $\Delta^{14}\text{C}$ value by $\sim 40\text{‰}$ has been reported from the GEOSECS measurements, with $\Delta^{14}\text{C}$ of -160‰ at $\sim 60^\circ\text{S}$ to -200‰ at $\sim 20^\circ\text{N}$ (Stuiver and Östlund, 1983; Somayajulu, *et al.*, 1999). This feature is not clearly discernible from the results of this study, within the short latitudinal range of the stations where deep water ^{14}C measurements were done.

The ^{14}C data, obtained for the two stations in the Andaman Sea (SS#172/4036 and SS#172/4037) show evidence of rapid vertical mixing below $\sim 1800\text{m}$. Water below this depth appears to be well mixed, from the near uniform distribution of various hydrographic and chemical properties (Appendix–D). The $\Delta^{14}\text{C}$ of the deep water (below 1500m) in the Andaman Basin is -170‰ , significantly higher than the deep water values of the open Bay of Bengal (-190‰ to -195‰). The basin is isolated from the main Bay of Bengal basin by the Andaman and Nicobar Islands in the west and southwest, and by the Asian landmass in the east. The high $\Delta^{14}\text{C}$ values in the deep water within this basin is a result of very rapid vertical mixing, which causes faster transfer of the surface waters to the deeper layers. The sea floor of the Andaman Basin is characterized by high heat flow values, ranging from $\sim 70\text{mW}\cdot\text{m}^{-2}$ to $\sim 220\text{mW}\cdot\text{m}^{-2}$ in the deepest portion of the basin (Burns, 1964; Vacquier and Taylor, 1966). The higher than normal geothermal heat flux from the floor of this enclosed basin possibly induces rapid convective mixing, which practically homogenizes the entire water column below $\sim 1500\text{m}$, and making all physical and chemical properties including ^{14}C to be almost depth invariant (Figs. 5–3 and 5–4). Rapid mixing with the intermediate waters and absence of mixing with aged deep water of the surrounding Indian Ocean maintain the $\Delta^{14}\text{C}$ of the deep water of the Andaman Basin below $\sim 1500\text{m}$ at about -170‰ .

5.5.1 Estimation of vertical diffusion and advection rates from natural ^{14}C distributions:

From the ^{14}C profiles obtained in this study from the Bay of Bengal and the equatorial Indian Ocean, the vertical eddy diffusion and advection rates are calculated, based on the intermediate and deep water ^{14}C distributions. The simple one-dimensional (1D) diffusion-advection model proposed by Munk (1966) and subsequently modified by Craig (1969) is used. In one dimension, the steady state distribution of a radioactive non-conservative tracer, *e.g.* ^{14}C , is governed by vertical advection, vertical diffusion, radioactive decay, and modification of its vertical distribution due to dissolution of sinking biological particles. The steady-state equation for a radioactive non-conservative tracer can be written as (Craig, 1969):

$$K \frac{d^2C}{dz^2} - w \frac{dC}{dz} - \lambda C + J = 0 \quad \dots(1)$$

where, C is the concentration of ^{14}C (atoms.g $^{-1}$), z is the vertical distance (positive upward), K is the vertical eddy diffusion coefficient, and w is the advection velocity. The disintegration constant of ^{14}C (λ) is taken as $1.2097 \times 10^{-4} \text{yr}^{-1}$. The parameter J is the zero-order, concentration-independent production rate. The equation (1) has the solution,

$$(C - J/\lambda) = \frac{\left\{ (C_m - J/\lambda) \left[\exp - \left(\frac{Z}{2z^*} \right) \right] \sinh \left(\frac{Az}{2z^*} \right) + (C_0 - J/\lambda) \left[\exp \left(\frac{z}{2z^*} \right) \right] \sinh \left(\frac{AZ}{2z^*} \right) \right\}}{\left\{ \sinh \left(\frac{Az_m}{2z^*} \right) \right\}} \quad \dots(2)$$

where, C_0 and C_m are the concentration of the tracer at the top and bottom of the mixing region, z^* ($= K/w$) is the mixing parameter, $Z = z_m - z$, and $A = [1 + 4z^*(\lambda/w)]^{1/2}$.

The z^* and J/w were first determined from the distributions of potential temperature and ΣCO_2 respectively, within the linear θ -S region. In case of upwelling the parameter z^* will be positive (since w is positive), while for downwelling regions, z^* will be negative. The value of A is determined from the best fit to the distributions of natural ^{14}C . Finally the values of w and K are determined from A , since z^* is known from the distribution of potential temperature. The results of analysis of the selected ^{14}C -profiles using 1D-model are shown in Table 5–6.

For the station SS#172/4030, the linear θ -S region was obtained only from 1000–1600m, where determination of the parameters J/w , w and K was not possible for this station due to considerable scatter in the distribution of ^{14}C within this short linear region. Analysis was also not attempted for the station SS#164/4018, due to bomb- ^{14}C penetration down to ~2000m (Fig. 5–8).

Table 5–6:
1D-model results for advection velocity (w) and vertical eddy diffusivity (K)

Station	Mixing interval (km)	z^* (km)	J/w (mmol/km g)	J^*/w ($\times 10^{-2}$) (atom/km g)	w (m.yr $^{-1}$)	K (cm 2 .sec $^{-1}$)
SS#152/3829	1.27-3.06	0.706	0.0441	2.950	9.2	2.1
SS#152/3846	0.85-3.66	0.960	0.0131	0.872	14.4	4.4
SS#172/4041	0.70-3.10	1.007	0.0230	1.531	5.4	1.7
SS#172/4036	0.70-1.91	0.339	0.0042	0.281	—	—
SS#172/4037	0.70-2.88	0.338	0.0124	0.829	—	—

The highest advection velocity (w) of ~14m.yr $^{-1}$ is measured at the equatorial Indian Ocean station (SS#152/3846). Vertical eddy diffusivity (K) is also the highest for this station, ~4cm 2 .sec $^{-1}$. For the two nearby stations in the Bay of Bengal, measured w range from 5 to 9m.yr $^{-1}$, and K from 1.7 to 2.1cm 2 .sec $^{-1}$. From the GEOSECS radiocarbon data, Stuiver, *et al.*, (1983) suggested an upwelling rate of 10m.yr $^{-1}$, for waters deeper than 1500m. Somayajulu, *et al.*, (1991) reported w and K of 17.4m.yr $^{-1}$ and 5.4cm 2 .sec $^{-1}$ for the GEOSECS station 420 near the Somali margin in the western equatorial Indian Ocean, based on deep-water ^{14}C distribution between 1.69–5.07km. The w and K obtained for the northern Indian Ocean stations also agree with these values.

No stable solutions for w and K could be obtained for the Andaman stations (SS#172/4036 & SS#172/4037), using the derived z^* values. The model gives a stable solution using the lowest z^* value of about 0.58, which yields w of ~240m.yr $^{-1}$. This points to very rapid vertical mixing rate in the Andaman basin, and the above rate being its lower limit.

5.6 Conclusion

The new results of ^{14}C measurements in the northern Indian Ocean show, the inventory of bomb- ^{14}C range from $3.1 \times 10^9 \text{ atoms.cm}^{-2}$ in the northern Bay of Bengal, to $5.5 \times 10^9 \text{ atoms.cm}^{-2}$ in the southern Bay of Bengal. Lowest bomb ^{14}C inventory is obtained in the northern Bay of Bengal where fresh water discharge is the maximum, while largest inventory has been obtained from the equatorial Indian Ocean ($9.5 \times 10^9 \text{ atoms.cm}^{-2}$), where lateral advection is highest. The input of ^{14}C -enriched water from the Pacific through the Indonesian archipelago from east, and the Sub Antarctic Mode Water from the south increases the bomb- ^{14}C inventory in the equatorial Indian Ocean. Within the main Bay of Bengal basin, changes in the inventories of bomb- ^{14}C are only marginal after two decades since the GEOSECS. However, bomb- ^{14}C has penetrated $\sim 80\%$ deeper during this time, from $\sim 177\text{m}$ in 1978 to $\sim 297\text{m}$ in 1999. From the time scale of penetration of bomb ^{14}C in the northern Indian Ocean, it is apparent that diffusive mixing is the main process that controls the temporal variation of bomb- ^{14}C in this region.

The air-sea exchange rates of CO_2 are determined from the atmospheric $^{14}\text{CO}_2$ curve for the post nuclear-era from tropical latitudes, and the measured oceanic bomb- ^{14}C inventories, following the procedures of Stuiver et al. (1980). The air-sea CO_2 exchange rates based on bomb- ^{14}C range from $7\sim 17 \text{ mol.m}^{-2}.\text{yr}^{-1}$. The distribution of these exchange rates is mainly a function of long-term wind speed. From the annual mean surface ocean pCO_2 and the bomb- ^{14}C based air-sea CO_2 exchange rates, net regional CO_2 source of $\sim 164 \text{ TgC.yr}^{-1}$ have been estimated for the northern Indian Ocean between 0° and 25°N .

The vertical advective velocity and eddy diffusivity calculated at the equatorial Indian Ocean are $\sim 14 \text{ m.yr}^{-1}$ and $\sim 4 \text{ cm}^2.\text{sec}^{-1}$ respectively. These are $5\sim 9 \text{ m.yr}^{-1}$ and $\sim 2 \text{ cm}^2.\text{sec}^{-1}$ in the southern Bay of Bengal.

The physical and chemical properties of the waters in the Andaman Basin are depth invariant below $\sim 1400\text{m}$. The deep-water $\Delta^{14}\text{C}$ values for the Andaman Sea are nearly uniform at -170‰ , significantly higher than that for similar depths in the open Bay of Bengal (-190 to -195‰). Results of 1D-model indicates, below 700m in the Andaman basin, the vertical advection rate is possibly much higher than 240 m.yr^{-1} .

Chapter 6
Synthesis and
Scope of future research

6.1 Important results of this study:

New information on the regional oceanic carbon cycle and the upper ocean circulation are gained from this work for the northern Indian Ocean region, using ^{14}C measurements in shells of pre-nuclear era, maritime atmosphere and in seawater column. The important results emerged from this study, are summarized below.

6.1.1 Pre-nuclear $\Delta^{14}\text{C}$, ^{14}C reservoir ages and ΔR correction values for the northern Indian Ocean:

^{14}C reservoir ages for the northern Indian Ocean are determined for the first time through ^{14}C analysis of archived marine shells from the pre-nuclear era. The pre-nuclear $\Delta^{14}\text{C}$ values for the northern Bay of Bengal (Chilika Lake), the Andaman Sea and the southern Bay of Bengal are $-50\pm 6\text{‰}$, $-55\pm 4\text{‰}$ and $-61\pm 3\text{‰}$ respectively, whereas in the northern Arabian Sea (at Dwarka and Port Okha) it is $-78\pm 3\text{‰}$.

The ^{14}C reservoir ages in the northern Indian Ocean range from $229\pm 56\text{yr}$ to $385\pm 37\text{yr}$ in the Bay of Bengal, and $390\pm 38\text{yr}$ to $500\pm 46\text{yr}$ in the northern Arabian Sea. The enclosed basin of the Gulf of Kutch has a much younger reservoir age of $264\pm 34\text{yr}$. The upper ocean circulation patterns in these basins are reflected in the distribution of these ^{14}C reservoir ages. Thus oldest reservoir ages are found in the Arabian Sea where mixing with deeper ^{14}C -depleted waters is favored through wind induced upwelling and lower isopycnal gradients. The ^{14}C reservoir ages are younger in the Bay of Bengal, where vertical mixing is strongly damped due to steep isopycnal gradients, maintained by large amount of fresh water input through river discharge and precipitation.

The ΔR correction values corresponding to these reservoir ages are $-65\pm 53\text{yr}$ for the northern Bay of Bengal (Chilika Lake), $11\pm 35\text{yr}$ for the Andaman Sea and $32\pm 20\text{yr}$ for the southern Bay of Bengal (Palk Bay). Highest ΔR value obtained in this study is $163\pm 30\text{yr}$, for the northern Arabian Sea. These new sets of ΔR correction values will be useful for calibrating the ^{14}C ages of calcareous microfossils used for dating marine sediments, and also for calibrating the ^{14}C ages of calcareous archeological samples from the northern Indian Ocean coasts.

6.1.2 ^{14}C in atmospheric CO_2 over the northern Indian Ocean and evidence of modulation of atmospheric $^{14}\text{CO}_2$ by El Niño/Southern Oscillation events:

$\Delta^{14}\text{C}$ in the air over the northern Indian Ocean has been $109\pm 3\text{‰}$ in 1997 over the Bay of Bengal, $97\pm 2\text{‰}$ in 1998 over the Arabian Sea and $88\pm 2\text{‰}$ in 1999 over the Bay of Bengal. Comparison of these values with the $\Delta^{14}\text{C}$ measured between 1993 and 1995 over the Arabian Sea yield an average e-folding time of $17.0\pm 0.2\text{yr}$ for the removal of atmospheric ^{14}C in this region.

These measurements reveal presence of both spatial and interannual variability of atmospheric $\Delta^{14}\text{C}$ over the northern Indian Ocean. The air over the Arabian Sea has relatively lower $\Delta^{14}\text{C}$ than that over the Bay of Bengal. This difference is due to evasion of ^{14}C -depleted CO_2 from the Arabian Sea, which is absent or much less in the Bay of Bengal. The maritime $\Delta^{14}\text{C}$ measurements over the Bay of Bengal during 1997 and over the Arabian Sea during 1998 coincided with the beginning and end of the very strong El Niño event of 1997-'98, when $\Delta^{14}\text{C}$ of atmospheric CO_2 over the northern Indian Ocean was significantly higher than the expected trend by $\sim 9\text{‰}$.

To examine the influence of El Niño events on atmospheric $\Delta^{14}\text{C}$, the atmospheric $\Delta^{14}\text{C}$ data both in the pre-nuclear and post-nuclear periods are analyzed with suitable indices for El Niño. Analysis of high precision tree ring $\Delta^{14}\text{C}$ for the past three centuries (1650-1950AD), in trees from the Pacific coast of northwest U.S.A., revealed significant modulation of atmospheric $\Delta^{14}\text{C}$ by the El Niño events. The positive anomalies in this tree-ring $\Delta^{14}\text{C}$ data are found to correlate with positive Niño3-SST anomalies, which are commonly associated with the El Niño events. Association of positive excursions of atmospheric $\Delta^{14}\text{C}$ with El Niño events are also observed by comparing the monthly tropospheric $\Delta^{14}\text{C}$ data from Wellington, New Zealand (1970-1993AD) with multivariate ENSO index. In both cases, the positive $\Delta^{14}\text{C}$ anomalies appear to start in the year prior to that of the El Niño events, which suggests early reduction in the upwelling of CO_2 rich waters in the equatorial Pacific prior to these events. These observations suggest $\Delta^{14}\text{C}$ in the atmosphere over the Pacific Ocean is significantly influenced by the El Niño events. Thus high-frequency $\Delta^{14}\text{C}$ variations in sub-decadal time scales (2 to 9yr) can be partly attributed to oceanic CO_2 flux anomalies, associated with the thermohaline circulation changes during the El Niño events.

6.1.3 ^{14}C in the northern Indian Ocean two decades after GEOSECS:

This study reports the changes in the distribution of ^{14}C in the water column of the Bay of Bengal, the equatorial Indian Ocean and near the Red Sea mouth, about two decades after the GEOSECS expedition in this region during 1977 and 1978.

The new measurements show, that on an average there is only marginal change in the inventory of nuclear-bomb produced ^{14}C in the Arabian Sea and the Bay of Bengal, in two decades between 1978 and 1999. In the Arabian Sea, the mean penetration depth has increased on an average from ~270m during 1978 to ~330m during 1994 and 1995. The relative increase of the mean penetration depth is much higher in the Bay of Bengal, from ~168m during 1978 to ~300m during 1997 and 1999. At one station in the equatorial Indian Ocean, the mean penetration depth has increased from 194m to 533m, while the bomb- ^{14}C inventory has almost doubled from $5 \times 10^9 \text{ atoms.m}^{-2}$ to $9.5 \times 10^9 \text{ atoms.m}^{-2}$, between 1978 and 1997. These values indicate lateral advection of ^{14}C rich waters from the Pacific from southeast.

The air-sea CO_2 exchange rates in the northern Indian Ocean, as determined from the nuclear bomb produced ^{14}C inventories range from 7 to $17 \text{ mol.m}^{-2}.\text{yr}^{-1}$. Except for the equatorial Indian Ocean, the ^{14}C -derived exchange rates are mostly a function of long-term wind-speeds over this region. From the average ^{14}C derived CO_2 exchange rates and reported annual surface seawater pCO_2 values, the net flux of CO_2 from the Indian Ocean in the late 1990s has been estimated to $\sim 164 \text{ TgC.yr}^{-1}$. The entire Arabian Sea (within 0° - 25°N and 45°E - 80°E) is acting as a source of CO_2 , with estimated net ocean-air CO_2 flux of $\sim 174 \text{ TgC.yr}^{-1}$. The Bay of Bengal (within 0° - 23°N and 80°E - 98°E) is a sink of CO_2 , the net uptake rate of atmospheric CO_2 by the entire basin has been estimated to $\sim 9 \text{ TgC.yr}^{-1}$. The northern Bay of Bengal (15°N - 23°N) with an net uptake rate of $\sim 0.8 \text{ mol.m}^{-2}.\text{yr}^{-1}$ is a larger sink compared to its southern counterpart (0° - 15°N), which has net uptake rate of $< 0.1 \text{ mol.m}^{-2}.\text{yr}^{-1}$.

Based on the distribution of natural ^{14}C in the waters below 700m in selected northern Indian stations and using an one dimensional diffusion–advection model, the vertical advection rates (w) range from 5 to 14 m.yr^{-1} and eddy diffusive coefficients range from 2 to $4 \text{ cm}^2.\text{yr}^{-1}$. In the enclosed Andaman Basin, the average $\Delta^{14}\text{C}$ values of waters deeper than 1400m is -170‰ , significantly higher than that for the open Bay of Bengal (-190‰ to -195‰), due to rapid mixing of deep waters with the intermediate water induced by high heat flow and absence of deep-water sources.

6.2 Scope of future research:

Following studies are suggested for further understanding of the coupled ocean-atmosphere processes using ^{14}C distributions in the northern Indian Ocean, and also the variation of ^{14}C in a global perspective.

6.2.1 Further measurements of ^{14}C reservoir ages for the northern Indian Ocean and its variation in the past:

Although this work presents the first results of ^{14}C reservoir age for the northern Indian Ocean, the data are still spatially inadequate. To fill the gaps, more pre-bomb ^{14}C measurements are needed, particularly from the northern Bay of Bengal and the southern Arabian Sea. In absence of archived marine shells of known age, to determine the marine ^{14}C reservoir age, one can also measure ^{14}C in coral bands formed during the pre-nuclear era, or in shells and charcoal (of terrestrial plants) collected from same stratigraphic horizon (Southon, *et al.*, 1992). Paired ^{14}C measurements in shell and charcoal, collected from long and coastal sediment cores could also provide information on past variations of marine ^{14}C reservoir ages.

6.2.2 Spatial variation of atmospheric $\Delta^{14}\text{C}$ over the northern Indian Ocean:

The Arabian Sea being a stronger source of CO_2 to the atmosphere than the Bay of Bengal, the regional contrast of oceanic CO_2 sources should get reflected in the $\Delta^{14}\text{C}$ values of the atmosphere overlying these regions. Contemporaneous $\Delta^{14}\text{C}$ measurements in the atmosphere over the Arabian Sea and the Bay of Bengal can throw light on the presence of possible zonal variation of $\Delta^{14}\text{C}$.

Maritime CO_2 samples for $\Delta^{14}\text{C}$ analysis can be collected over these two regions during same season, preferably during spring, when the winds speeds are minimum. Such differences could also be deciphered from ^{14}C analysis in the tree-rings of coastal trees from this region. For ^{14}C measurements, tree-ring samples from suitable tropical trees can be collected from the Arabian Sea and the Bay of Bengal coasts. To avoid contamination by fossil fuel CO_2 from the continents, it is preferable to choose trees growing in islands away from the continent, *e.g.*, the Andaman and Nicobar Islands in the Bay of Bengal and the Lakshadweep Islands in the Arabian Sea. The rings of teak tree (*Tectona grandis*) are best suited for the purpose, since most of the tropical trees do not develop well-defined growth rings, due to less contrast in seasonality the tropics.

6.2.3 *Interannual variation of atmospheric $\Delta^{14}\text{C}$ in the equatorial Pacific:*

ENSO related $\Delta^{14}\text{C}$ variations in the atmosphere are expected to be highest in the eastern equatorial Pacific region, where the ENSO induced oceanic CO_2 flux variations are largest. High precision $\Delta^{14}\text{C}$ measurements of rings in trees collected near the eastern equatorial Pacific (*e.g.*, from the coasts of Ecuador or Peru), can record variations oceanic CO_2 flux, for several years in the past.

6.2.4 *Post-bomb evolution of mixed layer $\Delta^{14}\text{C}$ in the Indian Ocean:*

For calibrating the ocean general circulation models, one-time measurements of oceanic $\Delta^{14}\text{C}$ profiles can only give a snapshot distribution of this tracer. However, in order to better calibrate these models, it is also necessary to understand the temporal variation of this tracer in the oceanic mixed layer (Mahadevan, 2001). In the oceanic mixed layer, variation of $\Delta^{14}\text{C}$ of DIC is the net result of the atmospheric $\Delta^{14}\text{C}$ variation, air-sea CO_2 exchange rates, mixing with deeper ^{14}C depleted water through upwelling and variation induced by lateral transport processes. In tropics, the oceanic response of the atmospheric bomb- ^{14}C pulse can be faithfully recorded in the annual growth bands of hermatypic or reef building corals (Druffel, 1980, 1981, 1989; Guilderson, *et al.*, 1998, 1999, 2000b), as they grow at depths <100m within the oceanic mixed layer and derive their carbon mainly from the oceanic DIC. High-resolution $\Delta^{14}\text{C}$ measurements in coral growth bands can also reveal inter annual variations of the seasonal oscillations of ^{14}C in the DIC of the mixed layer, in response to seasonal changes of upwelling or lateral advection of waters with varying ^{14}C concentrations (Brown, *et al.*, 1993).

From the northern Indian Ocean, only reported coral ^{14}C measurements are from the Gulf of Kutch (Moore and Krishnaswami, 1974; Chakraborty, 1993) and from the Red Sea (Cember, 1989). The oceanographic features of these enclosed basins are significantly different from that of the open Indian Ocean. The mixed layer bomb- ^{14}C history for the main Indian Ocean basin is unknown so far. There are several potential coral reefs in this region, where such studies need to be initiated. ^{14}C measurements in corals collected from the reefs of Lakshadweep Islands (southern Arabian Sea), Palk Bay (southern Bay of Bengal), Andaman and Nicobar Islands (Bay of Bengal) can provide the mixed layer $\Delta^{14}\text{C}$ history for the northern Indian Ocean.

In the absence of corals, ^{14}C measurements can also be done in the annual growth layers of giant bivalve shells like *Tridacna* (Weidman and Jones, 1993). ^{14}C analysis in archived otoliths or scales of marine fish can also provide information on oceanic $\Delta^{14}\text{C}$ evolution (Highham and Hogg, 1995; Kalish, *et al.*, 2000; Brown, *et al.*, 2000). Such data give $\Delta^{14}\text{C}$ history averaged over a wide oceanic region, within which the fish is expected to migrate during its lifetime. However, a thorough understanding about the geographic habitat and the migration pattern of the chosen species of fish is necessary to interpret the ^{14}C variations in fish otoliths or scales.

^{14}C measurements in very small samples of tree-rings, corals or otoliths can only be achieved using accelerator mass spectrometry (AMS), rather than conventional β -counting technique by LSC. If AMS is used for atmospheric ^{14}C measurements, sampling time of few hours will be sufficient to collect enough CO_2 for an analysis. This will enable to examine the finer detail of the spatial variability of $\Delta^{14}\text{C}$ over a region, through collection of larger number of samples.

Appendix – A
Reporting of ¹⁴C data

Methods of reporting radiocarbon data:

All notations used for reporting the radiocarbon data in this study are according to the conventions of Stuiver and Pollach (1977). The method is described in details in Mook and van der Plicht (1999), and outlined here briefly.

The permil enrichment or depletion of a sample in ^{13}C relative to ^{12}C , relative to that in Vienna Pee Dee belemnite (V-PDB) standard (Gonfiantini, 1984), is expressed by the conventional delta (δ) notation as,

$$\delta^{13}\text{C}_{\text{Sample}} = [({}^{13}\text{C}/{}^{12}\text{C})_{\text{Sample}}/({}^{13}\text{C}/{}^{12}\text{C})_{\text{PDB}} - 1] \times 1000 \text{ ‰} \quad \dots(1)$$

If A_S is the net ^{14}C activity of a given volume of benzene prepared from a sample and A_{OX} being the net ^{14}C activity of same volume of benzene prepared from the standard NBS Oxalic Acid-I (HOx-I), then their activities, normalized for isotopic fractionation are given by,

$$A_{\text{SN}} = A_S \times [1 - 2(\delta^{13}\text{C}_{\text{Sample}} + 25)/1000] \quad \dots(2)$$

and

$$A_{\text{ON}} = 0.95 \times A_{\text{OX}} \times [1 - 2(\delta^{13}\text{C}_{\text{Oxalic}} + 19)/1000] \quad \dots(3)$$

Since in all ^{14}C measurements in this study have been done using NBS Oxalic Acid-II (NIST SRM 4990C) as standard, which has an activity 1.2736 ± 0.0004 times higher than NBS Oxalic Acid-I (Mann, 1983), the term A_{ON} has been divided by this factor. Unlike HOx-I, the new HOx-II standard with $\delta^{13}\text{C} = -17.6\text{‰}$, is to be normalized to $\delta^{13}\text{C} = -25\text{‰}$. The relative enrichment or depletion of the ^{14}C activity with respect to the oxalic acid standard is given by,

$$\delta^{14}\text{C} = [A_S/A_{\text{ON}} - 1] \times 1000 \text{ ‰} \quad \dots(4)$$

Same, after correcting for isotopic fractionation of the sample to $\delta^{13}\text{C} = -25\text{‰}$,

$$\Delta^{14}\text{C} = [A_{\text{SN}}/A_{\text{ON}} - 1] \times 1000 \text{ ‰} \quad \dots(5)$$

or,

$$\Delta^{14}\text{C} = \delta^{14}\text{C} - 2(\delta^{13}\text{C} + 25)(1 - \delta^{14}\text{C}/1000) \times 1000 \text{ ‰} \quad \dots(6)$$

Using the Libby ^{14}C half-life of 5568yr, the age (t) of the sample before 1950 AD (in yr BP) is given by,

$$t = -8033 \ln (A_{\text{SN}}/A_{\text{ON}}) \quad \dots(7)$$

The *Percent Modern Carbon* (PMC) in a sample is given by,

$$\text{PMC} = (A_{\text{SN}}/A_{\text{ON}}) \times e^{\lambda(1950-x)} \times 100\% \quad \dots(8)$$

where, $\lambda = (1/5730)\text{yr}^{-1}$ and 'x' is the year of measurement.

Appendix – B

Calculation of ^{14}C reservoir ages & ΔR correction values

The details of determining the reservoir ages and the ΔR correction values from conventional ^{14}C ages of known age are summarized in Stuiver, *et al.*, (1993a). The methods are briefly summarized here.

Regional ^{14}C reservoir ages:

The reservoir ages are obtained as the difference between the conventional ^{14}C -age of the known age marine carbonate sample (shell or coral) and ^{14}C -age of contemporary terrestrial samples at any given time (Stuiver, *et al.*, 1986), *i.e.*,

$$^{14}\text{C reservoir age} = \text{Marine } ^{14}\text{C age} - \text{Tree ring } ^{14}\text{C age} \quad \dots(1)$$

The tree ring ^{14}C age is taken from the INTCAL98 dataset, for the northern hemisphere decadal samples (Stuiver, *et al.*, 1998a). As far as bivalve shells are concerned, their typical life span is $\sim 10\text{yr}$. For calculating the reservoir ages, the decadal tree-ring ^{14}C values reported for the decade of the growth of the shell sample have been subtracted from their measured ^{14}C ages.

Regional ΔR correction values:

The regional difference of local ^{14}C reservoir ages from the average global marine reservoir correction is designated as ΔR (Stuiver and Braziunas, 1998b), *i.e.*,

$$\Delta R = \text{Regional marine } ^{14}\text{C age} - \text{Modeled marine } ^{14}\text{C age} \quad \dots(2)$$

$$\text{or, } \Delta R = \text{Regional } ^{14}\text{C reservoir age} - \text{Global modeled } ^{14}\text{C reservoir age} \quad \dots(3)$$

Reporting pooled ^{14}C reservoir ages and ΔR correction values:

The individual reservoir ages obtained for different samples collected from a given region show considerable variations, hence it is preferable to report pooled mean or error-weighted values (Stuiver, *et al.*, 1986). The final regional ^{14}C reservoir ages and ΔR correction values are reported as the pooled mean of all samples analyzed, given by,

$$\mu \pm \sigma = \Sigma[x_i/\sigma_i^2] / \Sigma[1/\sigma_i^2] \pm \sqrt{\Sigma[1/\sigma_i^2]} \quad \dots(4)$$

Here x_i is the measured reservoir age or ΔR correction value with uncertainty σ_i , and μ is the error weighted mean with uncertainty σ .

Appendix – C

Determination of bomb-¹⁴C inventories & Air-sea CO₂ exchange rates

Determination of bomb-¹⁴C inventory:

The inventories of bomb-¹⁴C are calculated following the procedures of Broecker, *et al.*, (1985). The area (A) between the measured $\Delta^{14}\text{C}$ depth profile and the reconstructed pre-nuclear $\Delta^{14}\text{C}$ depth profile ($\Delta^{14}\text{C}^0$) is calculated as,

$$A = \int_0^{z^0} (\Delta^{14}\text{C} - \Delta^{14}\text{C}^0) dz \quad \dots(1)$$

Here, z^0 is the depth at which the difference between $\Delta^{14}\text{C}$ and $\Delta^{14}\text{C}^0$ becomes negligible (<1‰). The mean penetration depth (Z) of bomb-¹⁴C is obtained as,

$$Z = A / (\Delta\Delta^{14}\text{C}) \quad \dots(2)$$

Here, $\Delta\Delta^{14}\text{C} = (\Delta^{14}\text{C} - \Delta^{14}\text{C}^0)_{\text{surface}}$ is the measured excess of surface water $\Delta^{14}\text{C}$ from its pre-nuclear value (Fig. C-1). The total column-inventory of bomb-¹⁴C is given by,

$$\Sigma^{14}\text{C} = \Sigma\text{CO}_2 \times A \times k \quad \dots(3)$$

Here ΣCO_2 is the mean DIC of the water column up to which bomb-¹⁴C has penetrated. The proportionality constant 'k' takes into account average density of seawater (1025kg.m^{-3}), Avogadro's number ($6.023 \times 10^{23} \text{atoms.mol}^{-1}$), and the ¹⁴C/¹²C atom ratio of the NBS Oxalic Acid-I standard (1.176×10^{12} , Stuiver, *et al.*, 1981). The inventory of bomb-¹⁴C is expressed in units of atoms of ¹⁴C per square unit area of the seawater column. Following this procedure, the estimate uncertainty of the calculated inventory is about $\pm 10\%$ (Peng, *et al.*, 1998). To compute the bomb-¹⁴C inventories, the measured $\Delta^{14}\text{C}$, SiO_2 and ΣCO_2 values were interpolated to every 1m. Pre-nuclear $\Delta^{14}\text{C}$ profiles ($\Delta^{14}\text{C}^0$) were then reconstructed from the measured values of silicate, using the empirical relationship of Broecker, *et al.*, (1995), $\Delta^{14}\text{C}^0 (\text{‰}) = -70 - \text{SiO}_3 (\mu\text{mol.kg}^{-1})$. The reconstructed pre-nuclear $\Delta^{14}\text{C}$ of surface was forced, to match with the values obtained from pre-bomb shells. The excess (or bomb) $\Delta^{14}\text{C}$ are then integrated until the difference becomes negligible and the inventory of bomb-¹⁴C is obtained using eqns. 1 and 3.

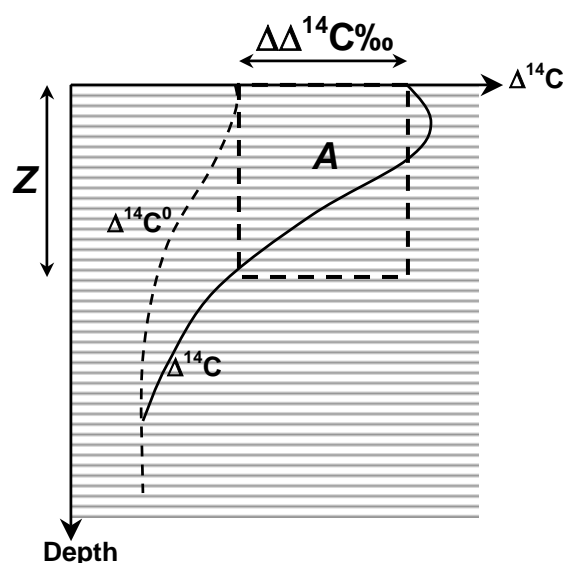


Figure C-1 Demonstration of integrating ¹⁴C profile to determine bomb-¹⁴C inventory in seawater column.

Determination of air-sea CO₂ exchange rate from bomb-¹⁴C inventory:

The air-sea CO₂ exchange rates were calculated following the procedure outlined by Stuiver, (1980), and is summarized below.

The total amount of bomb-¹⁴C penetrated in ocean is proportional to the air-sea exchange rate of CO₂ and the time integrated gradient of Δ¹⁴C between the atmosphere (Δ¹⁴C_{atm}) and the ocean surface mixed layer (Δ¹⁴C_{mix}). Assuming the mean steady state difference in Δ¹⁴C values between atmosphere and oceanic mixed layer is -60‰ for the northern Indian Ocean, the total amount of bomb-¹⁴C (Q_{14}), transferred per unit of ocean surface over time t (in years) is related to the air-sea exchange rate of CO₂ (F_{12}) as,

$$Q_{14} = 1.24 \times 10^{-15} F_{12} \int_0^t (\Delta^{14}\text{C}_{\text{atm}} - \Delta^{14}\text{C}_{\text{mix}} - 60) dt \quad \dots(4)$$

The constant term on the right hand side of *eqn. 4*, takes into account the isotopic fractionation factors for ocean-atmosphere transfer and normalization of ¹⁴C activity to δ¹³C value of -25‰ (Stuiver, 1980). Here Q_{14} is expressed in mol.m⁻² and F_{12} in mol.m⁻².yr⁻¹. For the onset of input of bomb-¹⁴C to the oceans, 1954 is taken as the initial year ($t = 0$).

The values of the integrals for Δ¹⁴C_{atm} and Δ¹⁴C_{mix} are obtained from Δ¹⁴C measurements in the atmosphere and in corals. The atmospheric Δ¹⁴C from 1954 and 1968 is adopted from the reported measurements from the tropical regions (*sec. 4.1*). From 1968 onward, an exponentially decreasing atmospheric Δ¹⁴C trend with e-folding time of 17yrs is adopted, fixing the Δ¹⁴C for the years 1980 and 1999 at 265‰ and 88‰ respectively. There are too few coral Δ¹⁴C measurements in the open northern Indian Ocean, to reconstruct the mixed layer Δ¹⁴C history for different regions. Between the years 1954 and 1973, the value of the integral of Δ¹⁴C_{mix} is taken as 1400 (Stuiver, 1980). From 1973 onward, a linear decrease of surface ocean Δ¹⁴C has been assumed, from a value of 140‰ in 1973 to 50‰ in 2000, to match with the observed values from the GEOSECS measurements during 1977-‘78 (Stuiver and Östlund, 1983) and during late 1990s (Bhushan, *et al.*, 2000, and the present study).

Q_{14} are calculated from the bomb ¹⁴C inventories for different stations, to determine the air-sea CO₂ exchange rates (F_{12}) using *eqn. 4*.

Appendix – D

Radiocarbon & hydrographic data

Station: SS#152/3829

Lat. 08° 31' E Long. 86° 02' E

Water depth: 3669m

Date sampled: February 16, 1997

Depth (m)	Potential Temp. (°C)	Salinity (PSU)	Potential density (σ_θ)	Dissolved Oxygen	Silicate	Phosphate	ΣCO_2	Radiocarbon results	
				(μmol.kg ⁻¹)				PRLCH code	$\Delta^{14}\text{C}$ (‰)
5	28.258	33.813	21.418	202.8	0.94	0.08	1936	564	38 ± 7
45	28.190	33.893	21.501	208.1	1.03	0.08	1915	591Q	64 ± 4
70	27.258	34.429	22.205	164.4	1.45	0.38	2000	592Q	-6 ± 4
150	19.929	34.852	24.668	30.9	6.40	1.86	2174	593Q	15 ± 5
300	12.123	35.015	26.577	32.8	40.07	2.45	2254	594Q	-62 ± 4
436	10.215	35.017	26.928	17.2	56.36	2.80	2277	595Q	-97 ± 4
504	9.519	35.002	27.035	31.4	41.68	2.55	2288	597Q	-105 ± 4
1275	4.818	34.855	27.582	126.4	—	2.49	2318	590Q	-169 ± 4
1670	3.169	34.792	27.704	118.8	136.83	2.75	2344	589Q	-194 ± 4
1821	2.760	34.774	27.727	122.6	153.00	2.64	2341	587Q	-174 ± 4
2004	2.393	34.758	27.746	120.2	115.19	2.54	2329	588Q	-172 ± 4
2057	2.314	34.755	27.750	—	134.38	2.70	2335	586Q	-184 ± 3
2476	1.832	34.735	27.772	—	131.24	2.80	—	585Q	-176 ± 4
2769	1.589	34.725	27.783	—	—	—	2310	584Q	—
3057	1.399	34.719	27.792	—	137.29	—	—	582Q	-179 ± 5

Station: SS#152/3846

Lat. 00° 01' N Long. 80° 03' E

Water depth: 4648m

Date sampled: March 1, 1997

Depth (m)	Potential Temp. (°C)	Salinity (PSU)	Potential density (σ_θ)	Dissolved Oxygen	Silicate*	Phosphate	ΣCO_2	Radiocarbon results		
				(μmol.kg ⁻¹)				PRLCH code	$\delta^{13}\text{C}$ (‰)	$\Delta^{14}\text{C}$ (‰)
5	29.028	34.889	21.792	209.4		0.18	1944	423	4.5	55 ± 7
50	28.118	35.173	22.486	205.3		—	1956	422	(0.0)	77 ± 7
100	20.194	35.249	24.706	129.8		0.90	2069	421	3.6	59 ± 7
175	14.158	35.123	26.249	47.3		1.46	2177	420	2.3	12 ± 6
271	11.869	35.055	26.656	83.9		1.59	2185	416	2.9	11 ± 7
347	10.585	35.003	26.852	74.9		1.86	—	415	1.5	-42 ± 6
440	10.072	34.988	26.930	69.6		1.95	2210	414	0.3	-52 ± 6
573	9.537	35.003	27.032	49.2		2.15	2233	413	0.4	-95 ± 6
665	9.077	34.995	27.102	58.0		2.23	2251	412	3.7	-100 ± 6
851	7.455	34.956	27.320	68.8		2.92	2271	411	0.4	-149 ± 5
1061	6.437	34.918	27.431	62.0		2.59	2297	410	3.8	-146 ± 6
1587	3.953	34.814	27.643	111.0		2.28	2297	408	1.4	-169 ± 5
1857	3.107	34.783	27.702	120.7		2.68	2311	407	(0.0)	-191 ± 5
2282	2.147	34.744	27.755	144.3		2.56	2311	409	(0.0)	-195 ± 4
2665	1.737	34.727	27.774	151.0		—	—	405	2.7	-180 ± 5
3380	1.293	34.713	27.794	169.9		2.52	2278	403	(0.0)	-183 ± 6
3658	1.186	34.709	27.799	155.1		2.29	2304	402	(0.0)	-187 ± 5

*Silicate not measured (GEOSECS 448 silicate data was used to reconstruct natural $\Delta^{14}\text{C}$)

Station: SS#164/4018

Lat. 13°21' N Long. 53°16' E

Water depth: 2830m

Date sampled: April 2, 1998

Depth (m)	Potential Temp. (°C)	Salinity (PSU)	Potential density (σ_θ)	Dissolved Oxygen	Silicate	Nitrate	Phosphate	ΣCO_2	Radiocarbon results		
				(μmol.kg ⁻¹)					PRLCH code	$\delta^{13}\text{C}$ (‰)	$\Delta^{14}\text{C}$ (‰)
4	28.902	35.400	22.400	199.2	0.82	1.16	0.18	2205	—	—	—
75	26.682	36.039	23.604	203.3	2.54	0.69	0.02	2016	449	(0.0)	43 ± 6
135	23.756	36.032	24.497	169.6	1.68	6.69	0.52	2062	448	1.4	35 ± 5
200	18.208	35.581	25.667	21.7	19.63	23.74	1.94	2230	460	(0.0)	30 ± 6
342	13.771	35.565	26.673	12.0	28.15	26.95	2.00	2266	459	-1.1	-20 ± 5
464	13.171	35.702	26.903	3.9	35.83	25.10	2.35	2275	458	1.9	-62 ± 5
640	11.495	35.607	27.157	7.6	46.07	28.77	2.41	2268	457	0.1	-99 ± 5
790	10.203	35.499	27.307	10.4	58.00	32.91	2.43	2290	456	-1.7	-126 ± 5
989	8.649	35.351	27.450	15.2	70.80	34.29	2.46	2332	454	(0.0)	-122 ± 6
1309	6.230	35.139	27.633	28.8	91.27	36.13	2.70	2346	464	2.3	-157 ± 4
1563	4.703	35.003	27.712	57.1	110.88	34.75	2.65	2357	463	0.0	-153 ± 8
1973	3.018	34.855	27.768	—	125.38	34.28	2.55	2347	462	1.4	-161 ± 4
2172	2.509	34.815	27.781	102.4	136.47	33.36	2.34	2341	461	(0.0)	-179 ± 5
2401	2.127	34.788	27.792	114.9	139.03	32.90	2.46	2334	447	-0.4	-209 ± 5
2601	1.889	34.772	27.798	124.0	141.59	32.44	2.36	2340	446	-1.8	-189 ± 6
2800	1.746	34.763	27.802	126.1	141.59	33.36	2.34	2330	445	(0.0)	-205 ± 7

Station: SS#172/4030

Lat. 18° 59' N Long. 89° 32' E

Water depth: 1851m

Date sampled: February 3, 1999

Depth (m)	Potential Temp (°C)	Salinity (PSU)	Potential density (σ_θ)	Dissolved Oxygen	Silicate	Nitrate	Phosphate	ΣCO_2	Radiocarbon results		
				(μmol.kg ⁻¹)					PRLCH code	$\delta^{13}\text{C}$ (‰)	$\Delta^{14}\text{C}$ (‰)
5	26.164	32.327	20.969	215.7	BDL	BDL	0.13	1866	560	-1.9	18 ± 6
58	26.319	33.846	22.065	155.8	1.16	4.33	0.57	1953	—	—	—
101	23.021	34.599	23.629	16.1	14.01	23.70	1.82	2128	571	-1.0	13 ± 5
200	14.831	34.913	25.943	2.8	29.20	31.04	2.32	2214	572	-0.3	-60 ± 4
300	11.893	34.989	26.602	4.0	35.62	34.39	2.54	2252	567	-0.5	-90 ± 5
397	10.775	34.999	26.816	4.3	40.88	36.11	2.61	2268	570	-1.2	-106 ± 4
551	9.646	34.992	27.006	6.7	49.64	37.59	2.87	2281	569	-0.6	-113 ± 4
701	8.686	34.971	27.146	12.8	59.57	38.32	2.91	2280	568	-2.0	-133 ± 4
850	7.789	34.946	27.263	24.6	68.69	38.71	2.72	2290	531	-1.1	-148 ± 4
1001	6.978	34.920	27.359	38.6	78.26	38.63	2.88	2298	533	-1.5	-136 ± 4
1201	5.657	34.868	27.492	56.4	94.90	38.80	2.86	2306	566	-1.0	-159 ± 3
1401	4.703	34.837	27.580	68.3	105.12	38.57	3.01	2315	565	-2.5	-165 ± 4
1600	3.673	34.790	27.653	89.1	122.06	38.14	3.24	2325	525	-1.3	-158 ± 4
1800	2.557	34.746	27.722	113.6	133.45	37.57	2.71	2329	524	-0.1	-185 ± 5

Station: SS#172/4036

Lat. 13° 04' N Long. 94° 06' E

Water depth: 1991m

Date sampled: February 13, 1999

Depth (m)	Potential Temp. (°C)	Salinity (PSU)	Potential density (σ_θ)	Dissolved Oxygen	Silicate	Nitrate	Phosphate	ΣCO_2	Radiocarbon results		
				(μmol.kg ⁻¹)					PRLCH code	$\delta^{13}\text{C}$ (‰)	$\Delta^{14}\text{C}$ (‰)
5	28.282	33.452	21.141	209.2	BDL	BDL	BDL	1875	521	3.1	44 ± 5
51	28.062	33.610	21.332	196.9	BDL	BDL	0.06	1888	520	5.7	55 ± 5
100	25.713	34.383	22.662	107.5	7.18	11.88	0.84	2028	519	(2.0)	14 ± 5
202	14.241	34.936	26.088	19.3	29.79	32.06	2.26	2218	517	4.3	-20 ± 6
299	11.408	35.011	26.710	20.6	37.77	35.44	2.36	2263	516	(2.0)	-81 ± 4
404	10.190	35.009	26.927	22.9	44.43	35.06	2.47	2256	514	(2.0)	-99 ± 5
500	9.567	34.999	27.025	-	50.86	35.76	2.57	2269	511	1.1	-111 ± 5
703	7.998	34.962	27.245	-	66.23	36.91	2.62	2289	510	-1.7	-147 ± 5
885	6.728	34.918	27.392	53.6	82.16	37.27	2.65	2299	509	4.4	-148 ± 4
1101	5.790	34.887	27.490	64.0	92.78	37.69	2.69	2312	504	0.7	-156 ± 4
1300	5.162	34.879	27.561	69.8	99.76	38.01	2.70	2322	503	1.7	-159 ± 4
1501	5.002	34.863	27.567	67.7	100.60	37.83	2.72	2323	502	(2.0)	-181 ± 5
1699	4.889	34.858	27.576	71.4	103.39	38.10	2.72	2323	501	(2.0)	-169 ± 5
1905	4.855	34.857	27.579	75.2	104.23	38.38	2.70	2326	498	(2.0)	-178 ± 4

Station: SS#172/4037

Lat. 10° 48' N Long. 94° 46' E

Water depth: 3186m

Date sampled: February 16, 1999

Depth (m)	Potential Temp. (°C)	Salinity (PSU)	Potential density (σ_θ)	Dissolved Oxygen	Silicate	Nitrate	Phosphate	ΣCO_2	Radiocarbon results		
				(μmol.kg ⁻¹)					PRLCH code	$\delta^{13}\text{C}$ (‰)	$\Delta^{14}\text{C}$ (‰)
6	28.465	33.094	20.813	211.1	BDL	BDL	0.18	1891	495	(0.0)	40 ± 5
52	28.032	34.693	22.155	188.8	0.61	0.51	0.27	1925	494	-3.5	52 ± 6
100	25.112	34.500	22.932	110.5	8.80	14.85	1.39	2065	493	2.9	22 ± 4
150	17.540	34.795	25.232	29.0	21.81	27.03	1.88	2180	492	4.0	-15 ± 5
201	12.945	34.930	26.350	12.7	29.04	32.21	2.31	2228	491	2.5	-58 ± 4
300	11.306	34.999	26.720	24.2	35.38	34.47	2.39	2253	490	(0.0)	-72 ± 4
401	10.556	35.022	26.873	25.9	38.41	35.54	2.54	2259	489	1.7	-93 ± 4
501	9.724	35.009	27.006	30.4	45.35	36.64	2.71	2271	488	(0.0)	-101 ± 5
702	8.430	34.980	27.193	39.5	58.50	37.64	2.61	2286	487	1.1	-124 ± 5
900	7.047	34.936	27.362	51.1	74.67	38.31	2.74	2293	486	(0.0)	-147 ± 5
1100	5.743	34.897	27.504	62.7	87.68	37.80	2.79	2305	485	0.5	-152 ± 5
1239	5.348	34.876	27.536	70.4	94.28	37.72	2.83	2311	484	0.4	-161 ± 5
1401	5.059	34.869	27.565	77.3	97.42	37.89	2.87	2317	483	2.8	-168 ± 5
1601	4.902	34.862	27.577	76.3	99.30	37.89	2.89	2314	482	(0.0)	-172 ± 5
1800	4.800	34.860	27.587	79.0	99.93	38.14	2.80	2328	481	1.4	-169 ± 5
2000	4.755	34.857	27.590	78.1	100.56	37.97	2.89	2323	480	-0.2	-167 ± 4
2400	4.716	34.855	27.593	79.8	101.19	38.14	2.82	2321	478	-0.3	-186 ± 5
2601	4.710	34.857	27.595	79.7	101.19	38.30	2.93	2325	477	-1.7	-166 ± 5
2875	4.707	34.853	27.592	79.8	101.19	38.14	2.82	2312	476	-0.4	-181 ± 5

Station: SS#172/4041

Lat. 05° 00' N Long. 86° 00' E

Water depth: 3996m

Date sampled: February 23, 1999

Depth (m)	Potential Temp. (°C)	Salinity (PSU)	Potential density (σ_θ)	Dissolved Oxygen	Silicate	Nitrate	Phosphate	ΣCO_2	Radiocarbon results		
				(μmol.kg ⁻¹)					PRLCH code	$\delta^{13}\text{C}$ (‰)	$\Delta^{14}\text{C}$ (‰)
6	28.912	34.500	21.774	223.4	BDL	BDL	BDL	1913	547	0.9	57 ± 5
71	26.802	35.217	23.053	178.7	2.05	4.11	0.32	1991	546	-0.7	62 ± 4
201	13.928	35.021	26.340	1.9	29.42	31.60	2.11	2223	535	-0.4	-51 ± 7
335	11.142	35.067	26.835	5.0	29.42	31.51	2.05	2225	534	1.4	—
412	10.578	35.057	26.938	23.3	40.37	35.22	2.42	2251	532Q	-0.3	-89 ± 4
499	9.826	35.042	27.050	31.2	45.16	35.55	2.46	2257	530	-1.5	-95 ± 4
701	8.174	35.007	27.253	33.7	61.58	37.03	2.62	2276	529Q	-0.4	-131 ± 4
900	7.003	34.954	27.373	38.1	78.47	38.35	2.75	2295	558	(0.0)	-149 ± 4
1102	5.899	34.910	27.489	56.3	90.91	38.34	2.75	2305	528	-2.3	-168 ± 4
1250	5.317	34.884	27.549	66.2	98.07	38.34	2.79	2310	527Q	-1.3	-168 ± 4
1502	4.183	34.850	27.647	85.3	108.97	37.77	2.73	2311	557Q	(0.0)	-168 ± 6
1750	3.264	34.807	27.714	107.7	118.51	37.36	2.68	2308	556Q	(0.0)	-199 ± 4
1999	2.543	34.775	27.752	126.6	127.36	36.95	2.65	2314	555	(0.0)	-187 ± 3
2200	2.215	34.767	27.774	—	131.45	36.62	2.58	—	553	(0.0)	-204 ± 4
2400	1.958	34.750	27.779	144.0	132.47	36.46	2.49	2314	551	-1.4	-197 ± 4
2599	1.717	34.742	27.787	156.0	135.53	36.21	2.51	2319	550	-1.2	-200 ± 4
2851	1.520	34.736	27.795	160.7	136.55	36.10	2.45	2305	549	-1.1	-207 ± 5
2973	1.461	—	—	153.4	136.89	36.10	2.46	2314	552	-1.2	-209 ± 3
3100	1.375	34.736	27.807	154.7	138.26	36.04	2.55	2309	548	-0.8	-197 ± 4

References

- Archer**, D.E., Takahashi, T., Sutherland, S., Goddard, J., Chipman, D., Rodgers, K., and Ogura, H. (1996) Daily, seasonal and interannual variability of sea-surface carbon and nutrient concentration in the equatorial Pacific Ocean. *Deep-Sea Research Part II – Topical Studies in Oceanography*, **43**:779–808.
- Bacastow**, R.B. (1976) Modulation of atmospheric carbon dioxide by the Southern Oscillation. *Nature*, **261**:116–118.
- Bacastow**, R.B., Adams, J.A., Keeling, C.D., Moss, D.J., and Whorf, T.P. (1980) Atmospheric carbon dioxide, the Southern Oscillation, and the weak 1975 El Niño. *Science*, **210**:66–68.
- Bard**, E. (1988) Correction of accelerator mass spectrometry ^{14}C ages measured in planktonic foraminifera: Paleoceanographic implications. *Paleoceanography*, **3**:635–645.
- Bard**, E., Arnold, M., Ostlund, G.H., Maurice, P., Monfray, P., and Duplessy, J.–C. (1988) Penetration of bomb radiocarbon in the tropical Indian Ocean measured by means of accelerator mass spectrometry. *Earth and Planetary Science Letters*, **87**:379–389.
- Bard**, E., Arnold, M., Toggweiler, J.R., Maurice, P., and Duplessy, J.–C. (1989) Bomb ^{14}C in the Indian Ocean measured by accelerator mass spectrometry: oceanographic implications. *Radiocarbon*, **31**:510–522.
- Bevington**, P.R. (1969) Data reduction and error analysis for the physical sciences. McGraw Hill, New York, 119pp.
- Bien**, G.S., Rakestraw, N.W., and Suess, H. (1965) Radiocarbon concentration in the Pacific and Indian Oceans and its relation to deep water movements. *Limnology and Oceanography*, **10**:R25–37.
- Bhushan**, R., Chakraborty, S., and Krishnaswami, S. (1994) Physical Research Laboratory (Chemistry) radiocarbon date list I. *Radiocarbon*, **36**:251–256.
- Bhushan**, R., Krishnaswami, S., and Somayajulu, B.L.K. (1997) ^{14}C in air over the Arabian Sea. *Current Science*, **73**:273–276.
- Bhushan**, R., Somayajulu, B.L.K., Chakraborty, S., and Krishnaswami, S. (2000) in the Arabian Sea water column: Temporal variations in bomb ^{14}C inventory since the GEOSECS and CO_2 air-sea exchange rates. *Journal of Geophysical Research*, **105**:14,279–14,282.

- Braziunas, T.F., Fung, I., and Stuiver, M. (1995)** The preindustrial atmospheric $^{14}\text{CO}_2$ latitudinal gradient as related to exchanges among atmospheric, oceanic, and terrestrial reservoirs. *Global Biogeochemical Cycles*, **9**:565–584.
- Broecker, W.S., Peng T.–H., and Stuiver, M. (1978)** An estimate of the upwelling rate in the equatorial Atlantic based on the distribution of bomb radiocarbon. *Journal of Geophysical Research*, **83**:6,179–6,186.
- Broecker, W.S., and Peng, T.–H. (1982)** *Tracers in the Sea*, Lamont-Doherty Geological Observatory Press, Palisades, New York.
- Broecker, W.S., Peng, T.–H., Östlund, H.G., and Stuiver, M. (1985)** The distribution of bomb radiocarbon in the ocean. *Journal of Geophysical Research*, **90**:6,953–6,970.
- Broecker, W.S., Sutherland, S. Smethie, W., Peng, T.–H., and Östlund, H.G. (1995)** Oceanic radiocarbon: Separation of the natural and bomb components. *Global Biogeochemical Cycles*, **9**:263–288.
- Brown, T.A., Farwell, G.W., Grootes, P.M., Schmidt, F.H., and Stuiver, M. (1993)** Intra-annual variability of the radiocarbon content of corals from the Galapagos Islands. *Radiocarbon*, **35**:245–251.
- Brown, T.A., Freidland, K.D. Quay, P.D., and Francis, R.C. (2000)** Salmon scale derived open-ocean surface water ^{14}C concentrations in the Labrador Sea. In: *Abstracts, 17th International Radiocarbon Conference*, June 18–23 2000, Judean Hills, Israel, 95pp.
- Buddemeier, R.W., Maragos, J.E., and Knutson, D.W. (1974)** Radiographic studies of reef coral exoskeletons: rates and patterns of coral growth. *Journal of Experimental Marine Biology and Ecology*, **14**:179–200.
- Burns, R.E. (1964)** Sea bottom heat-flow measurements in the Andaman Sea. *Journal of Geophysical Research*, **69**:4,918–4,919.
- Carpenter, J.H. (1965)** The Chesapeake Bay Institute. Technique for the Winkler oxygen method. *Limnology and Oceanography*, **10**:141–143.
- Cember, R. (1989)** Bomb radiocarbon in the Red Sea: A medium-scale gas exchange experiment. *Journal of Geophysical Research*, **94**:2,111–2,123.
- Chakraborty, S. (1993)** Environmental significance of isotopic and trace elemental variations in banded corals. *Ph.D.–Thesis, MS University of Baroda, Vadodara, India.*

- Chakraborty, S., Ramesh, R., and Krishnaswami, S.** (1994) Air-sea exchange of CO₂ in the Gulf of Kutch, northern Arabian Sea based on bomb-carbon in corals and tree rings. *Proceedings of the Indian Academy of Sciences (Earth & Planetary Science)*, **103**:231–242.
- Conway, T.J., Tans, P.P., Waterman, L.S., Thoning, K.W., Kitzis, D.R., Masarie, K.A., and Zhang, N.** (1994) Evidence for interannual variability of the carbon cycle from the National Oceanic and Atmospheric Administration/Climate Monitoring and Diagnostics Laboratory Global Air Sampling Network. *Journal of Geophysical Research*, **99**:22,831–22,855.
- Craig, H.** (1969) Abyssal carbon and radiocarbon in the Pacific. *Journal of Geophysical Research*, **74**:5,491–5,506.
- Damon, P.E.** (1995) A note concerning “Location-dependent differences in the ¹⁴C content of wood” by McCormac *et al.* *Radiocarbon*, **37**:829–830.
- Damon, P.E., Lerman, J.C., and Long, A.** (1978) Temporal fluctuations of atmospheric ¹⁴C: Causal factors and implications. *Annual Reviews of Earth & Planetary Science*, **6**:457–494.
- Damon, P.E., and Sternberg, R.S.** (1989) Global production and decay of radiocarbon. *Radiocarbon*, **31**:697–703.
- Damon, P.E., Cheng, S., and Linick, T.W.** (1989) Fine and hyperfine structure in the spectrum of secular variations of atmospheric ¹⁴C. *Radiocarbon*, **31**:704–718.
- Damon, P.E., Burr, G.S., and Peristykh, A.** (1999) $\Delta^{14}\text{C}$ and Ekman transport, spiral and west coast upwelling. In: (Storohmaier, B., comp.) *Abstracts, 8th International Conference on Accelerator Mass Spectrometry, 6–10 September 1999, Vienna, Austria*, 101pp.
- Damon, P.E., and Peristykh, A.N.** (2000) Radiocarbon calibration and application to geophysics, solar physics, and astrophysics. *Radiocarbon*, **42**:137–150.
- DOE** (1994) *Handbook of methods for the analysis of the various parameters of the carbon dioxide system in seawater; version 2*. Dickson, A.G., and Goyet, C. eds. CDIAC-74, Oak Ridge National Laboratory, Oak Ridge, Tennessee, USA.
- Druffel, E.R.M.** (1980) Radiocarbon in annual coral rings of Belize and Florida. *Proceedings of the 10th International ¹⁴C Conference, Radiocarbon*, **22**:363–371.

- Druffel, E.R.M.** (1981) Radiocarbon in annual coral rings from the eastern tropical Pacific Ocean. *Geophysical Research Letters*, **8**:59–62.
- Druffel, E.R.M.** (1987) Bomb radiocarbon in the Pacific: Annual and seasonal time-scale variations. *Journal of Marine Research*, **45**:667–698.
- Druffel, E.R.M.** (1989) Decade time scale variability of ventilation in the North Atlantic: High-precision measurements of bomb radiocarbon in banded corals. *Journal of Geophysical Research*, **94**:3,271–3,285.
- Druffel, E.R.M., and Linick, T.W.** (1978) Radiocarbon in annual coral rings of Florida. *Geophysical Research Letters*, **5**:913–916.
- Druffel, E.R.M., and Suess, H.** (1983) On the radiocarbon record in the banded corals: Exchange parameters and net transport of $^{14}\text{CO}_2$ between atmosphere and surface ocean. In: (Keeling, C.D., and Cicerone, R.J., eds.) *Proceedings of Bern CO₂ Symposium*, September 14–18 1981, Bern, Switzerland. *Journal of Geophysical Research*, **88**:1,271–1,280.
- Druffel, E.R.M., and Griffin, S.** (1993) Large variations of surface ocean radiocarbon: Evidence of circulation changes in the southwestern Pacific. *Journal of Geophysical Research*, **98**:20,249–20,259.
- Dupplessy, J.-C.** (1982) Glacial to interglacial contrasts in the northern Indian Ocean. *Nature*, **295**:494–498.
- Dutta, K., Bhushan, R., and Somayajulu B.L.K.** (2000a) Anthropogenic radiocarbon in Bay of Bengal: Two decades after GEOSECS. In: *Abstracts, 17th International Radiocarbon Conference*, June 18–23 2000, Judean Hills, Israel, 97pp.
- Dutta, K., Bhushan, R., and Somayajulu B.L.K.** (2000b) ^{14}C in archived marine shells from the Arabian Sea and the Bay of Bengal. In: *Abstracts, 17th International Radiocarbon Conference*, June 18–23 2000, Judean Hills, Israel, 99pp.
- Dutta, K., Bhushan, R., and Somayajulu, B.L.K.** (2001a) ΔR correction values for the Northern Indian Ocean. In: *Proceedings of the 17th International ^{14}C Conference. Radiocarbon*, **43** (in press).
- Dutta, K., Bhushan, R., and Somayajulu, B.L.K.** (2001b) $^{14}\text{CO}_2$ in maritime air over the northern Indian Ocean. In: *Proceedings of 3rd IAEA Conference on “The Study of Environmental Change Using Isotope Techniques,”* April 23–27 2001, Vienna, Austria.

- Dye, T.** (1994) Apparent ages of marine shells: implications for archeological dating in Hawai'i. *Radiocarbon*, **36**:51–57.
- Elliot, W.P., Angell, J.K., Thoning, K.W.** (1991) Relation of atmospheric CO₂ to tropical sea and air temperatures. *Tellus*, **43(B)**:144–155.
- Emery, W.J., and Meincke, J.** (1986) Global water masses: Summary and review. *Oceanologica Acta*, **9**:383–391.
- Enfield, D.B.** (1988) Is El Niño becoming more common? *Oceanography*, **1**:23–27.
- Enting, I.G., and Pearman, G.I.** (1982) Description of a one-dimensional global carbon cycle model. *Division of Atmospheric Physics Technical paper No. 42*, CSIRO, Melbourne, Australia.
- Feely, R.A., Wanninkhof, R., Goyet, C., Archer, D.E., and Takahashi, T.** (1997) Variability of CO₂ distributions and sea-air fluxes in the central and eastern Pacific during the 1991-1994 El Niño. *Deep-Sea Research Part II – Topical Studies in Oceanography*, **44**:1851–1867.
- Feely, R.A., Wanninkhof, R., Goyet, C., Archer, D.E., and Takahashi, T.** (1999) Influence of El Niño on the equatorial Pacific contribution to atmospheric CO₂ accumulation. *Nature*, **398**:597–601.
- Fine, R.A.** (1985) Direct evidence using tritium data for throughflow from the Pacific into the Indian Ocean. *Nature*, **315**:478–480.
- Fonselius, S., and Östlund, G.** (1959) Natural radiocarbon measurements on surface water from the North Atlantic and the Arctic Sea. *Tellus*, **11**:77–82.
- Gage, K.S., and Reid, G.C.** (1986) The tropical tropopause and the El Niño of 1982–1983. *Journal of Geophysical Research*, **91**:13,315–13,317.
- Gaudry, A., Monfray, P., Polian, G., and Lambert, G.** (1987) The 1982-1983 El Niño: A 6billion ton CO₂ release. *Tellus*, **39(B)**:209–213.
- George, M.D., Kumar, M.D., Naqvi, S.W.A., Banerjee, S., Narvekar, P.V., de Sousa, S.N., and Jayakumar, D.A.** (1994) A study of carbon dioxide system in the northern Indian Ocean during premonsoon. *Marine Chemistry*, **47**:243–254.
- Godwin, H.** (1962) Half-life of radiocarbon. *Nature*, **195**:984.

- Gonfiantini, R.** (1984) Stable Isotope Reference Samples for Geochemical and Hydrological Investigations. In: *Report Adv. Group meeting*, September 1983, IAEA, Vienna, Austria. 77pp.
- Goyet, C.** (1997) Partial pressure of CO₂ in water, along ship track. JGOFS Arabian Sea/TTN-044 – SeaSore cruise 2, onboard *Thomas Thompson*.
<<http://usjgofs.who.edu/jg/dir/jgofs/arabian/ttn-044>>
- Goyet, C., Millero, F.J., O’Sullivan, D.W., Eiseheid, G., McCue, S.J., and Bellerby, R.G.J.** (1998) Temporal variations of pCO₂ in the surface waters of the Arabian Sea in 1995. *Deep Sea Research Part I*, **45**:609–623.
- Goyet, C., Coatanoan, C., Eiseheid, G., Amaoka, T., Okuda, K., Healy, R., and Tsunogai, S.** (1999) Spatial variation of total CO₂ and total alkalinity in the northern Indian Ocean: A novel approach for the quantification of anthropogenic CO₂ in seawater. *Journal of Marine Research*, **57**:135–163.
- Guilderson, T.P., Schrag, D.P., Kashgarian, M., and Southon, J.** (1998) Radiocarbon variability in the western equatorial Pacific inferred from a high-resolution coral record from Nauru Island. *Journal of Geophysical Research*, **103**:24,641–24,650.
- Guilderson, T.P., Schrag, D.P., Kashgarian, M., and Southon, J.** (1999) Nauru Island Coral Radiocarbon Data, IGBP PAGES/World Data Center-A Paleoclimatology Data Contribution Series #1999-043. NOAA/NGDC Paleoclimatology Program, Boulder CO, U.S.A. (original reference Guilderson, *et al.*, 1998).
- Guilderson, T.P., Caldeira, K., and Duffy, P.B.** (2000a) Radiocarbon as diagnostic tracer in ocean and carbon cycle modeling. *Global Biogeochemical Cycles*, **14**:887–902.
- Guilderson, T.P., Schrag, D.P., Goddard, E., Kashgarian, M., Wellington, G. M., and Linsley, B.K.** (2000b) Southwest subtropical Pacific surface water radiocarbon in a high-resolution coral record. *Radiocarbon*, **42**:249–256.
- Gupta, S.K., and Polach, H.A.** (1985) Radiocarbon dating practices at ANU. *Radiocarbon Laboratory Handbook*, Research School of Pacific Studies, Australian National University, Canberra, Australia, 173pp.
- Higham, T.F.G., and Hogg, A.G.** (1995) Radiocarbon dating of prehistoric shell from New Zealand and calculation of the ΔR value using fish otoliths. In: *Proceedings of the 15th International ¹⁴C Conference*, *Radiocarbon*, **37**:409–416.

- Head, J.** (1979) Structure and chemical properties of fresh and degraded wood. *M.Sc.–Thesis*, Australian National University, Canberra, Australia.
- Hesshaimer, V.** (1977) Tracing the global carbon cycle with bomb radiocarbon. *Ph.D.–Thesis*, University of Heidelberg, Heidelberg, Germany.
- Hesshaimer, V., and Levin, I.** (2000) Revision of the stratospheric bomb ^{14}C inventory. *Journal of Geophysical Research*, **105**:11,641–11,658.
- Hua, Q., Barbetti, M., Jacobsen, G.E., Zoppi, U., and Lawson, E.M.** (2000) Bomb radiocarbon in annual tree rings from Thailand and Australia. *Proceedings of 8th AMS Conference, Nuclear Instruments and Methods in Physics Research– B*, **172**:359–365.
- Ingram, B.L.** (1998) Differences in radiocarbon age between shell and charcoal from a Holocene shell mound in northern California. *Quaternary Research*, **49**:102–110.
- Jain, A.K., Kheshgi, H.S., Hoffert, M.I., Wuebbles, D.J.** (1995) Distribution of radiocarbon as a test of global carbon cycle models. *Global Biogeochemical Cycles*, **9**:153–166.
- JGOFS** (Joint Global Ocean Flux Study) Report No. 19 (1996) Protocols for the JGOFS core measurements. *Intergovernmental Oceanographic Commission*, Bergen, Norway.
- Johnson, K.M., King, A.E., and Seiburth, J.M.** (1985) Coulometric TCO_2 analyses for marine studies; an introduction. *Marine Chemistry*, **16**:61–82.
- Jiricovic, J.L., and Kalin, R.M.** (1993) A possible paleoclimatic ENSO indicator in the spatial variation of annual tree-ring ^{14}C . *Geophysical Research Letters*, **20**:439–442.
- Kalish, J.M.** (1993) Pre- and post-bomb radiocarbon in fish otoliths. *Earth and Planetary Science Letters*, **114**:549–554.
- Kalish, J.M., Nydal, R., Neadraas, K., Burr, G.S., and Eine, G.L.** (2000) A 70 years long time series of radiocarbon from cod otoliths in the Barents Sea. In: *Abstracts, 17th International Radiocarbon Conference*, June 18–23 2000, Judean Hills, Israel, 94pp.
- Kalnay, E., Kanamitsu, M., Kistler, R., Collins, W., Deaven, D., Gandin, L., Iredell, M., Saha, S., White, G., Woollen, J., Zhu, Y., Chelliah, M., Ebisuzaki, W., Higgins, W., Janowiak, J., Mo, K.C., Ropelewski, C., Wang, J., Leetmaa, A., Reynolds, R., Jenne, R., and Joseph, D.** (1996) The NCEP/NCAR reanalysis 40-year project. *Bulletin of American Meteorological Society*, **77**:437–471.

- Keeling, C.D.,** and Revelle, R. (1985) Effects of El-Niño southern oscillation on the atmospheric content of carbon dioxide. *Meteoritics*, **20**:437–450.
- Keeling, C.D.,** Bacastow, R.B., Carter, A.F., Piper, S.C., Whorf, T.P., Heimann, M., Mook, W.G., and Roeloffzen, H. (1989) A three dimensional model of atmospheric CO₂ transport based on observed winds: 1. Analysis of observational data. In: (Peterson, D.H., ed.) *Aspects of Climate Variability in the Pacific and the Western Americas, Geophysical Monograph 55*, American Geophysical Union, Washington, D.C., U.S.A., 165pp.
- Keeling, C.D.,** Whorf, T.P., Wahlen, M., and van der Plicht, J. (1995) Interannual extremes in the rate of rise of atmospheric carbon dioxide since 1980. *Nature*, **375**:666–670.
- Keeling, C.D.,** and Piper, S.C. (2000) Interannual variations of exchanges of atmospheric CO₂ and ¹³CO₂ with the terrestrial biosphere and oceans from 1978 to 2000: III. Simulated sources and sinks. Scripps Institution of Oceanography Reference No. 00-14, University of California, San Diego, U.S.A., 68pp.
- Keeling, C.D.,** Whorf, T.P. (2001) Atmospheric CO₂ records from sites in the SIO air sampling network. In *Trends: A Compendium of Data on Global Change*. Carbon Dioxide Information Analysis Center, Oak Ridge National Laboratory, U.S. Department of Energy, Oak Ridge, Tenn., U.S.A.
<<http://cdiac.esd.ornl.gov/trends/co2/sio-mlo.htm>>
- Kessler, M.J.** (1989) Liquid Scintillation Science and Technology. Packard Instrument Company, Publication No. 169–3052, 413pp.
- Kumar, M.D.,** Rajendran, A., Somasundar, K., Ittekot, V., and Desai, B.N. (1992) Processes controlling carbon components in the Arabian Sea. In: (Desai, B.N. ed.) *Oceanography of the Indian Ocean*. Oxford-IBH, New Delhi, India, 313–325pp.
- Kumar, M.D.,** Naqvi, S.W.A., George, M.D., and Jayakumar, D.A. (1996) A sink for atmospheric carbon dioxide in the northeast Indian Ocean. *Journal of Geophysical Research*, **101**:18,121–18,125.
- Kusumgar, S.** (1965) *Study of the geophysical processes based on C¹⁴/C¹² ratios in the atmosphere. M.Sc.–Dissertation, University of Bombay, Bombay, India, 55pp.*
- Lal, D.,** and Krishnaswami, S. (1999) Carbon-14 dating and other applications in earth sciences. In: (Marshall, C.P., and Fairbridge, R.W. eds.) *Encyclopedia of Geochemistry* (Encyclopedia of Earth Sciences series). Kluwer Academic Publishers, Dordrecht, The Netherlands, 59–64pp.

- Lal, D.**, and Rama. (1966) Characteristics of global tropospheric mixing based on man-made C^{14} , H^3 , and Sr^{90} . *Journal of Geophysical Research*, **71**:2,865–2,874.
- Lassey, K.R.**, Manning, M.R., and O'Brien, B.J. (1990) An overview of oceanic radiocarbon: Its inventory and dynamics. *Reviews in Aquatic Sciences*, **3**:117–146.
- Levin, I.**, Münich, M., and Weiss, W. (1980) The effect of anthropogenic CO_2 and ^{14}C sources on the distribution of ^{14}C in the atmosphere. *Radiocarbon*, **22**:379–391.
- Levin, I.**, Kromer, B., Schoch–Fischer, H., Bruns, M., Münich, M., Beradu, B., Vogel, J.C., and Münich, K.O. (1985) 25 years of tropospheric ^{14}C observations in central Europe. *Radiocarbon*, **27**:1–19.
- Levin, I.**, Hesshaimer, V., and Kromer, B. (1997) Long-term observations of $^{14}CO_2$ in the global atmosphere. In: *Abstracts, 16th International Radiocarbon Conference*, June 16–20 1997, Groningen, The Netherlands, 115pp.
- Levin, I.**, and Kromer, B. (1997a) Twenty years of atmospheric $^{14}CO_2$ observations at Schauinsland station, Germany. *Radiocarbon*, **39**:205–218.
- Levin, I.**, and Kromer, B. (1997b) $^{14}CO_2$ records from two sites in central Europe. In *Trends: A Compendium of Data on Global Change*. Carbon Dioxide Information Analysis Center, Oak Ridge National Laboratory, U.S. Department of Energy, Oak Ridge, Tenn., U.S.A. <<http://cdiac.esd.ornl.gov/trends/co2/cent.htm>>
- Levin, I.**, Hesshaimer, V., Kromer, B., Neubert, R., and Schmidt, M. (1998) Global atmospheric observations and modeling of isotopes in CO_2 . In: (Heimann, M., ed.) *European Study of Carbon in the Ocean, Biosphere and Atmosphere (ESCOBA): Atmosphere Section*, Project No. ENV4-CT95-0116, Annual Report 1997, 15pp.
- Levin, I.**, Hesshaimer, V., Kromer, B., Neubert, R., Glatzel-Mattheier, H., and Schmidt, M. (1999) Global atmospheric observations and modeling of isotopes in CO_2 . In: (Heimann, M., ed.) *European Study of Carbon in the Ocean, Biosphere and Atmosphere (ESCOBA): Atmosphere Section*, Project No. ENV4-CT95-0116, Final Report 1996-1998, 21–32pp.
- Levin, I.**, and Hesshaimer, V. (2000) Radiocarbon — A unique tracer of global carbon cycle dynamics. *Radiocarbon*, **42**:69–80.
- Libby, W.F.**, Anderson, E.C., and Arnold, J.R. (1949) Age determination by radiocarbon content: World-wide assay of natural radiocarbon. *Science*, **109**:227–228.

- Libby, W.F.** (1955) *Radiocarbon dating*, 2nd edition. University of Chicago press, Chicago, U.S.A.
- Lingenfelter, R.E., and Ramaty, R.** (1970) Astrophysical and geophysical variations in C14 production. In: (Olsson, I.U., ed.) *Radiocarbon Variations and Absolute Chronology, Proceedings of 12th Nobel Symposium*, John Wiley & Sons, New York, 513pp.
- Linick, T.W.** (1975) Uptake of Bomb-produced Carbon-14 by the Pacific Ocean. *Ph.D.-Thesis, University of California, San Diego, U.S.A.*
- Little, E.A.** (1993) Radiocarbon age calibration at archeological sites of coastal Massachusetts and vicinity. *Journal of Archeological Science*, **20**:457–471.
- Louanchi, F., Metzl, N., Poisson, A.** (1996) Modelling the monthly sea surface f_{CO_2} fields in the Indian Ocean. *Marine Chemistry*, **55**:265–279.
- Madhupratap, M., Kumar, S.P., Bhattathiri, P.M.A., Kumar, M.D., Raghukumar, S., Nair, K.K.C., and Ramaiah, N.** (1996) Mechanism of the biological response to the winter cooling in the northeastern Arabian Sea. *Nature*, **384**:549–552.
- Maier-Reimer, E.** (1993) Geochemical cycles in an ocean general circulation model: Preindustrial tracer distribution. *Global Biogeochemical Cycles*, **7**:645–678.
- Mahadevan, A.** (2001) An analysis of bomb radiocarbon trends in the Pacific. *Marine Chemistry*, **73**:273–290.
- Malhi, Y., Nobre, A.D., Grace, J., Krujit, B., Pereira, M.G.P., Culf, A., and Scott, S.** (1998) Carbon dioxide transfer over a Central Amazonian rain forest. *Journal of Geophysical Research*, **103**:31,593–31,612.
- Mangerud, J., and Gulliksen, S.** (1975) Apparent radiocarbon ages of recent marine shells from Norway, Spitzbergen, and Arctic Canada. *Quaternary Research*, **5**:263–273.
- Mann, M.E., Bradley, R.S., and Hughes, M.K.** (2000) Long-term variability in the El Niño/Southern Oscillation and associated teleconnections. In: (Diaz, H.F., and Markgraf, V., eds.) *El Niño & the Southern Oscillation: Multiscale variability & its impacts on natural ecosystem and society*, Cambridge University Press, Cambridge, U.K., 321–372pp.
- Mann, W.B.** (1983) An international reference material for radiocarbon dating. *Radiocarbon*, **25**:519–522.

- Manning**, M.R., Lowe, D.C., Melhuish, W.H., Sparks, R.J., Wallace, G., Brenninkmeijer, C.A.M., and McGill, R.C. (1990) The use of radiocarbon measurements in atmospheric studies. *Radiocarbon*, **32**:37–58.
- Manning**, M.R., and Melhuish, W.H. (1994) Atmospheric ^{14}C record from Wellington. In *Trends: A Compendium of Data on Global Change*. Carbon Dioxide Information Analysis Center, Oak Ridge National Laboratory, U.S. Department of Energy, Oak Ridge, Tenn., U.S.A. <<http://cdiac.esd.ornl.gov/trends/co2/welling.htm>>
- Marland**, G., Boden, T., and Andres, R.J. (2000) National CO_2 emissions from fossil-fuel burning, cement manufacture, and gas flaring: 1751-1997. *NDP-030*, Carbon Dioxide Information Analysis Center, Oak Ridge National Laboratory, U.S. Department of Energy, Oak Ridge, Tenn., U.S.A.
- Masarie**, K.A., White, J., Vaughn, B., and Tans, P. (2000) Stable isotopic composition of atmospheric carbon dioxide (^{13}C and ^{18}O). INSTAAR, University of Colorado and NOAA Climate Monitoring and Diagnostic Laboratory (CMDL), Carbon Cycle Group. <<http://www.cmdl.noaa.gov/info/ftpdata.html>>
- McCormac**, F.G., Baillie, M.G.L., Pilcher, J.L., and Kalin, R.M. (1995) Location-dependent differences in the ^{14}C content of wood. *Radiocarbon*, **37**:395–408.
- Milliman**, J.D., and Mead, R.H. (1983) World delivery of riverine sediments to the oceans. *Journal of Geology*, **21**:1–21.
- Mook**, W.G., and van der Plicht, J. (1999) Reporting ^{14}C activities. *Radiocarbon*, **41**:227-239.
- Moore**, W.S., and Krishnaswami, S. (1974) Correlation of X-radiography revealed banding in corals with radiometric growth rates. In: *Proceedings, 2nd International Coral Reef Symposium*, Brisbane, Australia, 269–276pp.
- Moore**, W.S., Krishnaswami, S., and Bhat, S.G. (1973) Radiometric determination of coral growth rates. *Bulletin of Marine Science*, **23**:157–176.
- Munnich**, K.O., and Roether, W. (1967) Transfer of bomb ^{14}C and tritium from the atmosphere to the ocean: Internal mixing of the ocean on the basis of tritium and ^{14}C profiles. *Symposium on Radioactive Dating and Methods of Low Level Counting*, Report, UN DOC SM-87/22, IAEA, Vienna, 93–103pp.
- Munk**, W.H. (1966) Abyssal recipes. *Deep-Sea Research*, **13**:707–730.

- Nakamura, T., Nakazawa, T., Nakai, N., Kitagawa, H., Honda, H., Itoh, T., Machida, T., and Matsumoto, E.** (1992) Measurement of ^{14}C concentrations of stratospheric CO_2 by accelerator mass spectrometry. *Radiocarbon*, **34**:745–752.
- Nakazawa, T., Morimoto, S., and Aoki, S.** (1997) Temporal and spatial variations of the carbon isotopic ratio of atmospheric carbon dioxide in the western Pacific region. *Journal of Geophysical Research*, **102**:1,271–1,285.
- Noakes, J.E., Kim, S., and Stipp, J.J.** (1965) Chemical and counting advances in liquid scintillation age dating. In: (Chatter, R.M., and Olson, E.A., eds.) *Proceedings of International Conference on ^{14}C and Tritium Dating*, NBS, Washington, D.C., USAEC 650-652, 68–92pp.
- Noakes, J., and Valenta, P.** (1989) Low background liquid scintillation counting using an active sample holder and pulse discrimination electronics. *Radiocarbon*, **31**:332–341.
- Nozaki, Y., Rye, D.M., Turekian, K.K., and Dodge, R.E.** (1978) A 200 year record of Carbon-13 and Carbon-14 variations in a Bermuda coral. *Geophysical Research Letters*, **5**:825–828.
- Nydal, R.** (1963) Increase in radiocarbon from most recent series of thermonuclear tests. *Nature*, **196**:212–214.
- Nydal, R.** (1966) Variation of ^{14}C concentration in the atmosphere during the last several years. *Tellus*, **18**:271–279.
- Nydal, R., and Lövseth, K.** (1983) Tracing bomb ^{14}C in the atmosphere 1962–1980. In: (Keeling, C.D., and Cicerone, R.J., eds.) *Proceedings of Bern CO_2 Symposium*, September 14–18 1981, Bern, Switzerland. *Journal of Geophysical Research*, **88**:3,621–3,642.
- Nydal, R., and Gisslefoss, J.S.** (1996) Further application of bomb ^{14}C as a tracer in the atmosphere and ocean. *Radiocarbon*, **38**:389–406.
- Nydal, R., and Lövseth, K.** (1996) Carbon-14 measurements in atmospheric CO_2 from Northern and Southern Hemisphere sites, 1962–1993. *NDP-057*, Carbon Dioxide Information Analysis Center, Oak Ridge National Laboratory, U.S. Department of Energy, Oak Ridge, USA. <<http://cdiac.esd.ornl.gov/epubs/ndp/ndp057/ndp057.htm>>
- Oeschger, H., Siegenthaler, U., Schotterer, U., Gugelmann, A.** (1975) A box-diffusion model to study the carbon dioxide exchange in nature. *Tellus*, **27**:168–192.

- Olsson, I.U.** (1989) Recent ^{14}C activity in the atmosphere, clean air and the Chernobyl effect. *Radiocarbon*, **31**:740–746.
- Pacanowski, R.K., Dixon, K., and Rosati, A.** (1991) The GFDL Modular Ocean Model Users Guide, v 1.0, *GFDL Ocean Group Technical Report*, **2**, Geophysical Fluid Dynamics Laboratory, Princeton, NJ, U.S.A.
- Peng, T.-H., Key, R.M., and Östlund, H.G.** (1998) Temporal variations of bomb radiocarbon inventory in the Pacific Ocean. *Marine Chemistry*, **60**:3–13.
- Peristykh, A.N., and Damon, P.E.** (1998) Modulation of atmospheric ^{14}C concentrations by the solar wind and irradiance components of the Hale and the Schwabe solar cycles. *Solar Physics*, **177**:343–355.
- Quay, P.D., and Stuiver, M.** (1980) Vertical advection–diffusion rates in the oceanic thermocline determined from ^{14}C distributions. *Radiocarbon*, **22**:607–625.
- Rafter, T.A., and Ferguson, G.J.** (1957) “Atomic bomb effect” — recent increase of carbon-14 content of the atmosphere and biosphere. *Science*, **126**:557–558.
- Rafter, T.A., and O’Brien, B.J.** (1973) ^{14}C measurements in the atmosphere and in the South Pacific Ocean — A re-calculation of the exchange rates between the atmosphere and the ocean. In: (Rafter, T.A., and Grant-Taylor, T., eds.) *Proceedings of the 8th International Conference on radiocarbon dating*, The Royal Society of New Zealand, **1**:241–266pp.
- Rasmusson, E.M., and Wallace, J.M.** (1983) Meteorological aspects of the El Niño/Southern Oscillation. *Science*, **222**:1,195–1,202.
- Rayner, P.J., Law, R.M., and Dargaville, R.** (1999) The relationship between tropical CO_2 fluxes and the El Niño–Southern Oscillation. *Geophysical Research Letters*, **26**:493–496.
- Reimer, P.J. and Reimer, R.W.** (2001) A marine reservoir correction database and on-line interface. In: *Proceedings of the 17th International Radiocarbon Conference*. *Radiocarbon* (in press). <<http://www.calib.org/marine>>
- Rozanski, K., Levin, I., Stock, J., and Guevara Falcon, R.E.** (1995) Atmospheric $^{14}\text{CO}_2$ variations in the equatorial region. *Radiocarbon*, **37**:509–516.

- Rubin, M.**, and Suess, H. (1955) U.S. Geological Survey radiocarbon dates II. *Science*, **121**:481–488.
- Sabine, C.** and Key, R.M. (1997) Surface water and atmospheric underway carbon data obtained during the World Ocean Circulation Experiment Indian Ocean Survey Cruises (R/V Knorr, December 1994–January 1996). *NDP-064*, Carbon Dioxide Information Analysis Center, Oak Ridge National Laboratory, U.S. Department of Energy, Oak Ridge, USA. <<http://cdiac.esd.ornl.gov/epubs/ndp/ndp064/ndp064.htm>>
- Sarkar, A.**, Ramesh, R., Bhattacharya, S.K., Rajagopalan, G. (1990) Oxygen isotope evidence for a stronger winter monsoon current during the last deglaciation. *Nature*, **343**:549–551.
- Sarkar, Ashish**, Ramesh, R., Somayajulu, B.L.K., Agnihotri, R., Jull, A.J.T., and Burr, G.S. (2000) High resolution monsoon record from the eastern Arabian Sea. *Earth and Planetary Science Letters*, **177**:209–218.
- Sarma, V.V.S.S.**, Kumar, M.D., and George, M.D. (1998) The central and the eastern Arabian Sea as a perennial source of atmospheric carbon dioxide. *Tellus, Sec. B*, **50**:179–184.
- Sarma, V.V.S.S.**, Kumar, M.D., Gauns, M., and Madhupratap, M. (2000) Seasonal controls on surface pCO₂ in the central and eastern Arabian Sea. *Proceedings of Indian Academy of Science (Earth and Planetary Science)*, **109**:471–479.
- Schlitzer, R.** (2001) Ocean Data View 5.5. *Alfred Wegener Institute for Polar and Marine Research*, Bremerhaven, Germany. <<http://www.awi-bremerhaven.de/GEO/ODV>>
- Schulz, M.**, and Stettgen, K. (1997) SPECTRUM: Spectral analysis of unevenly spaced paleoclimatic time series. *Computers and Geosciences*, **23**:929–945.
- Schulz, M.**, and Mudelsee, M. (2001) REDFIT: Estimating red-noise spectra directly from unevenly spaced paleoclimate time series. *Computers and Geosciences*, (in press).
- Siani, G.**, Paterne, M., Arnold, M., Bard, E., Bernard, M., Tisnerat, N., and Bassinot, F. (2000) Radiocarbon reservoir ages in the Mediterranean Sea and the Black Sea. *Radiocarbon*, **42**:271–280.
- Somayajulu, B.L.K.** (1993) Age and mineralogy of the miliolites of Saurashtra and Kutch, Gujarat. *Current Science*, **64**:926–928.

- Somayajulu, B.L.K., Broecker, W.S., and Goddard, J. (1985)** Dating Indian corals by U-decay-series methods. *Quaternary Research*, **24**:235–239.
- Somayajulu, B.L.K., Rengarajan, R., Lal, D., and Craig, H. (1991)** GEOSECS Pacific and Indian Ocean ^{32}Si profiles. *Earth and Planetary Science Letters*, **107**:197–216.
- Somayajulu, B.L.K., Bhushan, R., and Narvekar, P.V. (1999)** $\Delta^{14}\text{C}$, ΣCO_2 and salinity of the western Indian Ocean deep waters: spatial and temporal variations. *Geophysical Research Letters*, **26**:2,869–2,872.
- Southon, J.R., Nelson, D.E., and Vogel, J.S. (1990)** A record of past ocean-atmosphere radiocarbon differences from the northeast Pacific. *Paleoceanography*, **5**:197–206.
- Southon, J.R., Nelson, D.E., and Vogel, J.S. (1992)** The determination of past ocean-atmosphere radiocarbon differences. In: (Bard, E., and Broecker, W.S. eds.) *The Last Deglaciation: Absolute and Radiocarbon Chronologies*. Springer-Verlag, Berlin, Germany, 219–227pp.
- Srinivasan, A., Rooth, C.G.H., Top, Z., and Olson, D.B. (2000)** Abyssal upwelling in the Indian Ocean: Radiocarbon diagnostics. *Journal of Marine Research*, **58**:755–778.
- Strickland, J.D.H., and Parsons, T.R. (1972)** *A practical Handbook of Sea-water Analysis*. Fisheries Research Board of Canada, Ottawa, Canada.
- Stuiver, M. (1980)** ^{14}C distribution in Atlantic Ocean. *Journal of Geophysical Research*, **85**:2,711–2,718.
- Stuiver, M. (1993)** A note on single-year calibration of the radiocarbon time scale, AD 1510–1954. *Radiocarbon*, **35**:67–72.
- Stuiver, M., and Polach, H.A. (1977)** Reporting of ^{14}C data. *Radiocarbon*, **19**:355–363.
- Stuiver, M. and Quay, P.D. (1981)** Atmospheric ^{14}C changes resulting from fossil fuel CO_2 release and cosmic ray flux variability. *Earth and Planetary Science Letters*, **53**:349–362.
- Stuiver, M., and Östlund H.G. (1983)** GEOSECS Indian Ocean and Mediterranean radiocarbon. *Radiocarbon*, **25**:1–29.
- Stuiver, M., and Quay, P.D. (1983)** Abyssal water Carbon-14 distribution and the age of the world oceans. *Science*, **219**:849–851.

- Stuiver, M., Pearson, G.W., and Braziunas, T.F.** (1986) Radiocarbon age calibration of marine samples back to 9000 cal BP. In: (Stuiver, M., and Kra, R.S. eds.) *Proceedings of the 12th International ¹⁴C Conference, Radiocarbon*, **28**:980–1,021.
- Stuiver, M., Braziunas, T.F., Becker, B., and Kromer, B.** (1991) Climatic, solar, oceanic, and geomagnetic influences on late-glacial and Holocene atmospheric ¹⁴C/¹²C change. *Quaternary Research*, **35**:1–24.
- Stuiver, M., and Braziunas, T.F.** (1993a) Modeling atmospheric ¹⁴C influences and ¹⁴C ages of marine samples to 10,000 BC. In: (Stuiver, M., Long, A., and Kra, R.S. eds.) *Calibration 1993, Radiocarbon*, **35**:137–189.
- Stuiver, M., and Braziunas, T.F.** (1993b) Sun, ocean, climate and atmospheric ¹⁴CO₂: an evaluation of causal and spectral relationships. *The Holocene*, **3**:289–305.
- Stuiver, M., and Braziunas, T.F.** (1998) Anthropogenic and solar components of hemispheric ¹⁴C. *Geophysical Research Letters*, **25**:329–332.
- Stuiver, M., Reimer, P.J., Bard, E., Beck, J.W., Burr, G.S., Hughen, K.A., Kromer, B., McCormac, G., van der Plicht, J., and Spurk, M.** (1998a) INTCAL 98 Radiocarbon age calibration, 24,000–0 cal BP. In: (Stuiver, M., and van der Plicht, J., eds.) *INTCAL 98: Calibration issue, Radiocarbon*, **40**:1,041–1,083.
- Stuiver, M., Reimer, P.J., and Braziunas, T.F.** (1998b). High precision radiocarbon age calibration for terrestrial and marine samples. *Radiocarbon*, **40**:1,127–1,151.
- Stuiver, M., Quay, P.D., and Braziunas, T.F.** (2000) Isotope and carbon cycle inferences. In: (Wigley, T.M.L., and Schimel, D.S., eds.) *The Carbon Cycle*, Cambridge University Press, Cambridge, U.K., 153–160pp.
- Takahashi, T., Feely, R.A., Weiss, R.F., Wanninkhof, R.H., Chipman, D.W., Sutherland, S.C., and Takahashi, T.T.** (1997) Global air-sea flux of CO₂: An estimate based on measurements of sea-air pCO₂ difference. *Proceedings of National Academy of Sciences, U.S.A.*, **94**:8,292–8,299.
- Talma, A.S.** (1990) Radiocarbon age calibration of marine shells. In: *Quarterly Report, Quaternary Dating Research Unit, CSIR*, Pretoria, South Africa. 10pp.
- Taylor, R.E., and Berger, R.** (1967) Radiocarbon content of marine shells from the Pacific coasts of Central and South America. *Science*, **158**:1,180–1,182.

- Tian, H., Melillo, J.M., Kicklighter, D.W., McGuire, A.D., Helfrich, J.V.K., Moore, B., and Vörösmarty, C.J.** (1998) Effect of interannual climate variability on carbon storage in Amazonian ecosystems. *Nature*, **396**:664–667.
- Toggweiler, J.R., and Trumbore, S.** (1985) Bomb-test ^{90}Sr in Pacific and the Indian Ocean surface water as recorded by banded corals. *Earth and Planetary Science Letters*, **74**:306–314.
- Toggweiler, J.R., Dixon, K., and Bryan K.** (1989a) Simulations of radiocarbon in a coarse-resolution world ocean model, 1. Steady state prebomb distributions. *Journal of Geophysical Research*, **94**:8,217–8,242.
- Toggweiler, J.R., Dixon, K. and Bryan K.** (1989b) Simulations of radiocarbon in a coarse-resolution world ocean model, 2. Distributions of bomb-produced Carbon 14. *Journal of Geophysical Research*, **94**:8,243–8,264.
- Trumbore, S.** (1997) Potential of soil organic carbon to global environmental change. *Proceedings of National Academy of Sciences, USA*, **94**:8,284–8,291.
- UNESCO.** (1978) *Technical Papers in Marine Science*, 28:35pp.
- Vacquier, U, and Taylor, P.T.** (1966) Geothermal and magnetic surveys of the coast of Sumatra. *Bulletin of Earthquake Research Institute*, **44**:531pp.
- von Rad, U., Schaff, M., Michels K.H., Schulz, H., Berger, W.H., Sirocko, F.** (1999) A 5000-yr record of climate change in varved sediments from the oxygen minimum zone off Pakistan, northeastern Arabian Sea. *Quaternary Research*, **51**:39–53.
- Wanninkhof, R., Ledwell, J., Broecker, W.S.** (1985) Gas exchange–wind speed relation measured with sulfur hexafluoride on a lake. *Science*, **227**:1224–1226.
- Wanninkhof, R.,** (1992) Relationship between wind speed and gas exchange over the ocean. *Journal of Geophysical Research*, **97**:7,373–7,382.
- Wanninkhof, R., and McGillis, W.R.** (1999) A cubic relationship between air-sea CO_2 exchange and wind speed. *Geophysical Research Letters*, **26**:1,889–1,892.
- Warren, B.A.** (1992) Circulation of north Indian deep water in the Arabian Sea. In: (Desai, B.N., ed.) *Oceanography of the Indian Ocean*, Oxford & IBH, New Delhi, India, 575–582pp.

- Weidman**, C.R., and Jones, G.A. (1993) A shell-derived time history of bomb ^{14}C on Georges Bank and its Labrador Sea implications. *Journal of Geophysical Research*, **98**:14,557–14,588.
- Weiss**, R.F. (1974) Carbon dioxide in water and seawater: The solubility of a non-ideal gas. *Marine Chemistry*, **2**:203–215.
- Wolter**, K., and Timlin, M.S. (1998) Measuring the strength of ENSO — how does 1997/98 rank? *Weather*, **53**:315–324.
- Wolter**, K. (2001) Multivariate ENSO index. NOAA-CIRES Climate Diagnostics Center, Boulder, Colorado, U.S.A. <<http://www.cdc.noaa.gov/~kew/MEI>>
- Wong**, C.S., Chan, Y-H., Page, J.S., Smith, G.E., and Bellegay, R.D. (1993) Changes in equatorial CO₂ flux and new production in estimated from CO₂ and nutrient levels in Pacific surface waters during the 1986/87 El Niño. *Tellus*, **45B**:64–79.
- Yang**, X., and Wang, M.X. (2000) Monsoon ecosystems control on atmospheric CO₂ interannual variability: inferred from a significant positive correlation between year-to-year changes in land precipitation and atmospheric CO₂ growth rate. *Geophysical Research Letters*, **27**:1671–1674.
- You**, Y. (1997) Seasonal variations of thermocline circulation and ventilation in the Indian Ocean. *Journal of Geophysical Research*, **102**:10,391–10,422.
- You**, Y., and Tomczac, M. (1993) Thermocline circulation and ventilation in the Indian Ocean derive from water mass analysis. *Deep-Sea Research Part II – Topical Studies in Oceanography*, **40**:13–56.

List of publications by the author:

List of papers:

1. **Dutta, K.**, Bhushan, R., and Somayajulu B.L.K. (2001) ΔR correction values for the Northern Indian Ocean. *Radiocarbon*, **43(2a)**:483–485.
2. **Dutta, K.**, Bhushan, R., and Somayajulu, B.L.K. (2001) $^{14}\text{CO}_2$ in maritime air over the Northern Indian Ocean. In: *Proceedings of 3rd IAEA Conference on “The Study of Environmental Change Using Isotope Techniques,”* April 23–27 2001, Vienna, Austria.
3. Bhushan, R., **Dutta, K.**, and Somayajulu, B.L.K. (2001) Concentrations and burial fluxes of organic and inorganic carbon on the eastern margins of the Arabian Sea. *Marine Geology*, **178**:95–113.
4. Bhushan, R., **Dutta, K.**, Somayajulu B.L.K., and Krishnaswami, S. (1999) Bomb radiocarbon in the Arabian Sea: Estimates of the rates of air–sea CO_2 exchange and upwelling. In: (Nojiri, Y., ed.) *Proceedings of the 2nd International Symposium on “CO₂ in the Oceans”*, Jan 18–22, 1999, Tsukuba, Japan, 231–234pp (Center for Global Environmental Research, Tsukuba, 1999).
5. Somayajulu, B.L.K., Agnihotri, R., Dixit, M., **Dutta, K.**, and Sharma, C. (1998) Arabian Sea Sediments and Paleoclimate. In: (Subbaraya, Rao, Desai, and Manikiam, eds.) *Global Climate Changes Scientific Results from ISRO–GBP*. ISRO, Bangalore, India, 207–221pp.
6. Agnihotri R., **Dutta, K.**, Bhushan, R., and Somayajulu, B.L.K. Evidence of solar forcing of the southwest monsoon during the last millennium (submitted to *Earth and Planetary Science Letters*).
7. **Dutta, K.** Coherence of tropospheric $^{14}\text{CO}_2$ with El Niño/Southern Oscillation (submitted to *Geophysical Research Letters*).

List of abstracts published in conference proceedings:

1. **Dutta, K.** (2001) Influence of El Niño/Southern Oscillation on tropospheric $^{14}\text{CO}_2$. In: *Abstracts of "6th International CO₂ Conference"*, October 1–5 2001, Sendai, Japan.
2. **Dutta, K.**, Bhushan, R., and Somayajulu B.L.K. (2001) $^{14}\text{CO}_2$ in maritime air over the Northern Indian Ocean. In: *Abstracts of "3rd IAEA Conference on The Study of Environmental Change Using Isotope Techniques"*, April 23–27 2001, Vienna, Austria.
3. **Dutta, K.**, Bhushan, R., and Somayajulu B.L.K. (2000) Anthropogenic radiocarbon in Bay of Bengal: Two decades after GEOSECS. In: *Abstracts of "17th International Radiocarbon Conference"*, June 18–23 2000, Judean Hills, Israel.
4. **Dutta, K.**, Bhushan, R., and Somayajulu B.L.K. (2000) ^{14}C in archived marine shells from the Arabian Sea and the Bay of Bengal. In: *Abstracts of "17th International Radiocarbon Conference"*, June 18–23 2000, Judean Hills, Israel.
5. **Dutta, K.**, Bhushan, R., and Somayajulu B.L.K. (2000) Application of nuclear bomb produced radiocarbon in environmental studies: Air–sea exchange rate of carbon dioxide over the Northern Indian Ocean. In: *Abstracts of "TROPMET–2000, National Symposium on Tropical Meteorology"*, Feb 1–4 2000, Cochin, India.
6. Agnihotri, R., **Dutta, K.**, Bhushan, R., and Somayajulu, B.L.K. (2001) Multi-decadal variability of South Asian monsoon: Proxy and instrumental records. In: *Abstracts of "1st ARTS Open Sciences Meeting"*, November 4–7 2001, Nouméa, New Caledonia.
7. Agnihotri, R., Bhushan, R., **Dutta, K.**, Ramesh, R., Sarkar, A., and Somayajulu, B.L.K. (2000) Retrieving high resolution paleomonsoon and paleoclimatic information from the margin sediments of the Eastern Arabian Sea. In: *Abstracts of "Chairman's review of ISRO–GBP projects and the 3rd workshop on scientific results from ISRO Geosphere Biosphere Programme"*, October 3–4 2000, ISRO headquarters, Bangalore, India.
8. Somayajulu, B.L.K., Sarkar, A., Agnihotri, R., Ramesh, R., **Dutta, K.**, and Bhushan, R. (1999) Holocene monsoonal and upwelling records from the margin sediments of the eastern Arabian Sea. In: *Abstracts of "IAPSO Symposium, IUGG General Assembly"*, July 19–31 1999, (P07) Birmingham, UK.
9. Agnihotri, R., Bhushan, R., **Dutta, K.**, Jull, A.J.T., Ramesh, R., Sarkar, A., and Somayajulu, B.L.K. (1998) Margin sediments of the Eastern Arabian Sea: geochronology, geochemistry and C and O isotope systematics. In: *Abstracts of "International Conference on Benthic Processes in Deep Arabian Sea"*, July 1–3 1998, Edinburgh, Scotland.
10. Agnihotri, R., Bhushan, R., Dubey, A., **Dutta, K.**, Karthikeyan, K., Rengarajan, R., and Somayajulu B.L.K. (1998) Ascertaining changes in physical and chemical properties of the Arabian Sea: Reoccupation of GEOSECS after two decades. In: *Abstracts of "Second International Conference on Environmental Science"*, December 2–4 1998, Regional Research Laboratory, Trivandrum, India.
11. Agnihotri, R., Bhushan, R., **Dutta, K.**, Sarkar, A., and Somayajulu, B.L.K. (1997) Deciphering monsoonal/climatic changes during the past millennium using the continental margin sediments of the west–coast of India. In: *Proceedings of the "International Conference on Isotopes in the Solar System"*, November 11–14 1997 Physical Research Laboratory, Ahmedabad, India.
12. Sarin M.M., Bhushan, R., and **Dutta, K.** (1997) Determination of organic carbon and nitrogen in marine sediments using elemental analyzer. In: *Abstracts of conference on "Recent Advances in Elemental Analysis"*, October 1997, Homi Bhabha Centre for Science Education (TIFR), Mumbai, India.